

A Systems Biology Approach to Unravel the Cellular Function of MicroRNAs

Dissertation

zur

Erlangung des akademischen Grades

Doktor-Ingenieur (Dr.-Ing.)

Promotionsgebiet Systembiologie

Fakultät für Informatik und Elektrotechnik

Universität Rostock

**Universität
Rostock**



Traditio et Innovatio

vorgelegt von

Xin Lai, geboren am 21. April 1983 in Chengdu, China

Gutachter:

Referent: Prof. Dr. Olaf Wolkenhauer, Universität Rostock

Korreferent: Prof. Dr. Bernd Schmeck, Philipps-Universität Marburg

Korreferent: Prof. Dr. Rui Alves, Universidad de Lleida

Datum der Einreichung: 10. September 2012

Datum der Verteidigung: 3. Dezember 2012

Mitglieder der Promotionskommission:

Prof. Dr. Adelinde Uhrmacher, Universität Rostock

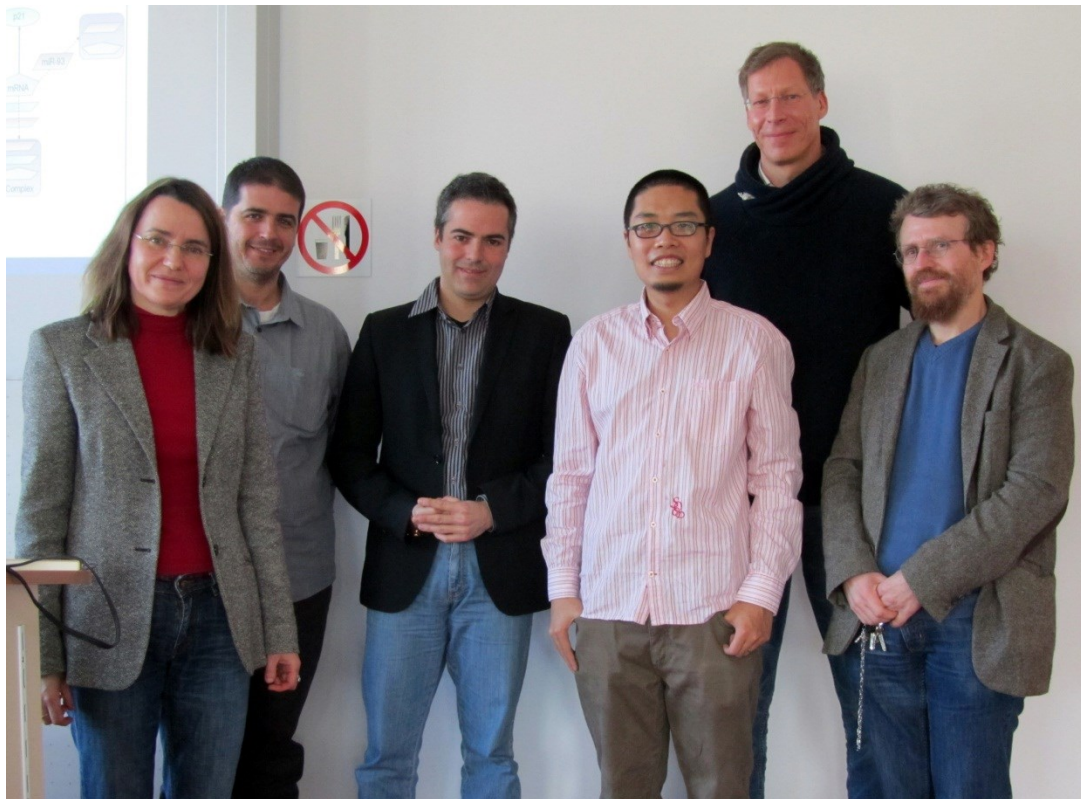
Prof. Dr. Olaf Wolkenhauer, Universität Rostock

Prof. Dr. Bernd Schmeck (via Skype), Universität Marburg

Prof. Dr. Rui Alves, Universidad de Lleida

Prof. Dr. Georg Füllen, Universität Rostock

Dr. Julio Vera, Universität Rostock



Von links nach rechts: Adelinde Uhrmacher, Rui Alves, Julio Vera, Xin Lai, Olaf Wolkenhauer und Georg Füllen.

If you cannot explain it simple, you do not understand it well enough.

- Albert Einstein

Science is an ongoing self-correcting process rather than an unassailable monolith of truth.

- Stephen Hawking

Stay hungry, stay foolish.

- Steve Jobs

To my grandmother Ren, Yafang, who passed away on 15 August 2012.
Thank you for your generous love and I will miss you forever.

Contents

Abstract	V
Acknowledgements	IX
Abbreviations	XI
1. Introduction	1
1.1 Systems biology	1
1.2 MicroRNAs	4
1.2.1 MicroRNA biogenesis and function	4
1.2.2 MicroRNAs and human diseases	9
1.3 Using a systems biology approach to study microRNA-mediated regulation ..	12
1.3.1 MicroRNA regulation of gene expression	12
1.3.2 MicroRNA inhibition at translation initiation.....	13
1.3.3 MicroRNA-mediated feedback and feedforward loops	14
1.4 Objectives of this thesis	17
1.5 Outline of this thesis	18
2. <i>In silico</i> modelling using ODEs	19
2.1 Model construction	19
2.2 Model calibration	24
2.2.1 Parameter estimation	25
2.2.2 Parameter identifiability	28
2.3 Model validation and analysis.....	30
2.3.1 Sensitivity analysis.....	31
2.3.2 Bifurcation analysis.....	34
2.4 Summary	38

3. MicoRNA-34a regulation of the p53/SIRT1 signalling pathway	41
3.1 The p53/SIRT1 signalling pathway	41
3.2 Materials and methods	44
3.2.1 Model construction	44
3.2.2 Model calibration	46
3.2.3 Model validation	47
3.3 Results	50
3.3.1 The post-transcriptional repression of SIRT1 by miR-34a	50
3.3.2 The regulatory effect of miR-34a on the activation of p53	53
3.4 Conclusion	55
4. Target hub gene repression by multiple and cooperative microRNAs	57
4.1 Target hub gene regulation	57
4.2 Materials and methods	59
4.2.1 Data retrieval	60
4.2.2 Construction and analysis of the p21 regulatory map	61
4.2.3 Model construction and calibration	62
4.2.4 Experimental verification for microRNA cooperativity	65
4.3 Results	66
4.3.1 Analysis of the p21 regulatory map	66
4.3.2 Identification of network motifs	69
4.3.3 Kinetic modelling of p21 regulation by multiple miRNAs	71
4.3.4 Computational analysis of miRNA cooperativity	74
4.3.5 The response of p21 to stimulus signals	80
4.3.6 Cooperative miRNA regulation of p21 expression	83
4.4 Conclusion	84
5. Conclusion and discussion	86
6. Appendix	90

6.1	Modelling SIRT1 repression by microRNA-34a	90
6.2	MicroRNA target hub network analysis and model simulations	91
6.2.1	Confidence scores	91
6.2.2	Model simulations.....	95
6.3	Experimental methods.....	99
6.3.1	Small RNA transfection and doxorubicin treatment.....	99
6.3.2	Immunoblotting.....	99
Bibliography.....		106
Scientific contributions.....		115
Curriculum vitae.....		124
Theses.....		126
Selbständigkeitserklärung		131

Abstract

MicroRNAs (miRNAs) are potent effectors of post-transcriptional gene regulation. They exert functions that affect cellular processes, and dysregulated miRNAs may cause pathologies such as cancer. Distinct interactions between miRNAs and their target genes are designed to implement particular functions within cells. Experimental approaches are used to study individual interactions between miRNAs and their targets, but these approaches cannot lead to a system-level understanding of the regulatory role of miRNAs. Therefore, the introduction of a systematic and complementary approach to investigate the function of miRNAs is needed.

The systems biology approach, combining biological data with mathematical modelling, provides the means to elucidate the functional role of miRNAs in signalling pathways and gene regulatory networks. The approach is characterised by a cyclic process, including biological network construction, mathematical modelling, simulation and experimental validation. In the process, biochemical networks are translated into kinetic models using nonlinear ordinary differential equations. Model parameter values are characterised using biological information from the literature, databases and/or estimated from experimental data using optimisation methods. Analytical tools, like sensitivity and bifurcation analysis, together with model predictions are adopted to unravel dynamic properties of kinetic models.

In this thesis, I first present a case study in which I investigate the regulatory role of miR-34a in a signalling pathway using a systems biology approach. The signalling pathway consists of the interactions among tumour protein 53 (p53), sirtuin 1 (SIRT1) and miR-34a. Kinetic modelling of the p53/SIRT1 signalling pathway identifies the mechanism by which miR-34a represses SIRT1 and shows the ability of miR-34a to recover the loss of active p53, which is caused by upregulation of SIRT1.

Second, the investigation of the regulation of a miRNA target hub by multiple and cooperative miRNAs is presented. Using targeting prediction algorithms and experimental evidence, the putatively cooperating miRNA pairs for cyclin-dependent kinase inhibitor 1 (p21) are identified, and a comprehensive regulatory map of p21 is constructed. Subsequently, experimental results verify the method for identifying cooperative miRNA pairs, and a kinetic model is developed on the basis of the p21 regulatory map. The characterised and validated model is further used to decipher the regulation of p21 by multiple and cooperative miRNAs in different biological scenarios.

Zusammenfassung

MicroRNAs (miRNAs) sind potente Effektoren posttranskriptioneller Genregulation. Sie beeinflussen zelluläre Prozesse und können bei Fehlregulation Krebs und andere Krankheiten auslösen. Die Prozessregulation erfolgt über individuelle Interaktionen zwischen miRNAs und ihren Zielgenen (Targets). Diese Interaktionen wurden für verschiedene miRNAs und deren Targets mit Hilfe experimenteller Methoden aufgeklärt, ungeklärt jedoch bleibt dabei die regulatorische Rolle von miRNAs auf Systemebene. Daher ist die Einführung eines systematischen und komplementären Ansatzes zur Erforschung der Funktionen von miRNAs erforderlich.

Der systembiologische Ansatz integriert die mathematische Modellierung mit biologischen Daten und erlaubt somit die Aufklärung der Funktion von miRNAs in Signalwegen und genregulatorischen Netzwerken. Charakteristisch für diesen Ansatz ist ein zyklischer Prozess, welcher die Konstruktion biologischer Netzwerke, die mathematische Modellierung, Simulation sowie die experimentelle Validierung vereint. Dabei werden die biochemischen Netzwerke mittels gewöhnlicher Differentialgleichungen in kinetische Modelle umformuliert. Die Modellparameter werden aus der Literatur und biologischen Datenbanken extrahiert oder durch Optimierungsmethoden geschätzt. Analytische Werkzeuge, wie zum Beispiel die Sensitivitäts- und die Bifurkationsanalyse, zusammen mit Modelvorhersagen werden dazu genutzt, die dynamischen Eigenschaften des kinetischen Modells zu ermitteln.

In der vorliegenden Arbeit stelle ich zunächst eine Fallstudie vor, in der ich, mit Hilfe eines systembiologischen Ansatzes, die regulatorische Rolle von miR-34a in einem Signalweg untersuche. Dieser Signalweg beinhaltet die Interaktion zwischen dem Tumorphprotein 53 (p53), Sirtuin 1 (SIRT1) und miR-34a. Die kinetische Modellierung des p53/SIRT1 Signalweges identifiziert die Mechanismen, mit denen miR-34a das Protein SIRT1 reprimiert. Dadurch kompensiert die miR-34a Aktivität in den Simulationen den Verlust an aktiven p53 durch ein hohes SIRT1 Level.

Danach analysiere ich die Regulation eines miRNA-Targethubs durch vielfache und kooperativ wirkende miRNAs. Unter Zuhilfenahme von Zielvorhersagealgorithmen und experimenteller Daten, identifiziere ich putativ kooperierende miRNA Paare für den CDK-Inhibitor 1 (p21) und konstruiere daraus eine umfassende Übersichtskarte zur p21 Regulation. Anschließend, wird die Methode zur Identifizierung kooperierender miRNAs mit experimentellen Ergebnissen validiert. Schließlich entwickle ich ein kinetisches Modell auf Basis der Übersichtskarte zur p21 Regulation. Das parametrisierte und validierte Modell erlaubt die Entschlüsselung der p21 Regulation durch multiple und kooperierende miRNAs in verschiedenen biologischen Szenarien.

Acknowledgements

This work was funded from June 2008 to September 2012 by German Federal Ministry of Education and Research (BMBF) as a part of the project CALSYS-FORSYS (Project Number: 0315264).

I would like to thank my advisor Prof. Olaf Wolkenhauer for his sustained support during my Ph.D. study. As the head of the department of Systems Biology and Bioinformatics (SBI), Prof. Wolkenhauer has outstanding visionary attitude to solving biological problems by applying control system theories and mathematical methods. Prof. Wolkenhauer also provides an excellent working environment for young researchers fascinated by interdisciplinary subjects.

I am grateful for Dr. Julio Vera who provides his generous support for my research work. As a colleague Dr. Vera is a passionate and creative group leader, and as a friend he also shows kind concern for my personal life.

I would like to say a big thank you to the current and former SBI colleagues including Dr. Daniel Guebel, Dr. Manfred Drack, Dr. Simone Frey, Dr. Dagmar Waltemath, Dr. Johannes Wollbold, Dr. Katja Rateitschak, Dr. Anuradha Chauhan, Dr. Thomas Millat, Dr. Mukhtar Ullah, Dr. Jiri Jablonsky, Ulf Schmitz, Ulf Liebal, Angelyn Lao, Peggy Sterling, Virginia Knaack, Stefan Pauleweit, Sonja Boldt, Felix Winter, Florian Wendland, Faiz Muhammad Khan, Sherry Freiesleben, Kann Vearasilp, Yvonne Schmitz, Tobias Breidenmoser, Falko Lange, Christina Kossow, Ron Henkel, Sylvia Haus, Peter Raasch, Arne Bittig, Dinto Jose, Andreas Frost and Rebekka Alm. During my four year research at SBI, I have received a lot of support and help from you, and I will never forget the joyful time when we worked together.

With a great pleasure I want to thank my collaborators. Prof. Bernd Schmeck, Dr. Alexandra Sittka and Christine Schulz provided pleasant arrangements and accommodations for my every visit. Every discussion with them is a great experience for me, because they not only broaden my knowledge about lung inflammation and vision in science but also inspire me morally. Prof. Svetoslav Nikolov and Dr. Shailendra Gupta

share their great knowledge about modelling nonlinear dynamics and bioinformatics analyses with me. Prof. Manfred Kunz and Animesh Bhattacharya carried out the experiments to verify the model-driven hypotheses about miRNA cooperativity.

I give thanks to my big family for their great love and support. I would like to show my gratitude to my parents. My father (Lai, Anping) brought me up and sent me to study in Germany, without him I would never have achieved what I have made until today. Although my mother (Chen, Chaogui) passed away when I was nine years old, but her spiritual support will be with me forever and encourage me to make greater achievements in the future. My step mother (Han, Defen) and parents in law (Luo, bing and Wu, hui) also give me big support and care for my life.

Finally, I would like to thank my wife (Luo, Wenlan) for her support and understanding for the academic career.

Abbreviations

Biological terms and abbreviations

14-3-3σ	A protein belongs to the 14-3-3 protein family
5-FU	5-Fluorouracil, a genotoxic stress-inducing agent
Ago	Argonaute protein
CCR4-NOT	The carbon catabolite repressor protein 4-Negative on TATA complex which can catalyses the deadenylation of mRNAs
CDK	Cyclin-dependent kinase, a family of protein kinases which can regulate cell cycle
DBC1	Deleted in breast cancer 1, a protein can inhibit the deacetylation of p53 by sirtuin 1
DCP	mRNA-decapping enzyme
Deacetylation	A chemical process that describes the removal of an acetyl group from a chemical compound
Deadenylation	The process of the removal of the poly(A) tail from the mRNA 3' end
DGCR8	A microprocessor complex subunit encoded by DiGeorge syndrome critical region gene 8
Dicer	An endoribonuclease in the RNase III family
DNA	Deoxyribonucleic acid
DND1	A protein named as dead end 1
Drosha	A Class 2 RNase III enzyme
eIF4E	Eukaryotic translation initiation factor 4E
E2F	A family of transcriptional factors contains eight members
Epo	Erythropoietin, a hormone that induces red blood cell production
EpoR	Erythropoietin receptor
ErbB	A protein family contains four members ErbB-1, -2, -3 and -4 that can be activated by growth factor ligands
EZH2	An enzyme named as Histone-lysine N-methyltransferase 2
FMRP	Fragile X mental retardation protein
GW182	Glycine-tryptophan protein of 182 kDa
HCT116	Human colorectal carcinoma cells
HOXD10	Homeobox D10 protein
HuR	A protein named as human antigen R

IRES	Virus internal ribosome entry site
JAK2	Janus kinase 2
m⁷G	5'-terminal 7-methylguanosine cap
Mdm2	The murine double minute protein that negatively regulates p53
miRISC	miRNA-induced silencing complex
miRNA	MicroRNA
miR-17-92 cluster	A set of six miRNAs transcribed from physically adjacent miRNA genes
mRNA	Messenger RNA
Myc	A transcriptional factor
ORF	Open reading frame
p21	Cyclin-dependent kinase inhibitor 1
p53	Tumour protein 53
PABP	Poly(A)-binding protein
P-bodies	Processing bodies, which are cytoplasmic foci enriched for proteins that are involved in RNA degradation
Pol II	RNA polymerase II
PUF	Pumilio-Fem-3-binding factor proteins
Ran-GTP	Guanosine triphosphate binding protein Ran
Ras	A protein named as rat sarcoma
RBP	RNA-binding protein
RNase III	A kind of enzymes specifically bind to and cleave double-stranded RNA
RNA	Ribonucleic acid
SIRT1	Sirtuin 1, an enzyme that can deacetylate p53
Sk-Mel-147	Melanoma cell lines with wild type p53
STAT5	Signal transducer and activator of transcription 5
TF	Transcriptional factor
TRBP	The human immunodeficiency virus transactivating response RNA-binding protein
UTR	Untranslated regions in mRNA sequences

Key mathematical terms and abbreviations

ODE	Ordinary differential equation which is formulated to describe the time evolution of a biochemical system
Deterministic model	A class of mathematical models which is used to describe the time evolution of a biochemical system in a way that the model always perform the same output for a given set of parameter values
Stochastic model	A class of mathematical models which is used to describe the time evolution of a biochemical system in a way that takes account of random variations in model variables
Mass action kinetics	Mass action kinetics defines chemical reaction rates as a product of a rate constant and the concentrations of the reactants
Model variables	In biochemical systems variables change their values over time and they are typically the concentrations of molecular species
Model parameters	Kinetic rate constants and initial concentrations that have fixed values
Initial concentrations	Concentrations of model variables at the start of the reaction
Michealis-Menten kinetics	A simplification of mass action kinetics typically used for enzyme–substrate interactions when the concentration of the substrate is in excess of the enzyme, and is also used to describe saturation kinetics
Quasi-steady state	A condition in which a product or reactant is nearly constant in concentration over a limited time scale
Hill equation	An equation that describes the extent of cooperative binding of multiple proteins, and is also used to describe sigmoid steepness
Power-law	An alternative formalism for modelling biochemical reactions
Parameter estimation	The regression process by which parameters are characterised by comparing model simulations with experimental data
Cost function	An expression quantifying the deviation between a simulation and experimental data for a given set of parameter values
Parameter identifiability	The process by which parameter uncertainties are evaluated, A parameter is identifiable if its value can be determined by estimation
Model simulation	The process of studying the responses and properties of a biochemical system under differing conditions by configuring the model with different parameter values or using different model structures
Sensitivity analysis	Determining the change in model variables associated with changes in parameter values
Bifurcation analysis	An analysis that shows how the qualitative behaviour of a model changes as a function of critical model parameters

Bistability

Bistability means that a dynamical system has two stable steady states for a certain set of parameters

Model validation

The process of evaluating the ability of a calibrated model to reproduce the dynamics of the experimental data which are not used for parameter estimation

Chapter 1

Introduction

1.1 Systems biology

Systems biology is an emerging research field, which aims at understanding of the dynamics interactions between components of a living system (Kitano, 2002a and 2002b). Systems biology focuses on studying complex biological systems as networks of interconnected components rather than their individual properties, and it covers a broad range of areas from modelling cellular signalling pathways to the development of novel therapeutic strategies. For example, data-driven multiscale models have been developed to understand the mechanisms of how altered signalling pathways induced by mutations in ErbB-1 leads to the onset of oncogenic transformations (Liu *et al.*, 2007; Purvis *et al.*, 2008). Based on model-based computational analyses a drug for cancer treatment by targeting ErbB-3 has been developed (Schoeberl *et al.*, 2009).

With the development of new experimental techniques, large amounts of quantitative experimental data are being generated. However, with the ever increasing flood of information simply collecting and classifying cellular components (e.g. genes, RNAs and proteins) and their molecular properties prevent us from improving our understanding of how they interact to bring about cellular structure and functions (Wolkenhauer *et al.*, 2005). Thus, it is becoming increasingly evident that certain aspects of biology can only be understood at the system-level (Kitano, 2002a). The systems biology approach, integrating experiments in interactive cycles with computational modelling, simulation and theory, provides us with a promising way to address biological questions (Pastori *et al.*, 2008).

To investigate a biological system, a cyclic process including four key steps is needed (Figure 1.1). (I) **Biological network construction**: for the system under investigation, a biological network can be constructed by establishing the interactions among molecular entities (such as genes, proteins and metabolites) from experimental

evidence, which can be obtained from published literature and databases. (II) **Model construction**: depending on the biological problem and available experimental data, the biological network together with hypotheses can be translated into a particular mathematical model, which can be constructed using a particular modelling framework (e.g. deterministic or stochastic models). Model parameter values can be characterised using biological information from the literature, databases and/or estimated from experimental data using optimisation methods. (III) **Computational analysis and simulation**: after the determination of model structure and the characterisation of model parameter values, analytical tools (e.g. sensitivity and bifurcation analysis) and model simulations help us to unravel and study complex properties and behaviour of the biological system. (IV) **Experimental validation**: in this step model predictions together with biological explanations are integrated to guide and design new experiments, which in turn validate or falsify the model. If the model predictions are in line with the experiments, the model justifies biological hypotheses behind the model, and these hypotheses, which provide reasonable explanations for biological phenomenon, lead to a novel understanding of the biological system. Otherwise, the model has to be modified accordingly until it is validated.

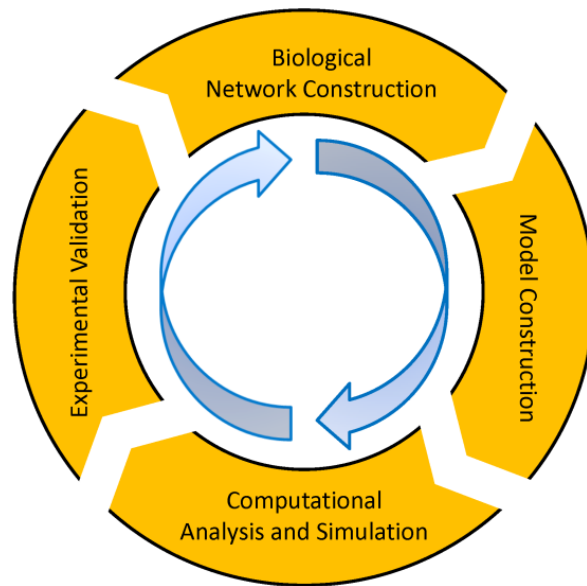


Figure 1.1: Scheme of the systems biology approach. Biological systems are investigated in an iterative systematic approach. With the help of advanced experimental techniques and computational methods, the approach provides a systemic and comprehensive way to study complex biological systems (Kitano, 2002a).

The subject of systems biology encompasses biological systems, the characteristics of which can be quantitatively measured, and for which mathematical models can be constructed to study their behaviour (Demin and Goryanin, 2009). Biological systems are composed by intricate interconnections among components within cells. These interconnections, which can be described by biochemical reactions and biophysical interactions, are the foundation of biological networks such as cellular signalling pathways and gene regulatory networks. Signalling pathways are important for cellular communication where the cell receives (and responds to) external stimuli from other cells and from the environment (Gomperts *et al.*, 2009); gene regulation controls the expression of genes and, consequently, all cellular functions (Machado *et al.*, 2011). As a result, complexity of biological networks emerges, and thus the systems biology approach is needed to unravel the kinetic mechanisms underlying biological systems.

Despite the fact that systems biology is still in its infancy, many studies have proved its success in basic (understanding complex mechanisms) and applied (e.g. prediction of drug targets) biological problems. Through the continuous collaboration between experimental and computational research, hybrid modelling linking the molecular scale to the cellular scale provides quantitative insights into the connections between phenotype and tumour morphology (Sanga *et al.*, 2007). Analysing cancer network motifs such as feedback loops in a systematic manner has increased our understanding of their mechanistic and practical implications in cancer (Cloutier and Wang, 2011). Schoeberl *et al.* (2009) constructed a kinetic model of the cancer-related signalling pathway induced by ErbB and analysis of the model has made valuable contributions to find effective prediction of novel and non-intuitive cancer therapeutic drug targets. Systemic analysis of biological problems provides an efficient way to understand complex mechanisms that are difficult to be dissected by purely experimental methods, and to generate hypotheses that push forward our comprehension of complicated interactions and their functionality (Hübner *et al.*, 2011). Although systems biology is still far from its ultimate goal, which is to provide insights into the processes of organelles, cells, organs and even whole organisms, its potential benefits are considerable in both basic and applied research. In the near future, as systems biology matures, it will revolutionise our understanding of biology and medicine.

In this thesis, I adopt a systems biology approach, whose framework is briefly described in Figure 1.1, to study two aspects of miRNA functions: the regulatory role of an individual miRNA in a cancer-specific signalling pathway and the regulation of a cancer-related gene by multiple and cooperative miRNAs.

1.2 MicroRNAs

miRNAs are a class of small endogenous non-coding RNAs with a length of around 22 nucleotides (nt). miRNAs are evolutionarily conserved regulatory molecules that, in most cases, modulate the stability and/or translation of target mRNAs through direct binding to the 3' UTR of their target mRNAs (Bartel, 2004). Recently, over 1000 miRNA sequences have been identified in the human genome and have been registered in the miRbase database (Kozomara and Griffiths-Jones, 2011). The identified miRNAs are estimated to regulate more than 30% of all protein-coding genes (Friedman *et al.*, 2009). This indicates their pervasive roles in the regulation of cellular processes, like proliferation, differentiation and apoptosis. In addition to exerting critical functions during normal development and cellular homeostasis, miRNA dysregulation has been found in many human diseases, like cancer (Hwang and Mendell, 2006). Thus, understanding the function of miRNAs in gene regulation is crucial for assisting us to unravel the mechanisms underlying human pathogenesis and to improve therapeutic approaches in human diseases. In this section, I give a comprehensive introduction to the biological background of miRNAs, ranging from their basic functions to their relations with human diseases. This knowledge is important and indispensable, and it is the basis of the research presented in this thesis.

1.2.1 MicroRNA biogenesis and function

The miRNA biogenesis pathway is a complex process (Berezikov, 2011; Filipowicz *et al.*, 2008; Kim, 2005; Krol *et al.*, 2010). The process is composed of multiple steps (Figure 1.2). At first, long primary transcripts known as pri-miRNAs are transcribed from miRNA genes by RNA polymerase II (Pol II). The composition of pri-miRNAs begins with a 5'-terminal 7-methylguanosine (m⁷G) cap, which is extended by a hairpin structure with a terminal loop and a ~32 nt long imperfectly base-paired stem, and ends

with a 3' poly(A) tail. Depending on the features of miRNA genes, pri-miRNAs can contain single (solo) or multiple (clustered) miRNA sequences that appear in pairs to form a hairpin structure. Next, with the help of the complex, which includes Drosha and its binding partner DGCR8, pri-miRNAs are processed into precursor miRNAs (pre-miRNAs) of ~70 nt hairpin structures with a characteristic 2 nt 3' overhang. Then, through the recognition of the 2 nt overhang, exportin 5 in conjunction with the cofactor Ran-GTP exports pre-miRNAs from the nucleus into the cytoplasm. After that, cytoplasmic processing by another complex, which is composed of Dicer, an Argonaute protein (Ago) and a TAR RNA binding protein (TRBP), cleaves a pre-miRNA into a ~22 nt double-stranded miRNA duplex (also known as mature miRNAs). Finally, one strand of the miRNA duplex known as the active strand is loaded into an Ago-containing miRNA-induced silencing complex (miRISC) which will further target mRNAs for subsequent cleavage or translation repression. The complementary strand known as the passenger strand will be degraded.

Except for the canonical miRNA biogenesis pathway described above, mature and functional miRNAs can also be produced in other alternative pathways. These pathways can be classified into Drosha- and Dicer-independent pathways (Figure 1.2; Miyoshi *et al.*, 2010). In the Drosha-independent pathway a class of miRNA genes, which originates from pre-miRNA-sized short introns (termed as mirtrons), can be directly processed into pre-miRNA hairpins without the participation of Drosha. These pre-miRNAs are further cleaved by Dicer in the cytoplasm to produce mature miRNAs (Ruby *et al.*, 2007). In the Dicer-independent pathway, although the process in the nucleus proceeds normally, the step in which a pre-miRNA is diced into a miRNA duplex by Dicer is skipped, for example, miR-415 is produced through an Ago-dependent pathway for maturation (Miyoshi *et al.*, 2010).

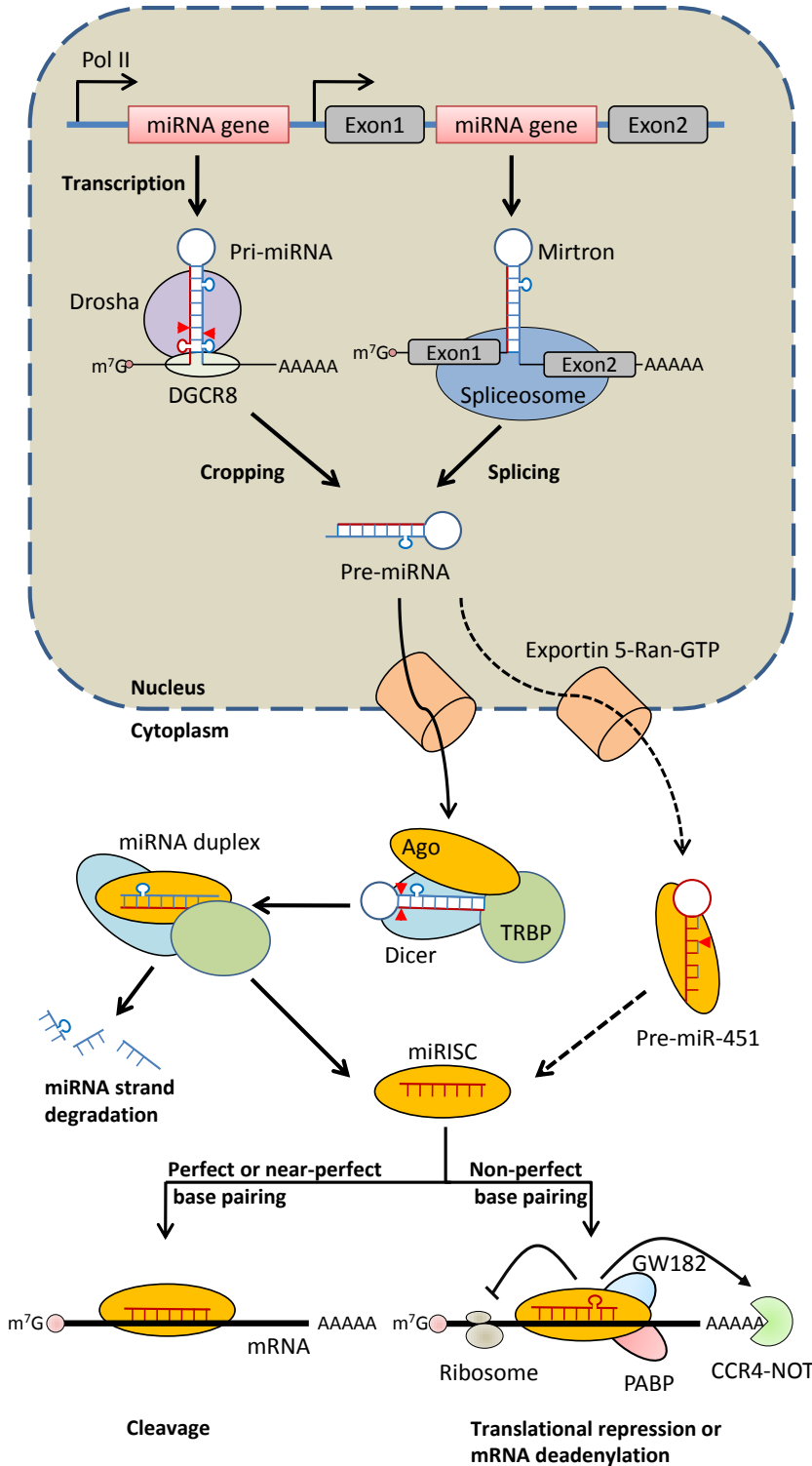


Figure 1.2: miRNA biogenesis pathways.

A miRNA can be processed either from a pri-miRNA or a mirtron. The pri-miRNA, containing a 5' terminal m⁷G cap and a 3' poly(A) tail (AAAAA), is transcribed from miRNA genes by Pol II and is subsequently cropped (red arrowheads) by Drosha with the cofactor DGCR8 and becomes a pre-miRNA. The mirtron situated between two exons is spliced and becomes a pre-miRNA without the requirement of Drosha-DGCR8 complex. The pre-miRNA is transported from the nucleus to the cytoplasm by exportin 5 with Ran-GTP. In the cytoplasm, most pre-miRNAs are processed into double-stranded miRNA duplexes with the help of Dicer and TRBP. One strand of the duplexes is loaded into the Ago containing miRISCs, whereas the other strand is degraded. When a miRNA is perfectly or near-perfectly pairing to its target mRNA, it can result in the cleavage of the mRNA. Otherwise, non-perfect base pairing between a miRNA and its target mRNA leads to translation repression or target mRNA deadenylation. Both processes are implemented through the interaction of miRISCs with GW182 and PABP. It is important to note that although most miRNAs are generated through a Dicer-dependent pathway, there also exist some exceptions. For example, pre-miR-451 is processed by Ago in a Dicer-independent pathway. Nevertheless, miR-451 exerts the same repressive function like other miRNAs. The figure is modified from Krol *et al.* (2010).

After the maturation of miRNAs, in most cases the active strands act as guides and direct miRISCs to bind to the 3' UTR of target mRNAs, resulting in the repression of the target genes at the post-transcriptional level (Figure 1.2). Some miRNAs are able to exert repressive function on target genes when their binding sites are placed in the 5' UTR or the coding regions of target mRNAs (Lytle *et al.*, 2007). In addition, a few miRNAs can bind to the 5' UTR of its target mRNA and activate gene expression (Ørom *et al.*, 2008). The mechanism by which target mRNAs are regulated is determined by the degree of complementarity between miRNAs and their target mRNAs. When a miRNA perfectly or near-perfectly pairs with its target mRNA, mostly occurring in plants, the target mRNA cleavage is triggered. Imperfect base pairing between a miRNA and its target, predominating in animals, leads to translation repression or destabilization of the target mRNA (Bartel, 2004). Based on experimental and bioinformatics analyses, in animals several miRNA binding motifs have been identified such as 8-mer, 7-mer and 6-mer (Bartel, 2009). These miRNA binding motifs are defined by the number of continuous base pairings in the seed region of miRNAs; for example, 7-mer means that in the seed region of a miRNA there are continuous 7 base pairings between the miRNA and its target mRNA (Bartel, 2009). The repressive efficacies of these binding motifs identified in animals are determined by the content of regional base pairing between the miRNA and its target, which follows a set of rules (Figure 1.3; Filipowicz *et al.*, 2008):

- The seed region (miRNA nucleotides from position 2 to 8) base pairing between a miRNA and its target mRNA. A continuous seed region base pairing is crucial for assuring target repression, if there are G-U pairs (guanine-uracil) or mismatches in this region, the target repression will be greatly affected. However, the appearance of an A (adenine) at position 1 of the miRNA and an A or U appearing at position 9 can improve the repressive efficiency, although they are not required to base pair with the target mRNA.
- The central region (miRNA nucleotides from position 10 to 12) of the miRNA-mRNA duplex. In this region, bulges or mismatches must be present.

- The complementary region (miRNA nucleotides from position 13 to the last one). The base pairing between the miRNA and its target mRNA is typically quite loose in this region. Thus, good complementarity, particularly for miRNA nucleotides from position 13 to 16, becomes important when mismatches or bulges appear in the seed region.

In addition to the binding motifs, other factors can also affect miRNA repression efficacy. For example, multiple miRNA binding sites in close proximity on the 3' UTR of a single mRNA can enhance the repression of the target (Doench and Sharp, 2004; Saetrom *et al.*, 2007); RNA-binding proteins (RBPs), which can interact with miRISCs on the 3' UTR of target mRNAs, can either facilitate or counteract miRNA-mediated repression (Krol *et al.*, 2010).

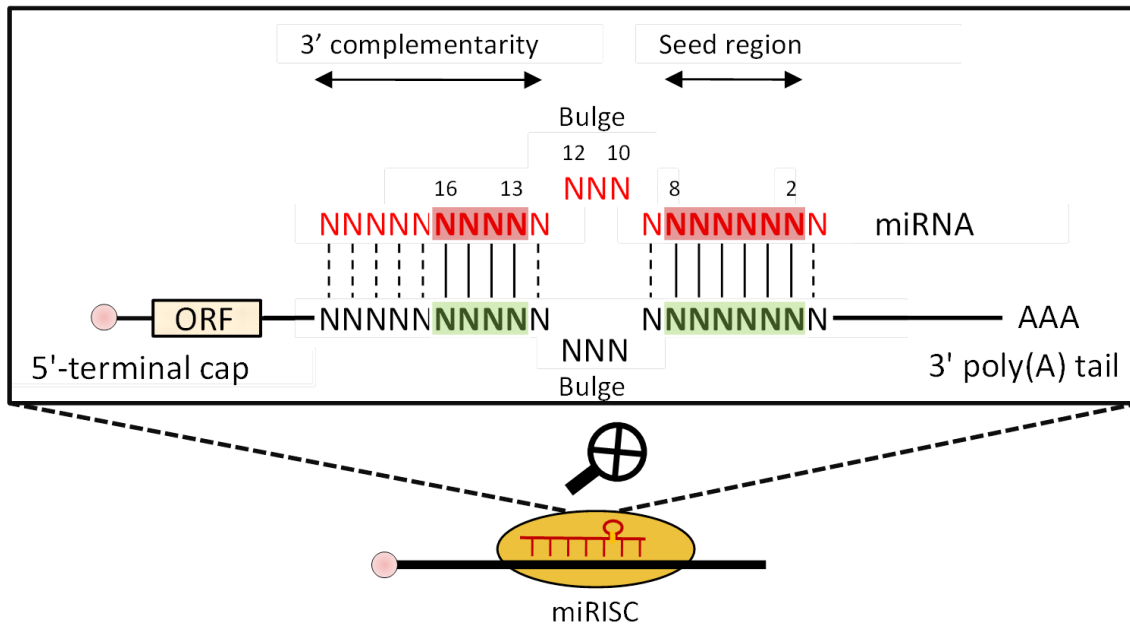


Figure 1.3: Base pairing principles between miRNAs and their target mRNAs in animals. In the seed region, continuous Watson-Crick pairing (vertical solid lines) is crucial for determining the efficacy of miRNA-mediated repression. When a mismatch (vertical dashed lines) or a bulge appears in the seed region, Watson-Crick pairing centring on miRNA nucleotides 13-16 of the 3' complementarity region can compensate and thereby construct a functional miRNA binding site. The figure is modified from Filipowicz *et al.* (2008).

In mammalian cells most of the binding motifs between miRNAs and target mRNAs are non-perfect base pairing, which can result in two main mechanisms by which miRNAs reduce protein production. The two mechanisms are translation repression and destabilisation of the target mRNAs. More particularly, miRNAs can inhibit translation of target mRNAs by affecting the initiation or post-initiation stage of mRNA translation (Fabian *et al.*, 2010). At the initiation stage, the miRISC can inhibit translation by interfering with eIF4E-cap recognition and 40S small ribosomal subunit recruitment or by antagonizing 60S subunit joining and preventing 80S ribosomal complex formation (Figure 1.4a). At the post-initiation stage, the miRISC can inhibit translation by inhibiting ribosome elongation, inducing ribosome drop-off, or facilitating proteolysis of the nascent polypeptides (Figure 1.4b). For miRNA-mediated mRNA degradation, with the participation of GW182 and PABP the miRISC facilitates deadenylation of the poly (A) tail by interacting with the CCR4-NOT deadenylase complex. Then, the 5' terminal m⁷G cap is removed by the decapping DCP1-DCP2 complex, resulting in the degradation of the target mRNA (Figure 1.4c).

1.2.2 MicroRNAs and human diseases

Although miRNAs are physically small, they play a major role in regulating numerous cellular processes including proliferation, differentiation and apoptosis (Bartel, 2004). Thus, aberrantly expressed miRNAs are associated with a wide variety of human diseases such as cancer, cardiovascular disorders and inflammatory lung diseases (Shenouda and Alahari, 2009; Ono *et al.*, 2011; Oglesby *et al.*, 2010). In addition, due to the vast and important miRNA-mediated post-transcriptional regulation of gene expression, miRNAs are gradually becoming potential therapeutic targets for treating human diseases.

Recently, *in vitro* and *in vivo* studies have shown that abnormal expression of specific miRNAs can lead to different cardiovascular disorders like cardiac fibrosis and arrhythmia. For example, several individual studies have demonstrated that the upregulation of miR-21 expression during cardiac fibrosis contributes to cardiac dysfunction in diverse pathological conditions (Ono *et al.*, 2011). Furthermore, a firm link between inflammatory lung diseases and unique miRNA expression profiles has been

established. Aberrantly expressed miRNAs can lead to several inflammatory lung diseases, like cystic fibrosis, chronic obstructive pulmonary disease, asthma and idiopathic pulmonary fibrosis (Ha, 2011). For instance, miR-155 is an important regulator involved in the Toll-like receptor signalling pathways, which are often underlying lung inflammatory responses. An *in vivo* mice study has shown that loss of miR-155 can lead to immunodeficiency and increased lung airway remodelling (Oglesby *et al.*, 2010). Moreover, aberrant miRNA expression profiles impinge upon the normal regulation of cellular processes, and thus dysregulated miRNA expression has key functions in tumourigenesis. Depending on targets, miRNAs can act as oncogenes or tumour suppressors. As an example, after induction through twist-related protein miR-10b shows oncogenic property by targeting HOXD10. The repression of HOXD10 by miR-10b results in increased cell migration and invasion (Shenouda and Alahari, 2009). In contrast, miR-101, whose expression is downregulated in prostate and breast cancer, has been demonstrated to be a tumour suppressor by repressing EZH2, an enzyme that can promote oncogenic and metastatic activity (Shenouda and Alahari, 2009).

With a growing number of miRNAs being associated with the development of human cancers, using them as therapeutic targets provides new hope for treating different cancers (Kasinski and Slack, 2011). miR-21 has been reported to be one of the most prominent miRNAs involved in the biogenesis and progression of human cancers such as breast and liver cancer. Repression of miR-21 expression can lead to decreased tumour cell proliferation, migration and invasion. This suggests miR-21 knockdown as a novel therapeutic approach for the treatment of human cancers (Feng *et al.*, 2010). Among several miRNAs, the expression of miR-26 has been identified to be most downregulated in Myc-induced hepatocellular carcinoma, and therefore restoration of miR-26 expression using a virus vector suggests a miRNA-based therapy for liver cancer (Rossi, 2009). Downregulation of some tissue-specific miRNAs (e.g. miR-1 and miR-206 in muscle cells or miR-124 in brain cells) have been reported to favour the formation of tumour cells in different tissues. Thus, re-expression of these miRNAs in cancerous cells could be used to treat cancer (Mishra and Merlino, 2009).

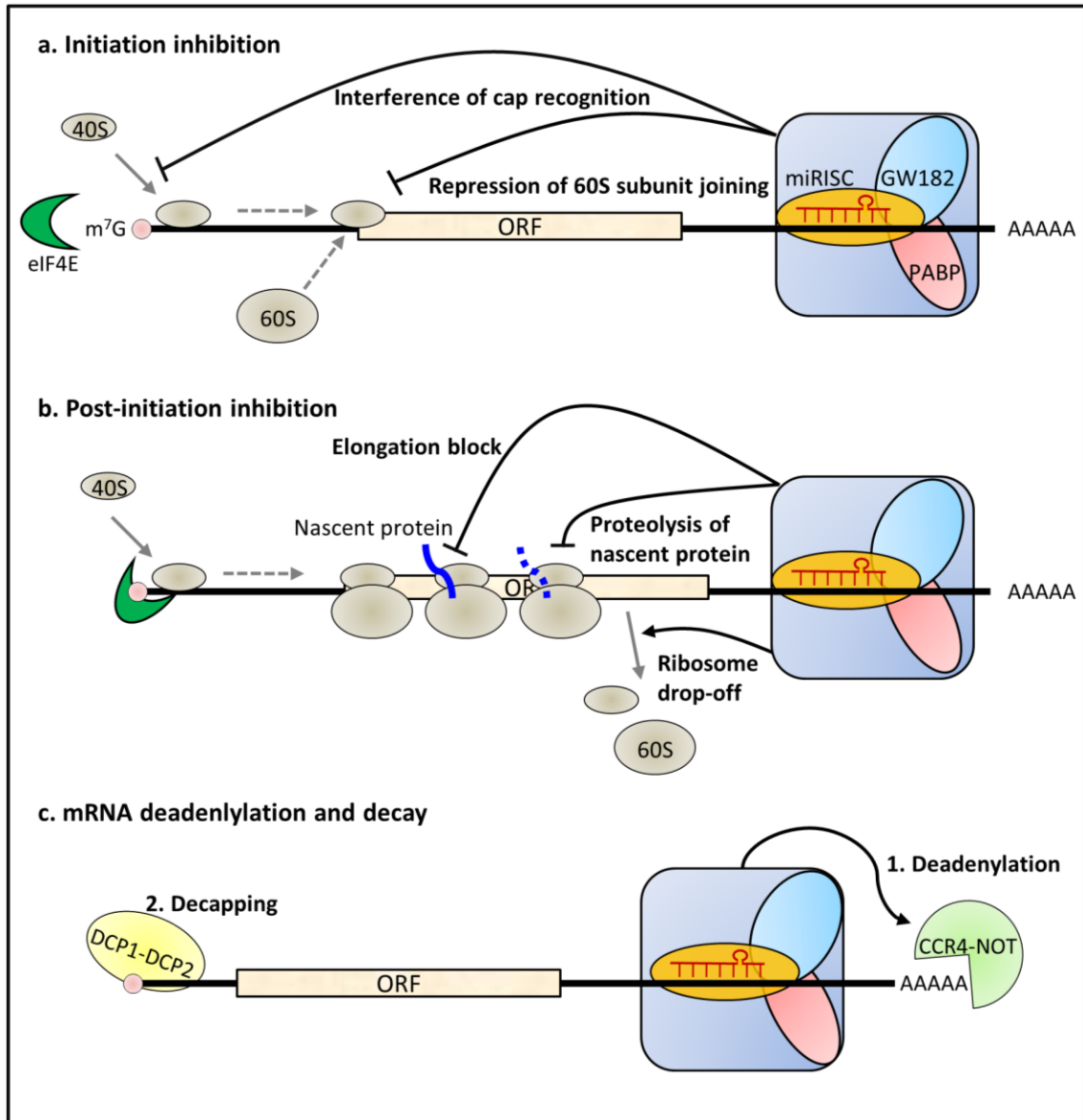


Figure 1.4: miRNA-mediated translation repression mechanisms. With the help of GW182 and PABP, miRISCs can repress translation at the initiation and post-initiation stage, or induce the deadenylation and decay of target mRNAs. **(a)** At the initial stage, binding of the miRISC complexed with GW182 and PABP to the target mRNA can repress translation by either interfering with the cap recognition or by repressing the 60S subunit joining. **(b)** The miRISC can inhibit translation at the post-initiation step by blocking translation elongation, causing ribosome drop-off or proteolytic cleavage of the nascent polypeptides. **(c)** Deadenylation of the target mRNA is facilitated by the interaction of the miRISC with CCR4-NOT. Subsequently, the decay of the target mRNA happens after the remove of 5'-terminal m⁷G cap by the decapping DCP1-DCP2 complex. The figure is reproduced from Fabian *et al.* (2008).

1.3 Using a systems biology approach to study microRNA-mediated regulation

Due to the fast development of systems biology, data-driven models have been widely applied in the studies of miRNA-mediated regulation. In this section, the most relevant publications using such an approach to investigate the regulatory roles of miRNAs in different biological contexts are reviewed and discussed, and the findings concerning the underlying principles on miRNA target regulation are highlighted.

1.3.1 MicroRNA regulation of gene expression

To investigate the mechanism by which gene expression is regulated by miRNAs, the mathematical models concerning miRNA-mediated gene regulation were developed. Levine *et al.* (2007) set up a quantitative model to show how local and global properties of the gene repression mechanism mediated by miRNAs can affect the mRNA and protein levels of target genes. Through analysing the model, the authors suggested that the number of miRNA binding sites on target mRNAs (local property) can result in different repressive effects on the targets. On the other hand, under different cellular conditions (global property) the same miRNA-target pairing can exhibit different behaviours. Whichard *et al.* (2011) constructed a mechanistic model that accounts for miRNA-mRNA complex formation and subsequent transcript sequestration or degradation. By applying sensitivity analysis to the model steady state solution, the results indicated that miRNA synthesis commonly acts to fine-tune target protein concentrations; however, for a small subset of miRNA-mRNA pairs characterised by slowly produced miRNAs, the miRNA synthesis is the dominant control element. Vohradsky *et al.* (2010) developed a model based on a set of microarray data, which shows the temporal gene expression after the treatment with miR-124a mimics. The data-driven model revealed a novel mechanism by which miR-124a can organize its target mRNA response in a switch-like manner, i.e. the miRNA has an enormous influence on the mRNA decay and the influence drops to zero transiently.

In addition, to investigate the effects of miRNAs on target gene expression in single cells, Mukherji *et al.* (2011) adopted a two-colour fluorescent reporter system which allows them to measure the change of gene expression when miRNA binding sites are

present or absent within reporters. Through their single-cell analysis, two intriguing features were found: 1) although the average level of protein repression by miRNAs is modest, which is in agreement with previous population-based measurements, the repression among individual cells varies dramatically (the maximum difference can reach 40-fold); 2) regulation by miRNAs establishes a threshold level of the target mRNA, which determines the degree of the repression of protein production. Below the threshold the protein production is highly repressed, however, slightly above this threshold the protein expression responds sensitively to the target mRNA. This result is consistent with the model simulations, which described the effect of molecular titration on the sensitive response of transcription above a threshold. The model showed that with the increasing abundance of the mRNA targets, the availability of the miRNA for repression is diluted; the strength of the interaction between the miRNA and its target and their relative abundance decide the sharpness of the switch from full repression to escaping from miRNA repression.

In conclusion, the publications mentioned above focus on gene regulation by individual miRNAs. However, recent experiments suggest the possibility that the regulation of gene expression can be simultaneously mediated by multiple miRNAs (Doench and Sharp, 2004; Saetrom *et al.*, 2007). In this thesis, the chapter about the regulation of a target hub gene by multiple and cooperative miRNAs not only complements the research field of miRNA-mediated regulation of gene expression, but also provides guidance for studying other miRNA target hubs.

1.3.2 MicroRNA inhibition at translation initiation

mRNA translation consists of three steps: initiation, elongation and termination. To investigate how protein production is affected by possible miRNA-mediated inhibition at the translation initiation step, Nissan and Parker (2008) developed a mathematical model accounting for miRNA repression on a variety of target genes whose translation could be cap-dependent (the target mRNA contains a functional m⁷G cap or a non-functional ApppN cap structure) or cap-independent (the target mRNA contains a IRES). Through their analysis, they found that miRNAs are affecting a late stage in the translation initiation such as AUG recognition or 60S subunit entry. Furthermore, their results

suggested that different rate-limiting steps in the translation initiation can explain the divergent results in literature. For example, the mRNA containing IRES may be resistant to miRNA inhibition because the translation initiation is not a rate-limiting step for such mRNA. Moreover, they demonstrated that the effect of miRNAs on translation can not be observed if a miRNA is acting on a step which is not rate-limiting. In case of ApppN-capped mRNAs, if miRNAs affect a step downstream of the inefficient cap recognition process of these mRNAs, their effect could be masked since the upstream step is rate-limiting.

1.3.3 MicroRNA-mediated feedback and feedforward loops

miRNAs are important components embedded in gene regulatory networks and are found to establish different kinds of network motifs with their TFs and targets. The most common miRNA-mediated network motifs are feedback and feedforward loops. These loops can be further differentiated into subtypes. The feedback loops can be either positive or negative if a miRNA and its TF are positively or negatively coregulated by each other. The feedforward loops can either be coherent or incoherent, if a miRNA and its TF consistently or oppositely regulate their common target (Figure 1.5).

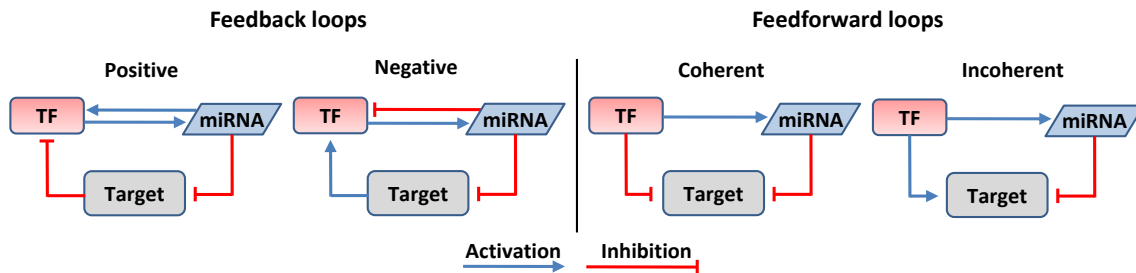


Figure 1.5: miRNA-mediated feedback and feedforward loops. **Left:** Feedback loops are classified into positive and negative loops. In positive loops, both the miRNA and the TF have the same overall effect on each other, and this effect can be direct or indirect. In negative loops, the overall effect of the miRNA and the TF on each other is opposite. **Right:** Feedforward loops are classified into coherent and incoherent loops. In coherent feedforward loops, the miRNA and the TF have the same effect on their common target. In incoherent feedforward loops, the miRNA and the TF have opposite effect on their common target.

In order to detect miRNA-mediated motifs contained in gene regulatory networks, analysing large-scale biological data using network biology tools is a powerful and popular approach. By using this approach, Tsang *et al.* (2007) detected that the miRNA-mediated motifs are conserved among different species. Particularly, the coherent feedforward and negative feedback loops mediated by miRNAs unregulated in neuronal cells were identified to be prevalent in mature neurons. The recurrences of these miRNA-mediated motifs suggest important biological functions of miRNAs in mammals, which are related to the robustness of gene regulation in mammalian genomes. Similarly, Re *et al.* (2009) identified a total of 638 putative miRNA-mediated feedforward loops in human gene regulatory networks and further filtered these feedforward loops using cancer relevant features. Their analyses showed that some miRNA-mediated feedforward loops are not only computationally identified but also experimentally verified to be involved in various aspects of organism development and differentiation, suggesting a crucial role of miRNA-mediated feedforward loops in gene regulatory networks. In addition, some researchers focused on searching for gene-specific network motifs containing miRNAs. For example, feedback and feedforward loops containing p53 and miRNAs were identified and studied by Sinha *et al.* (2008). The authors revealed the miRNA-mediated network motifs underlying p53 regulatory networks. This result suggested the important contribution of miRNAs regulating p53 signalling pathways, which are involved in tumour suppression. Martinez and Walhout (2009) compiled multiple experimentally verified feedback and feedforward loops, which are composed of miRNAs and their TFs. Their analysis showed that the existence of these miRNA-mediated network motifs reveals not only the reciprocal regulation by the miRNAs and the TFs but also their coordination in regulating shared target genes at the genome-scale level.

In addition to identifying the miRNA-mediated network motifs using computational methods, the employment of mathematical models focuses on unravelling the dynamic properties, which are thought to be essential for maintaining the operation of gene regulatory networks. Some *in silico* models showed that the existence of miRNA-mediated network motifs can lead to more effective noise buffering in gene expression. In support of this, Xu *et al.* (2009) studied miRNA-mediated network motifs by using

deterministic and stochastic models. The properties of the network motifs were further analysed for four types of external input signals: 1) the same signal acts on a miRNA and its target gene, 2) two different signals act on the miRNA and the target gene respectively, 3) the signal acts only on the target gene and 4) the signal acts only on the miRNA. Their numerical simulations indicated that for these signals the miRNA-mediated network motifs exhibit strong robustness to external stochastic perturbations in target gene expression. Similarly, Osella *et al.* (2011) investigated the role of miRNA-mediated feedforward loops in buffering noise in the target gene expression by using a mathematical model. They demonstrated that compared to the simple gene activation by a TF, the system containing miRNA-mediated repression shows a greater ability to dampen fluctuations in the target gene expression. Furthermore, mathematical modelling of miRNA-mediated network motifs embedded in specific networks revealed particularly intriguing properties of specific miRNAs. For example, Aguda and colleagues (2008) derived a mathematical model for a specific cancer network which includes feedback loops formed by Myc, the E2F protein family and the miR-17-92 cluster. By analysing the consequence of coupling the miRNA-mediated negative feedback loop with the E2F/Myc positive feedback loop, they showed the critical role of the miRNA cluster in shaping bistable behaviour in E2F/Myc protein levels and demonstrated the oncogenic and tumour suppression properties of the miRNA cluster. Moreover, the oscillatory behaviour of genes was mathematically proved to be affected by miRNAs. Xie *et al.* (2007) incorporated a miRNA into a gene regulatory network, in which the miRNA is involved in a negative feedback loop. They showed that the effect of the miRNA on mRNA stability can determine whether the expression of the corresponding gene oscillates or not.

In this thesis, I present a novel approach that combines miRNA and TF target prediction algorithms with experimental evidence to identify miRNA-mediated network motifs for p21. Compared to those purely predictive approaches, this approach provides more accurate and refined results. Furthermore, I construct a data-driven kinetic model to investigate the regulatory role of a feedback loop mediated by miR-34a in the p53/SIRT1 signalling pathway.

1.4 Objectives of this thesis

The involvement of miRNAs in gene regulatory networks and signalling pathways increase the complexity of biological systems. Thus, the systems biology approach, which combines mathematical modelling with experimental data, is required to address various roles played by miRNAs within cells. For advancing our understanding of the principles (mechanisms) by which miRNAs and other cellular molecules interact to realize their functions, I consider the following objectives:

- p53 is well known for its tumour suppression function and has been recently experimentally verified to upregulate the expression of miR-34a. In turn, miR-34a enhances the activation of p53 through repressing SIRT1. The involvement of miR-34a increases the complexity of the p53/SIRT1 signalling pathway composed by biochemical reactions. Thus, the objective is to investigate the regulatory role of miR-34 using a systems biology approach. To do so, a kinetic model of the p53/SIRT1 signalling pathway is constructed, and it is characterised and validated by quantitative experimental data. The model is further used to distinguish the different possible designs of the repression mechanism by which miR-34a represses SIRT1 and to generate experimentally verifiable predictions concerning the activation of p53 mediated by miR-34a.
- A miRNA target gene can be simultaneously repressed by multiple miRNAs, and such a gene is defined as a miRNA target hub. p21 is a miRNA target hub, which is experimentally verified to be targeted by more than 15 miRNAs. In addition to the repression of p21 by individual miRNAs, synergistic repression exerted by multiple targeting miRNAs is also experimentally proved to be possible. Therefore, the objective is to construct a kinetic model that can represent the comprehensive regulation of p21 by its targeting miRNAs. To do so, a novel approach is developed to construct the regulatory map of p21. The kinetic model, which is constructed based on the map, is further used to show the regulation of p21 by multiple and cooperative miRNAs for different biological scenarios.

1.5 Outline of this thesis

The remaining chapters of this thesis are structured as follows:

Chapter 2 presents the process of kinetic modelling using ordinary differential equations (ODEs), and this process includes model construction, model calibration, model validation and model analysis. I discuss the basic principles of the kinetic model construction using ODEs. In addition, various analytical tools used to study ODE-based models are introduced.

Chapter 3 shows the use of a systems biology approach for the analysis of the regulatory role of miR-34a in the p53/SIRT1 signalling pathway. First, the construction and validation of a kinetic model using quantitative experimental data are presented. Next, the discrimination of hypothetical mechanisms by which miR-34a represses SIRT1 is demonstrated with the help of the model. Finally, the investigation of the ability of miR-34a to compensate the loss of active p53 is shown.

Chapter 4 focuses on studying the mechanism by which a miRNA target hub is repressed by multiple miRNAs. A novel approach, combining target prediction algorithms with experimental data to generate a regulatory map for the miRNA target hub p21, is presented. This is followed by the utilisation of a kinetic model to show the regulation of p21 by its targeting miRNAs, which can function independently and cooperatively.

Chapter 5 concludes this work by discussing the main results.

Chapter 2

In Silico Modelling Using ODEs

A major challenge in systems biology is to choose an appropriate modelling approach for studying the dynamics of biological systems. This chapter focuses on the ODE approach, which is most frequently used to study the dynamics of biochemical systems over time. Systematically studying a biochemical system using the ODE approach requires four steps: model construction, model calibration, model validation and model analysis. Therefore, I first introduce the common kinetic laws used in ODEs, which ensure the accurate translation from biochemical reactions into mathematical representations. Next, characterisation of model parameter values using mathematical optimisation methods and identification of estimated parameter values are presented. Then, I show the process of model validation and introduce a series of analytical tools used for detecting the properties of dynamical systems. Finally, I briefly summarise some of my published research works, where the ODE modelling approach was used to study different biochemical systems.

2.1 Model construction

Biochemical systems are composed of biochemical reaction processes, in which substrates are converted into specific products through single or multiple steps within cells. ODEs can describe the temporal concentration profile of biochemical systems, which is affected by production, consumption and degradation of biochemical species (e.g. proteins, RNAs and metabolites). An ODE model can be constructed using appropriate kinetic laws such as the law of mass-action, which states that the rate of a chemical reaction is proportional to the probability that the reacting species collide. This collision probability is in turn proportional to the concentration of the reactants (Voit, 2000). The general representation of ODE-based models using mass-action kinetics can be determined by the following equation (Crampin *et al.*, 2004)

$$\frac{dx_i}{dt} = \sum_{\mu=1}^m c_{i\mu} \cdot k_{\mu} \cdot \prod_{j=1}^n x_j^{g_{\mu j}} \quad i \in \{1, 2, \dots, n\}, \quad (2.1)$$

where x_i represents the molar concentration of the i^{th} biochemical specie. Every biochemical reaction μ is described as a product of a rate constant (k_{μ}) and biochemical species ($x_j, j \in \{1, 2, \dots, n\}$) that are involved in the reaction. $c_{i\mu}$, the so-called stoichiometric coefficients, relates the number of reactant molecules consumed to the number of product molecules generated in the reaction μ . $g_{\mu j}$ denotes kinetic orders which are equal to the number of species of x_i involved in the biochemical reaction μ .

To illustrate how biochemical systems can be formulated in ODEs, I construct a model accounting for several basic processes within cells. These processes include gene expression, molecule degradation and protein phosphorylation (Figure 2.1). The model is used to explain the principles underlying the construction of ODE-based models. The process of gene expression is composed of two steps: the transcription of a gene into mRNA and the translation of the mRNA into a protein. By applying mass-action kinetics, I obtain the following equations

$$\frac{dM}{dt} = k_{syn}^{mRNA} - k_{deg}^{mRNA} \cdot M, \quad (2.2)$$

$$\frac{dP}{dt} = k_{syn}^{protein} \cdot M - k_{deg}^{protein} \cdot P, \quad (2.3)$$

where the rate constants k_{syn}^{mRNA} and $k_{syn}^{protein}$ represent the synthesis of mRNA (M) and the translation of a protein (P), respectively. The rate constants k_{deg}^{mRNA} and $k_{deg}^{protein}$ stand for the degradations of the mRNA and the protein. The production of the protein is termed by a product of the kinetic constant and the mRNA, which means that its production is proportional to the concentration of the mRNA. However, for the simplicity the production of the mRNA is only termed by a rate constant, meaning that the transcription of the gene into the mRNA is not affected by other molecules. The degradations of the mRNA and the protein are proportional to their concentrations. In this established ODE model, P and M are defined as model state variables, which describe the dynamics of the concentrations of the protein and the mRNA over time (t); the rate constants and the initial concentrations (i.e. concentrations at $t = 0$) of the protein ($P(0)$) and the mRNA ($M(0)$) are model parameters.

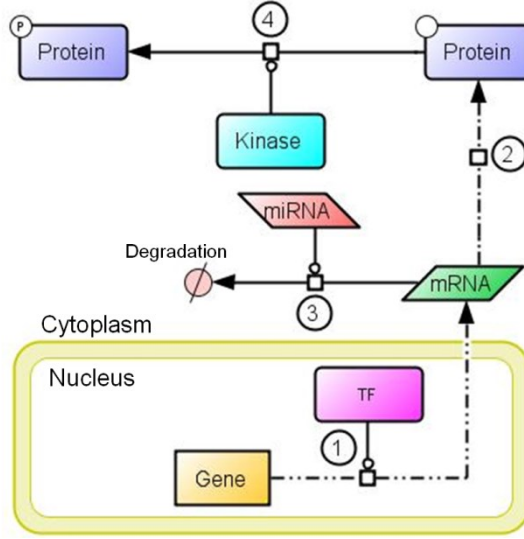


Figure 2.1: Scheme of the gene expression process. In the model, the basic biological processes considered are: gene transcription mediated by TFs (①), mRNA translation (②), miRNA-mediated degradation of mRNA (③) and protein phosphorylation (④). Each process is used as a separate example to explain the most common kinetic laws used in ODE-based models. The scheme is drawn using CellDesigner, which is a structured diagram editor for constructing biochemical schemes (Funahashi *et al.*, 2008).

Besides mass-action kinetics, other kinetic rate laws such as Michaelis-Menten kinetics and the Hill equation are also frequently used in ODE models. Michaelis-Menten kinetics is often used as an approximation of mass-action kinetics to model enzyme catalysed reactions such as protein phosphorylation. Michaelis-Menten kinetics not only simplifies the model in mass-action kinetics but also can be used to generate saturation kinetics of enzymatic equations (Aldridge *et al.*, 2006). For example, the protein (P) described above can further form a temporary complex (C) with a kinase (E), which is a type of enzyme and can facilitate the protein phosphorylation process to produce phosphoprotein (P^* ; Figure 2.1). If the kinase is not consumed and degraded during this process ($E_{total} = C + E$) and is in much lower initial concentration compared to the initial concentration of the protein ($P(0) \gg E(0)$), the quasi-steady-state approximation which assumes rapid equilibrium of the intermediate complex ($\frac{dC}{dt} \approx 0$) can be applied in the original ODEs. After the approximation, the model is simplified resulting in the Michaelis-Menten equation. The biochemical reactions are shown below and the simplification of the original ODEs using Michaelis-Menten kinetics are formulated in Equation (2.4) and (2.5).

Biochemical reactions	
$P + E \rightleftharpoons C \rightarrow P^* + E$	
Mass-action kinetics	
$\frac{dM}{dt} = k_{syn}^{mRNA} - k_{deg}^{mRNA} \cdot M$	
$\frac{dP}{dt} = k_{syn}^{protein} \cdot M - k_{deg}^{protein} \cdot P + k_{dis}^{complex} \cdot C - k_{ass}^{complex} \cdot P \cdot E$	
$\frac{dE}{dt} = (k_{dis}^{complex} + k_{pho}^{protein}) \cdot C - k_{ass}^{complex} \cdot P \cdot E$	(2.4)
$\frac{dC}{dt} = k_{ass}^{complex} \cdot P \cdot E - (k_{dis}^{complex} + k_{pho}^{protein}) \cdot C$	
$\frac{dP^*}{dt} = k_{pho}^{protein} \cdot C$	
Michaelis-Menten kinetics	
Quasi – steady – state ($P(0) \gg E(0)$): $\frac{dC}{dt} \approx 0$	
Mass conservation law: $E_{total} = C + E$	
$\Rightarrow C = \frac{E_{total} \cdot P}{K_m + P}$ with $K_m = \frac{k_{dis}^{complex} + k_{pho}^{protein}}{k_{ass}^{complex}}$	(2.5)
$\Rightarrow \frac{dP^*}{dt} = \frac{V_{max} \cdot P}{K_m + P}$ with $V_{max} = k_{pho}^{protein} \cdot E_{total}$	
$\frac{dP}{dt} = k_{syn}^{protein} \cdot M - k_{deg}^{protein} \cdot P - \frac{V_{max} \cdot P}{K_m + P}$	

where $k_{ass}^{complex}$ and $k_{dis}^{complex}$ are the association and the disassociation rate constants of the complex respectively, and $k_{pho}^{protein}$ is the phosphorylation rate constant of the protein. V_{max} is the maximum phosphorylation rate catalysed by the kinase, and K_m , known as the Michaelis constant, is the protein concentration at which its phosphorylation rate is half of V_{max} . E_{total} represents the total amount the kinase. $P(0)$ and $E(0)$ represent the initial concentrations of the protein and the kinase, respectively.

The Hill equation was first introduced by Hill and can be used for describing the cooperative interactions between the same or different molecules (Hill, 1910; Yagil and Yagil, 1971). For example, the mRNA (M) mentioned above may have multiple binding sites for a miRNA (S), which can target the mRNA and mediate its degradation (Figure 2.1). The multiple miRNA binding sites may have cooperative effect to enhance the degradation of the target mRNA. In other words, the already bound miRNAs can significantly increase the affinity of other binding sites targeted by subsequent miRNAs.

This phenomenon can result in quicker degradation of the target mRNA and be described using the equation below

$$\frac{dM}{dt} = k_{syn}^{mRNA} - k_{deg}^{mRNA} \cdot M - R \quad (2.6)$$

$$\text{with } R = D_{max} \cdot h(S, \theta, n), h(S, \theta, n) = \frac{S^n}{\theta^n + S^n}$$

where the degradation rate of the mRNA is represented by R , which is a function of the maximum mRNA degradation rate (D_{max}) and the Hill function (h). In the Hill function, the Hill constant θ corresponds to the concentration of miRNA (S) at which R reaches half-maximal degradation rate ($\frac{D_{max}}{2}$). Different values of the Hill coefficient n account for different miRNA-mediated effects on the mRNA degradation. If $n=1$, there is no cooperative effect for the miRNAs. Bigger values of n ($n>1$) account for miRNA cooperative effect, which can produce steep sigmoid shape for R (Figure 2.2).

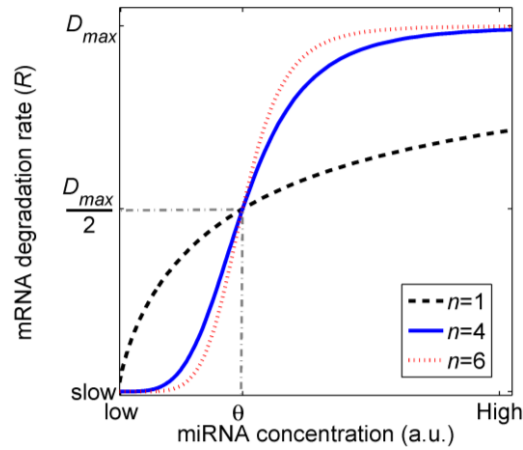


Figure 2.2: Using the Hill equation to describe miRNA-mediated degradation of the mRNA. With the low concentration of miRNA, the mRNA degradation rate is slow and stable ($n=4$ and 6). Until the miRNA concentration reaches θ , the mRNA degradation rate is $\frac{D_{max}}{2}$. The bigger the Hill coefficient n is, the steeper the transition from slow to D_{max} is.

The power-law formalism was originally presented by Savageau and is an alternative approach for modelling biochemical reactions (Savageau, 1969a and 1969b; Rui *et al.*, 2008). Compared to conventional kinetic models represented by Equation (2.1) in which kinetic orders are positive integers, power-law models allow non-integer values for the kinetic orders. Based on available structural information used to construct biochemical systems, two types of power-law models can be formulated: detailed and simplified power-law models. In detailed power-law models, due to the well-known

structural information of biochemical systems, kinetic orders have positive real values, which are related to the effects of molecular crowding and inhomogeneity in intracellular compartments (Savageau, 1992); however, incomplete information of biochemical systems and the need for simplification and aggregation lead to simplified power-law models, in which both positive and negative real values are applied for kinetic orders (Vera *et al.*, 2007). Positive values represent activation, translocation and degradation, while negative values are an intuitive representation for inhibition (Vera *et al.*, 2007). For example, the transcription of a gene can be regulated by several TFs (T), and TFs can play different roles through interacting with different regions of the gene (Figure 2.1). If a TF promotes the transcription of the gene, a positive number is assigned to the kinetic order (g). Otherwise, a negative kinetic order should be used for characterising the process in which a TF inhibits the gene transcription. The ODE formulated in power-law and the possible roles of TFs represented by different values of g are shown in Equation (2.7) and Figure 2.3.

$$\frac{dM}{dt} = k_{syn}^{mRNA} \cdot T^g \quad (2.7)$$

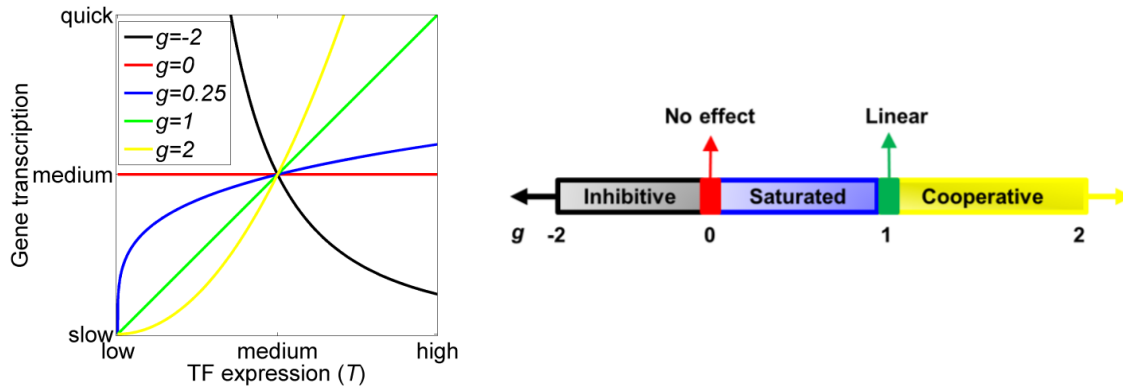


Figure 2.3: Using the power-law formalism to describe the TF-mediated gene transcription. When $g=-2$, the TF inhibits the synthesis of the mRNA (black line). When $g=0$, the TF is involved in the synthesis of the mRNA but not affects the transcription of the gene (red line). For positive values of g , the TF can activate the gene transcription in different manners: saturated (blue line), linear (green line) and cooperative activation (yellow line).

2.2 Model calibration

Once a biochemical system has been converted into a preliminary ODE model, the next step is model calibration, a process by which parameter values are adjusted in order to make model simulations match experimental observations as good as possible. To do so,

there are two possible means: characterisation of parameter values using available biological information or estimation of parameter values using optimisation methods. Some parameter values can be directly measured or obtained from the literature or databases. For example, the half-life ($t_{1/2}$) of some molecules (e.g. protein) can be measured *in vitro* via western blot data, and this information can be used to characterise their degradation rate constants through the equation $k_{deg} = \frac{\ln 2}{t_{1/2}}$ (e.g. if the half-life of a protein P is 10 hr, its corresponding $k_{deg}^P \approx 0.07 \text{ hr}^{-1}$). The database SABIO-RK provides a platform for modellers of biochemical networks to assemble information about reactions and kinetic constants (Wittig *et al.*, 2012). However, for most model parameters, whose values cannot be measured in laboratories or be accessed from the literature or databases, a process named as parameter estimation is adopted to characterise their values. Before running parameter estimation, initial parameter values and boundaries should be set within physically plausible ranges. To do so, the database BioNumbers provides modellers with key numbers in molecular and cell biology, ranging from cell sizes to metabolite concentrations, from reaction rates to generation times, from genome sizes to the number of mitochondria in a cell (Milo *et al.*, 2010).

2.2.1 Parameter estimation

Parameter estimation is a process, by which parameter values are determined using optimisation methods, to minimise the distance between model simulations and experimental data. To illustrate how this process is implemented, major steps in parameter estimation are described below.

Model definition

Given that there is an ODE-based model containing N state variables (x), which can be mapped to a set of M observables (y) through an observation function g as follows (Raue *et al.*, 2009)

$$\frac{dx(t)}{dt} = f(x(t), k), \quad (2.8)$$

$$x(t_0) = x(0), \quad (2.9)$$

$$y(t) = g(x(t), s) + \epsilon, \quad (2.10)$$

where $x(t)$ is a vector for all state variables, k is a vector for rate constants, $x(0)$ is the vector for all initial concentrations of the state variables, s is a vector comprising scaling or additional offset parameters of the observation function g , ϵ is a vector of measurement errors or noises. Both functions $f(\cdot)$ and $g(\cdot)$ are required to be continuously differentiable, and for partially observed models the dimension of observations is smaller than the dimensions of model state variables ($M < N$).

Rate constants k , initial concentrations $x(0)$ together with the parameters of the observation function s are defined as the set of problem specific parameters (p) of the model

$$p = \{x(0), k, s\} = \{p_1, p_2, \dots, p_n\}. \quad (2.11)$$

In biochemical systems the parameter values must be biologically meaningful, and therefore rate constants and initial concentrations should not be negative real numbers.

Cost function

Intuitively, a good fitting model should minimise the deviation between model simulations and experimental data (Figure 2.4). The cost function is used to evaluate the agreement between model simulations and measured experimental data and is commonly defined as the weighted sum of squared residuals ($R_{ij}(p)$) using the following equation

$$\chi^2(p) = \sum_{i=1}^M \sum_{j=1}^H (R_{ij}(p))^2, \quad (2.12)$$

$$R_{ij}(p) = \frac{y_i^{data}(t_j) - y_i(p, t_j)}{\sigma_{ij}^{data}}, \quad (2.13)$$

where $y_i^{data}(t_j)$ denotes the number of H data points for each observable i , which is measured at time point t_j . σ_{ij}^{data} represents the corresponding noise or the standard deviation of the experimental data, and $y_i(p, t_j)$ is the i^{th} observable predicted by the model that is configured with the parameter set p for time point t_j . The optimal parameter set (p^*) can be estimated numerically by

$$p^* = \min_p [\chi^2(p)]. \quad (2.14)$$

Equation (2.14) is a standard least square minimisation problem. Because of the nonlinear and constrained nature of this problem, in the next step of parameter estimation I will introduce some optimisation methods which are used to solve it.

Given that the measurement noises are normally distributed $\epsilon \sim N(0, \sigma^2)$, the deviations between measurements and model simulations are also normally distributed. In this case, maximum likelihood estimation is equivalent to standard least-squares minimisation (Raue *et al.*, 2009). An optimal parameter set (p^*) can be obtained by maximizing the likelihood of the data y^{data} with respect to the parameter set p

$$L(y^{data}|p) = \prod_{i=1}^M \prod_{j=1}^H \frac{1}{\sqrt{2\pi\sigma_{ij}}} \exp\left(-\frac{1}{2}\left(\frac{y_i^{data}(t_j) - y_i(p, t_j)}{\sigma_{ij}^{data}}\right)^2\right), \quad (2.15)$$

$$-\log(L(y^{data}|p)) = \sum_{i=1}^M \sum_{j=1}^H \frac{1}{2} \left(\frac{y_i^{data}(t_j) - y_i(p, t_j)}{\sigma_{ij}^{data}}\right)^2 + \frac{1}{2} \log(2\pi\sigma_{ij}^{data}), \quad (2.16)$$

$$\chi^2(p) = const - 2 \log(L(y^{data}|p)), \quad (2.17)$$

where $L(y^{data}|p)$ is the likelihood. χ^2 will be used as the placeholder for the likelihood in the next section.

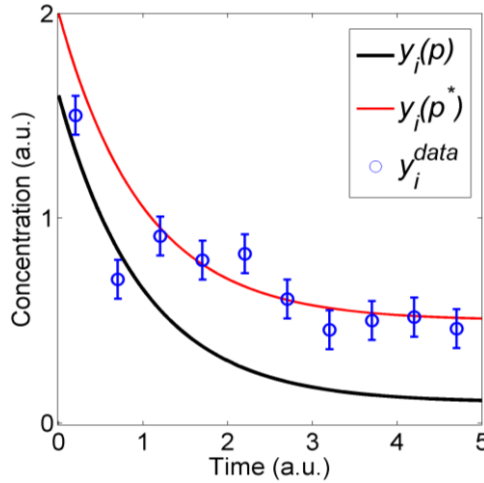


Figure 2.4: Illustration of Parameter estimation. Optimisation methods are used to tune the parameter values to minimise the distance between the initial model simulations ($y_i(p)$) and the experimental data (y_i^{data} ; the bars crossing the circles represent standard deviations of the experimental data). After parameter estimation, the optimal model simulation ($y_i(p^*)$) is obtained. a.u.: arbitrary unit.

Minimisation of the cost function

The minimisation of the cost function (i.e. to find the optimal parameter set p^*) measures the goodness of fit of the model with respect to given experimental data sets. Towards this end, local and global optimisation methods are usually adopted. The easiest and simplest local optimisation methods are gradient-based, such as the Gauss-Newton method, which minimise the cost function through an iterative procedure (Burke and Ferris, 1995). In each step of the procedure, the gradient of the residuals is used to

calculate a parameter update until the convergence criterion is fulfilled (e.g. the cost function does not decrease from one iteration to the next). However, local optimisation methods usually do not work for realistic problems, because they always converge to local solutions (local minimums; Figure 2.5). To prevent the search process being trapped in local minimums, researchers developed global optimisation methods, which are more efficient and robust to find the global solution (global minimum). Based on the algorithms adopted, global optimisation can be further differentiated into deterministic (e.g. DIRECT algorithm; Jones *et al.*, 1993) and stochastic methods (e.g. particle swarm pattern search algorithm; Vaz and Vicent, 2007). Compared to stochastic methods, which rely on probability approaches, deterministic methods show better convergence to global solutions, however, easy implementation and less time consuming properties of stochastic methods compensate their relative weak ability to guarantee global optimums (Ashyraliyev *et al.*, 2009).

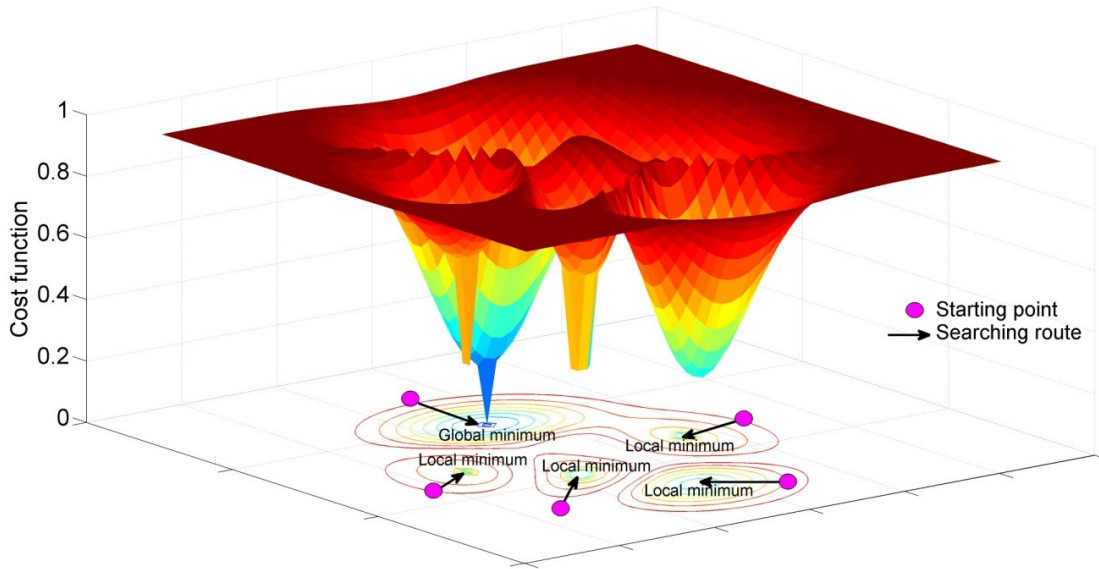


Figure 2.5: Gradient-based local optimisation methods. Due to the local nature of gradient-based methods, their search processes from the starting points are often trapped into local minimums. An intuitive way to overcome this problem is to apply different starting points (i.e. initial parameter sets within constraints) to improve the possibilities to find the global minimum.

2.2.2 Parameter identifiability

After parameter estimation, one major concern of modellers is uncertainties of estimated parameters values. Usually, the uncertainties represented as confidence intervals are determined by model structure and the quality of experimental data used in the

parameter estimation. A confidence interval $[p_i^-, p_i^+]$ of a parameter estimate \hat{p}_i with a significance level α signifies that the true value p_i^* is located within this interval with probability $1-\alpha$ (Raue *et al.*, 2009).

The confidence interval of a parameter estimate (p_i) can be obtained by using a threshold (Δ_α) in the likelihood

$$\{p_i | \chi^2(p_i) - \chi^2(\hat{p}_i) < \Delta_\alpha\} \text{ with } \Delta_\alpha = \chi^2(\alpha, df), \quad (2.18)$$

where the threshold Δ_α is the α quantile of the χ^2 -distribution with df degrees of freedom. $df=1$ gives point-wise confidence intervals that hold individually for each parameter, $df=\#p$, being the number of parameters, gives simultaneous confidence intervals that hold jointly for all parameters.

For complex ODE-based models, optimisation methods can yield more than one set of parameter estimates that make the cost function show the same minimal value. In this case, the parameter estimates are non-identifiable. More specifically, if the parameter estimate \hat{p}_i cannot lead to a unique minimum of the cost function, the parameter p_i is structurally non-identifiable (Figure 2.6; Raue *et al.*, 2009). This problem arises from the model structure only and is independent from the experimental data. However, the structurally identifiable parameter p_i may be practically non-identifiable. This can arise due to insufficiency and low quality of experimental data or the chosen measurement time points. A parameter is practically non-identifiable if the likelihood-based confidence interval (Equation 2.18) is infinitely extended in the direction of p_i indicated by the likelihood staying below a desired Δ_α (Figure 2.6; Raue *et al.*, 2009). By increasing the amount and quality of the measured data and/or choosing different time point t_j , more rigorous conditions on the parameter estimation are imposed. This leads to a tightening of confidence intervals that ultimately will remediate a practical non-identifiability, yielding finite confidence intervals (Figure 2.6; Raue *et al.*, 2009; Balsa-Canto *et al.*, 2010). Moreover, it is noteworthy that non-identifiability of parameters does not imply a poor fit to the experimental data, but that parameters cannot be constrained to unique values given the current model structure and experimental data. As a result of non-identifiability, the predictive ability of the model will be undetermined, and this can lead to uncertainties in model predictions.

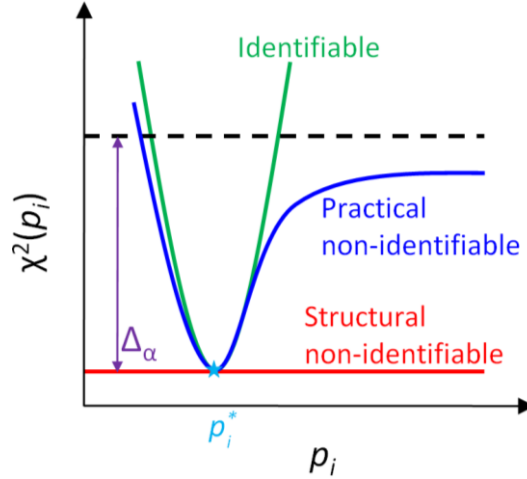


Figure 2.6: Illustration of parameter identifiability analysis. The identifiability of parameter p_i are accessed from the profile likelihood $\chi^2(p_i)$. The red solid line illustrates a structural non-identifiable p_i meaning the alternation of p_i can lead to more than one optimal solution; the blue solid line illustrates practical non-identifiable p_i , meaning the alteration of p_i leads to a unique optimal parameter set but one direction of its confidence interval is infinite below the threshold Δ_α ; and the green solid illustrates identifiable p_i meaning its alteration can lead to a unique solution and the corresponding confidence interval is finite below the threshold Δ_α . The dashed line indicates Δ_α which is utilised to assess likelihood-based confidence intervals of p_i and the light blue star corresponds to the minimum $\chi^2(p_i)$ at the optimal parameter p_i^* .

2.3 Model validation and analysis

After model calibration, the next step is to run predictive simulations, which are helpful to study the dynamic properties of biochemical systems and guide the future experiments in the laboratory. Usually, the model simulations are compared with the experimental data which are used during the parameter estimation. However, just a good agreement between the model simulations and those experimental data is not enough to prove its predictive ability, and therefore it is necessary to validate the model with other experimental data that is not used during the parameter estimation. This process is called model validation and can ensure more reliable and accurate model predictions. To do so, the data generated from new experiments or extracted from the literature are compared with new model simulations, which are usually obtained by configuring the model according to new experimental settings. Once a model is validated, it is appropriate for making predictions. In addition, analytical tools such as sensitivity and bifurcation analysis can be used to study complex properties and behaviour of the model. In the following sections, I will introduce these analytical tools with some concrete examples.

2.3.1 Sensitivity analysis

The most common way to carry out model predictions is through perturbing parameter values (i.e. model inputs) which are responsible for controlling model outputs. In contrast to model inputs, model outputs are defined as model behaviours (e.g. steady states). In a complex biochemical network, the behaviour of a component could be affected by most or all reactions in the network. Thus, it is needed to develop a tool, which can systematically identify the influence of reactions on the component behaviour. Sensitivity analysis is such a tool, which can evaluate the influence of model parameters (e.g. initial concentrations of the state variables and rate constants) on model outputs. Depending on strategies used for perturbing model parameters, sensitivity analysis can be classified into two types: local and global sensitivity analysis. Local sensitivity analysis provides a description of the behaviour near a specified operating condition, whereas global sensitivity analysis uses wide ranges of parameter spaces and addresses global behaviour of model parameters using statistical methods (Saltelli *et al.*, 2000). Based on these results, valuable information can be extracted for choosing right experimental targets, and thus with the help of sensitivity analysis the time and expenses used for designing new experiments can be reduced (Saltelli *et al.*, 2000).

Local sensitivity analysis

Local sensitivity analysis investigates sensitivities of model outputs with respect to particular points in parameter space. Mathematically, at a time point t , a local sensitivity coefficient S_{ij} is the first order derivative of a model variable (x_i) with respect to a model parameter (p_j ; Ingalls, 2008)

$$S_{ij} = \frac{\partial x_i(t)}{\partial p_j} \cong \frac{x_i(p_j + \Delta p_j, t) - x_i(p_j, t)}{\Delta p_j}, \quad (2.19)$$

where S_{ij} is computed at a point $p^0 = (p_1^0, p_2^0, \dots, p_j^0, \dots, p_n^0)$ where all the parameters are fixed to their nominal values. In other words, S_{ij} implies the variation of the model variables (x_i) due to the variation of the parameter (p_j) around the nominal value p^0 at the time point t . For example, if at the time point t , x_i reaches its steady state (denoted by x_i^{ss}) then $S_{ij} = \frac{\partial x_i^{ss}(t)}{\partial p_j}$ is obtained; if $S_{ij} = 1$, it indicates that an increase of Δ in p_j can lead to Δ increase of x_i^{ss} , for values of p_j near its nominal value p_j^0 . S_{ij} can be computed

by the finite difference approximation, and the accuracy of the approximation depends on the parameter perturbation size (Δp_j). Alternatively, Equation (2.19) can be written as follows (Ingalls, 2008)

$$S_{ij} = \frac{p_j}{x_i(t)} \frac{\partial x_i(t)}{\partial p_j}, \quad (2.20)$$

where S_{ij} is scaled with $\frac{p_j}{x_i(t)}$ to generate a relative sensitivity coefficient, which implies the relative change of the model variable (x_i) due to the relative variation of the parameter (p_j) at the time point t . After the scaling S_{ij} becomes dimensionless, which allows direct comparison of S_{ij} with other sensitivity coefficients and gives a more intuitive understanding of the sensitivity coefficients. By applying Equation (2.20) to the previous example, $S_{ij} = \frac{p_j}{x_i^{ss}} \frac{\partial x_i^{ss}}{\partial p_j}$ is obtained and $S_{ij} = 1$ indicates that an increase of $\Delta\%$ in p_j can lead to $\Delta\%$ increase of x_i^{ss} for values of p_j near its nominal value p_j^0 . The relative sensitivity coefficient is also referred to as logarithmic sensitivities or logarithmic gains since (Ingalls, 2008)

$$S_{ij} = \frac{\partial x_i(t)/x_i(t)}{\partial p_j/p_j} = \frac{\partial \ln(x_i(t))}{\partial \ln(p_j)}. \quad (2.21)$$

The use of local sensitivity analysis has a long tradition in biochemistry in work on Metabolic Control Analysis (MCA). Within MCA, sensitivity coefficients are referred to as flux control coefficients, which describe the dependence of pathway flux on individual reaction rates (Fell, 1997). As the local sensitivity analysis allows only a small perturbation of each model parameter value, it is a measure of local behaviour, i.e. it describes the behaviour for parameters close to their nominal values. The use of local sensitivity analysis is inherently restricted to small regions of parameter space, and thus global sensitivity analysis is proposed to address global behaviour over a wide range of parameter values.

Global sensitivity analysis

Global sensitivity analysis investigates the parametric influence on model outputs by simultaneously perturbing model parameter values over large ranges, and thus nonlinear effects and interactions among parameters can be examined. The parameter ranges are based on parameter estimates and are constrained by upper and lower bounds or

probability densities (Ingalls, 2008). Statistical methods are often used to guide sampling of parameter values within the specified domains of parameter ranges. The global sensitivity analysis methods are usually implemented by using sampling-based methods, thus an efficient sampling method is important for determining its efficacy. Latin hypercube sampling is such a method, which not only samples random parameter values but also guarantees a uniformed distribution of parameter values in their defined ranges (Figure 2.7; Tang, 1993). Most of current global sensitivity analysis methods adopt the Latin hypercube sampling method to generate parameter vectors, and for each vector there exists a corresponding model output. By visualizing parameter values and model outputs in scatter plots, their relationships such as non-linearities and non-monotonicities can be revealed. Depending on these relationships, modellers should choose an appropriate global sensitivity analysis method (Frey and Patil, 2002; Saltelli *et al.*, 2000). More specifically, for nonlinear but monotonic models, sensitivity coefficients calculated based on rank transforms like Partial Rank Regression Coefficient (PRRC) will perform well. For nonlinear nonmonotonic models, sensitivity coefficients calculated based on decomposing the variance like the Fourier Amplitude Sensitivity Test (FAST) and Sobol's method are the best choice. For the detailed implementation of these methods, the interested reader is referred to Saltelli *et al.*(2000).

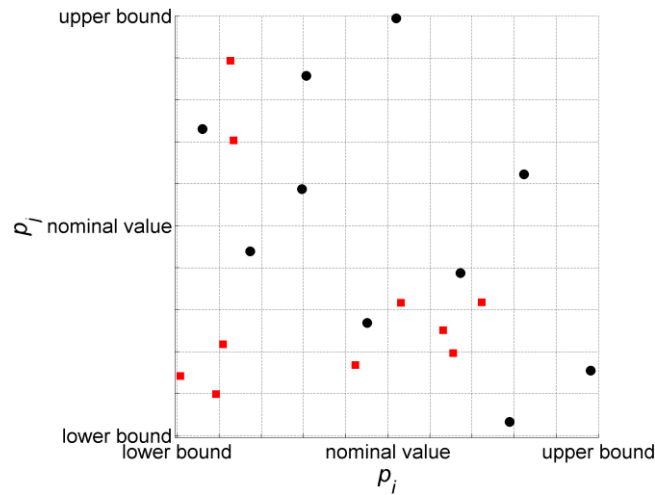


Figure 2.7: Latin hypercube sampling method. Compared to the simple random sampling method (red squares), Latin hypercube sampling (black dots) generates uniformly distributed samples for the parameter vector $[p_i, p_j]$ within predefined boundaries. The vectors obtained using simple random sampling may fall into the same small intervals indicated by grids; however, Latin hypercube sampling ensures that the samples are evenly distributed over the whole range and do not overlap in rows and columns.

2.3.2 Bifurcation analysis

As discussed in the previous section, sensitivity analysis identifies the most influential parameters which can affect model behaviour. Besides, another analytical tool called bifurcation analysis is employed to detect control parameters (also known as bifurcation parameters) whose variations are able to change the stability of fixed points (or equilibrium points) of ODE-based models (Strogatz, 2000). In other words, bifurcation analysis can explain how a change in dynamics of biochemical systems, from one stable steady state to another or from resting state to oscillations, happens. A coarse classification of bifurcations distinguishes local and global bifurcations. The local bifurcations describe local phenomena which occur near fixed points. Particularly, important local bifurcation behaviours in ODE models include transcritical bifurcations, saddle-node bifurcations and Hopf bifurcations. The former two generate bistability when a system switches from one stable steady state to another, while the latter gives rise to oscillations (Strogatz, 2000).

Bistability

A system, which can exhibit two stable steady states, is defined as a bistable system. Such a system toggles between two discrete, alternative stable steady states, in contrast to a monostable system, which always shows one steady state (Angeli *et al.*, 2004). This interesting system-level property can be produced even in relative simple biochemical networks such as a two-component positive feedback loop. The existence of bistability in biochemical systems is quite common, and it is crucial for modellers to understand its influence on basic cellular functioning, such as decision-making processes in cell cycle progression, cell differentiation and apoptosis (Ferrell and Machleder 1998; Gardner *et al.*, 2000).

Here, I use concrete examples to illustrate how bistability is triggered in two-component positive feedback loops by the alteration of bifurcation parameters. Based on the interaction types between the components, positive feedback loops can be classified into mutual activation and mutual inhibition systems (Tyson *et al.*, 2003; Figure 2.8). Both systems are able to produce switch-like behaviour. The behaviour appears when the bifurcation parameter passes its critical value (bifurcation point) resulting an unstable

steady state for the system, and therefore the system jumps to a new steady state. Mathematically, an unstable steady state is equal to an unstable fixed point. In terms of linear stability analysis, if a small perturbation away from a fixed point grows, the fixed point is unstable; if a small perturbation away from a fixed point decays, the fixed point is stable (Strogatz, 2000). As shown in Figure 2.8 left, the mutual activation positive feedback loop can produce one-way switch behaviour. In this case, the steady states of non-active protein (X) remain in the lower branch for weak stimulus signals (S), and the levels of the steady states are linearly dependent on the signal strength until the strength reaches a saddle node bifurcation point (Figure 2.8 left ①). At this point, the stable lower branch collides with the unstable middle branch. As two types of the steady states collide at the bifurcation point, a further increase in the signal strength results in a switch to the stable upper branch (Figure 2.8 left ②). In the upper branch, when the signal strength increases, the system follows the same behaviour as in the lower branch (stronger stimulus signals lead to higher steady state levels of X). However, when the signal strength decreases, the steady state levels of X are trapped in the upper branch and cannot go back to the lower one (Figure 2.8 left ③). This is due to the fact that the other bifurcation point, which should appear in the upper branch, lies outside of the physically reasonable interval for the signal strength (e.g., the value of the bifurcation point is negative). This one-way switch behaviour was demonstrated in a cancer-related network composed of the miR-17-92 cluster and the E2F family including E2F1, E2F2 and E2F3 (Aguda *et al.*, 2008). In contrast to the one-way switch behaviour, the toggle switch behaviour can be produced by the mutual inhibition feedback loop (Figure 2.8 right). In such a system two saddle-nodes bifurcation points exist in the physically reasonable interval, and therefore the alternation of the bifurcation parameter makes the switch from the lower branch to the upper branch reversible (Figure 2.8 right ①, ②, ③ and ④). Such phenomenon is referred to as hysteresis, which means that the equilibrium that the system attains for a given signal strength depends on the history of the system (Tyson *et al.*, 2003). In biology, hysteresis behaviour has been found to be important for governing cell fate decisions (Xiong and Ferrell, 2003) and driving cell cycle transitions (Sha *et al.*, 2003).

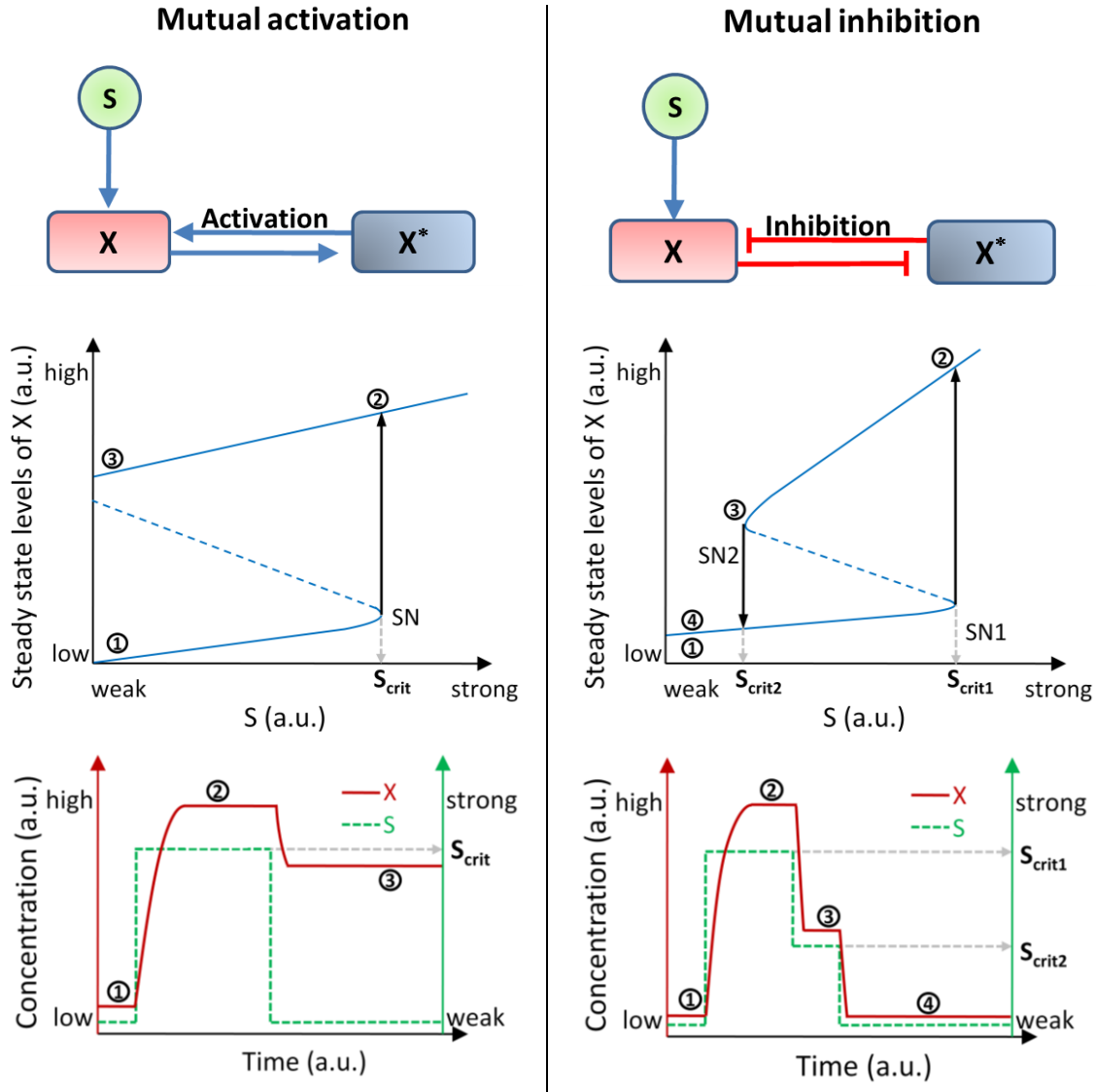


Figure 2.8: Illustration of bistability analysis. **Top:** The mutual activation and inhibition positive feedback loops are characterised by mutual activation or inhibition between the non-active protein X and active protein X^* , respectively. Here, the strength of the stimulus signal (S) is a bifurcation parameter whose alteration controls the behaviour of the system. **Middle:** Bifurcation diagrams are employed to analyse how the level of the steady states of X changes depending on the alteration of S . In these plots, the blue solid and dashed lines represent the S -dependent stable and unstable steady states of X , respectively. The black solid lines with arrow heads represent the switch of the steady state of X after S crosses the saddle-node bifurcation point (SN), which has the corresponding value S_{crit} indicated by the grey dashed line. **Bottom:** The plots show the response of X (red solid line) for different S (green dashed line) over time. The symbols ①, ②, ③ and ④ in these plots are corresponding to the ones in the bifurcation diagrams.

Oscillation

From an analytical point of view, the emergence of oscillations generally relates to a transition through a Hopf bifurcation point (Andronov *et al.*, 1966). This local bifurcation is the simplest and most common mechanism, in which a stable solution arises beyond the bifurcation point in the form of a periodic solution (corresponds to a closed curve or limit cycle) surrounding an unstable solution (Goldbeter, 2007). A Hopf bifurcation point may be subcritical or supercritical. In the supercritical case, a stable solution (or fixed point) becomes unstable, while a stable periodic solution is born. Mathematically, a periodic solution is stable if solutions that begin close to the limit cycle remain close to the limit cycle for all positive time; in other words, a periodic solution can attract other nearby solutions (Strogatz, 2000). In the subcritical case, an unstable fixed point becomes stable, while an unstable periodic solution is born. Similarly, a periodic solution is unstable if its nearby solutions spiral away from the limit cycle (Strogatz, 2000).

Here, I focus only on the supercritical Hopf bifurcation, which describes how sustained oscillations arise when a fixed point loses its stability. In biochemical systems, the negative feedback oscillator is a network motif that can trigger oscillatory behaviour in protein synthesis and circadian rhythms (Tyson *et al.*, 2003; Figure 2.9). As shown in Figure 2.9, the strength of stimulus signal (S) is the bifurcation parameter, which controls the overall behaviour of the system. When the signal strength is weak, protein X3 shows dampened oscillation that converges towards a stable steady state (Figure 2.9 ① and ②). With the increase of the signal strength, X3 starts to show sustained oscillation once the strength of the signal crosses the first Hopf bifurcation point (Figure 2.9 ③). In mathematical terms, the emergence of the oscillatory solution in the system is caused by the change of the eigenvalues of the Jacobian matrix via the variation of the bifurcation parameter. More specifically, with the alternation of the bifurcation parameter if the complex conjugate eigenvalues of the system cross the imaginary axis of the complex plane and show positive real numbers, the system will show oscillation (Strogatz, 2000). After entering the unstable solution area, the limited cycle becomes a new attractor for X3 and its amplitude is dependent on the signal strength. As the signal

strength is increased further to pass the second Hopf bifurcation point, the oscillation of X3 again dampens and converges towards the stable steady state (Figure 2.9 ④).

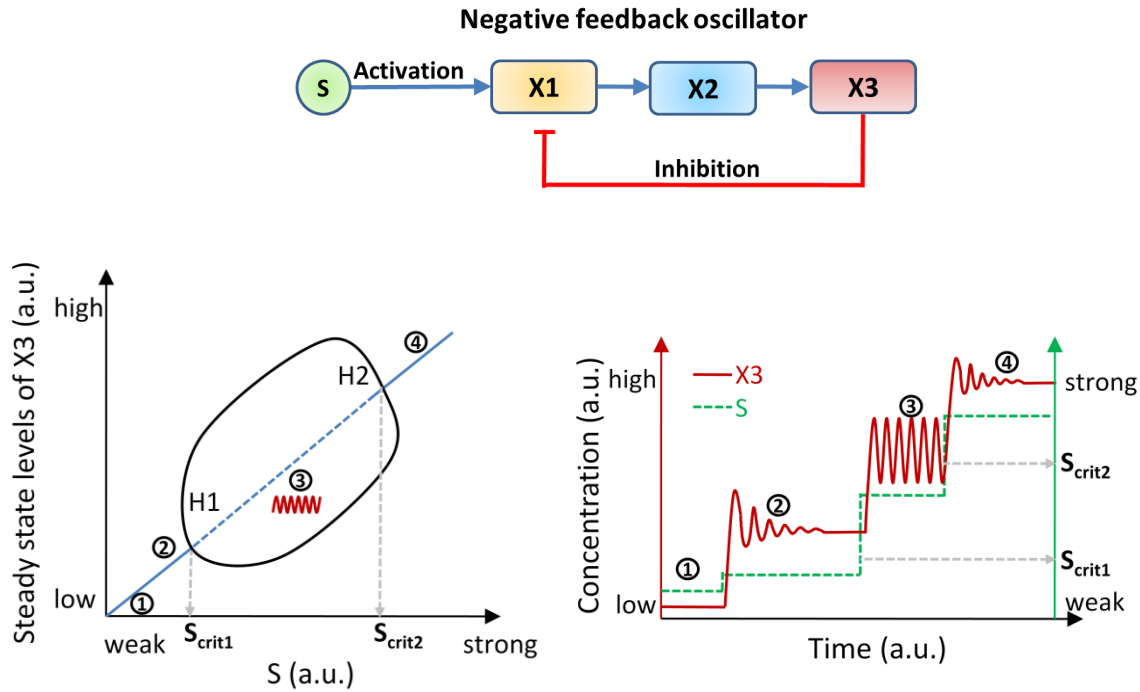


Figure 2.9: Illustration of Hopf bifurcation analysis. The negative feedback oscillator (top panel) is characterised by three-component interactions, in which protein X1 activates X3 through an intermediate protein X2. In turn, X3 inhibits X1 directly. The Bifurcation diagram (bottom left panel) is employed to illustrate how the oscillation of X3 emerges and disappears depending on the alteration of the bifurcation parameter S, which represents the strength of the stimulus signal. In this plot, the blue solid and dashed line represents the stable and unstable steady states of X3, respectively. The curve represents the limited cycle that connects the two Hopf bifurcation points (H1 and H2), whose corresponding values for S are S_{crit1} and S_{crit2} . The bottom right plot shows the response of X3 (red solid line) for different S (green dashed line) over time. The symbols ①, ②, ③ and ④ in this plot are corresponding to the ones in the bifurcation diagram.

2.4 Summary

In systems biology, the utilisation of ODE-based models is a very popular and powerful method for investigating biochemical systems. Using the ODE modelling approach together with numerical simulations and relevant analytical tools provides a useful and efficient means to gain insights into biochemical networks. This not only saves the experimental efforts but also makes *in silico* experiments possible. By using this approach, I together with some colleagues have published several research works regarding different biochemical systems. Some of these studies are briefly summarised below and the others are to be presented in the subsequent two chapters.

For example, we set up a multi-level model using the power-law formalism, which accounts for the JAK2-STAT5 signalling pathway in erythropoiesis (Lai *et al.*, 2009). The constructed model was calibrated using quantitative data, which were measured at molecular (e.g. protein expression) and physiological (e.g. hematocrit) levels. We used the model to investigate the effects of dysregulation of key proteins involved in the JAK2-STAT5 signalling pathway during erythropoiesis. The simulation results suggested that downregulation in any of the three components (Epo, STAT5 and EpoR/JAK2) has considerable effects on the hematocrit level. In addition, the model predicted that the traditional therapy, using exogenous Epo injection, can compensate the effect of the downregulation of Epo, STAT5 or EpoR/JAK2 expression levels individually. However, it is insufficient to counteract the combined downregulation of any two of Epo, STAT5 and EpoR/JAK2. We further developed a methodology by integrating sensitivity and bifurcation analysis, aiming for designing more informative predictive simulations in ODE models through finding critical parameters (Nikolov *et al.*, 2010). Particularly, under defined biological scenarios we first evaluated the influence of parameters on the model outputs, like steady state and oscillation amplitude; then, the parameters with high sensitivities to the model outputs were investigated to determine their bifurcation points and stability regions in the system's phase space. To test our methodology, we applied it in the multi-level model of the JAK2-STAT5 signalling pathway in erythropoiesis. Our analysis revealed that in contrast to the time delays related to intracellular signalling and hypoxia-controlled physiological dynamics, the physiological time delays caused by the differentiation process of the red blood cells are critical to induce pathological sustained oscillation. Moreover, the simulation results suggested that the system is able to recover from partial impairment of intracellular signalling processes, but it cannot survive from failure of the physiologically critical processes that can provoke the emergence of pathological oscillation.

In another publication (Vera *et al.*, 2011), we set up an ODE-based model to investigate the propagation of p53 oscillation to its transcriptional targets. The model showed that the turnover rates of the targets are key factors to determine whether they can successfully inherit the oscillation from p53. More particularly, the model suggested that the oscillation of p53 is only able to propagate to its transcriptional targets, when the

mRNA and protein of the targets show fast turnover rates (i.e. short half-lives). Furthermore, we investigated the effect of p53 oscillation on its targets when p53 is simultaneously involved in an additional negative feedback loop mediated by 14-3-3 σ . The Hopf bifurcation analysis and numerical simulations suggested that the regulation via 14-3-3 σ can induce quick cessation of p53 oscillation. Moreover, by analysing the interplay between upstream stimuli of p53 (e.g. stress signals that can cause DNA damage) and the regulation by 14-3-3 σ , we found that p53 can show bistability with sustained oscillation.

Chapter 3

MicroRNA-34a Regulation of the p53/SIRT1 Signalling Pathway

miRNAs are a family of small regulatory RNAs that post-transcriptionally regulate gene expression. The complexity of signalling pathways increases with the consideration of miRNA-mediated regulation. Due to the regulation by miRNAs, a variety of feedback loops is formed by miRNAs and other components in signalling pathways. miRNA-mediated feedback loops have great potential to influence the dynamic properties of signalling pathways.

In this chapter, I present a study investigating the regulatory role of miR-34a in the p53/SIRT1 signalling pathway, which has been published in Lai *et al.* (2012a). Using a systems biology approach, which integrates biological data into a kinetic model, we identify the mechanism by which miR-34a represses SIRT1. Moreover, the model simulations show the function of miR-34a under a cancerous condition caused by abnormal upregulation of SIRT1.

3.1 The p53/SIRT1 signalling pathway

Any attempt to update the paradigm of the genetic information flow represented by the central dogma of molecular biology (DNA→mRNA→protein) should include TFs and miRNAs. Both are involved in transcriptional and post-transcriptional regulation, respectively (Figure 3.1). Key elements in gene regulation are TFs, a class of proteins able to promote and regulate the expression of genes. Experimental evidence suggests that TFs are involved in a variety of feedback loop signalling systems, ensuring the processing of genetic information in reliable, robust and responsive manners in response to internal and external signals (Nelson *et al.*, 2003).

In the last decade, it has been shown that miRNAs, whose main function is to regulate the activity and stability of target genes through interacting with their target

mRNAs, are involved in post-transcriptional regulatory mechanisms (Chendrimada *et al.*, 2007). Usually, a miRNA can target multiple mRNAs and this property increases the challenge to attribute distinct functions to different miRNAs (Zhao *et al.*, 2008). The identified miRNAs are estimated to regulate more than 30% of all protein-coding genes, making them one of the most abundant gene regulators (Friedman *et al.*, 2009; Bueno *et al.*, 2008; Khanin and Vinciotti, 2008). Moreover, miRNAs are involved in tumour progression of several cancer types by targeting different genes such as CDKs, Ras, and Myc, which play key roles in tumour development and progression (Chan *et al.*, 2005; Schultz *et al.*, 2008). Depending on the identified role of their targets, miRNAs can act as tumour suppressors downregulating oncogenes (Takamizawa *et al.*, 2004; Johnson *et al.*, 2005; Akao *et al.*, 2006), or as oncogenic miRNAs negatively regulating the expression of tumour suppressor genes (Chan *et al.*, 2005; Iorio *et al.*, 2005).

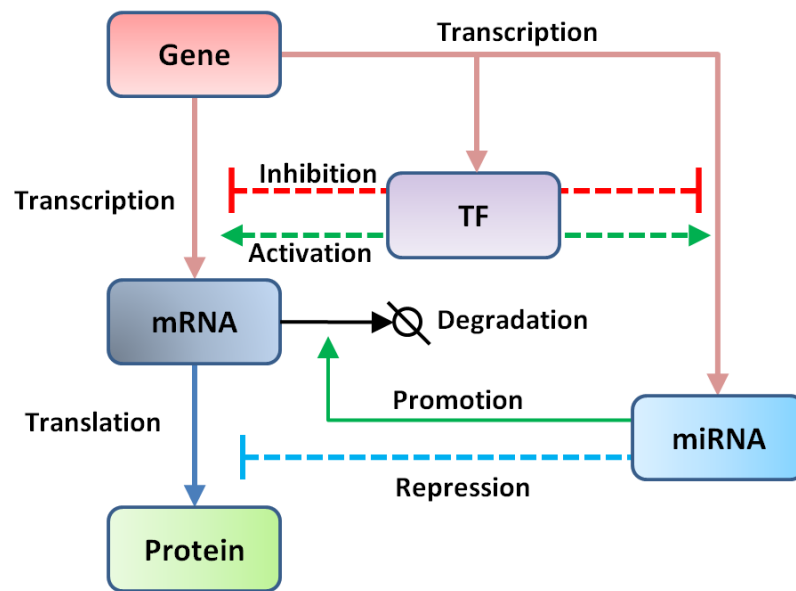


Figure 3.1: Sketch of genetic information flow. The discovery of miRNAs expands the central dogma of molecular biology. Most miRNAs can downregulate gene expression through interacting with mRNAs: promote mRNA degradation or repressing translation. The transcription process is controlled by TFs that can work as activators or inhibitors. TFs and miRNAs are themselves encoded by genes and subject to regulation.

In signalling pathways, a number of network motifs composed of miRNAs, TFs and other signalling proteins have been identified (Shalgi *et al.*, 2007). Among these motifs, there are positive or negative feedback loops (Figure 3.2), in which given TFs activate

the syntheses of miRNAs, and the miRNAs in turn inhibit the TFs through up- or downregulating the upstream regulators of the TFs. These kinds of feedback loops are linked with complex dynamic properties of biochemical systems (Shalgi *et al.*, 2007; Aguda *et al.*, 2008; Brosh *et al.*, 2008). When one or more of these network motifs appear in a signalling pathway, purely experimental methods are not enough to dissect dynamic properties of the complex biochemical system. Thus, to gain full insights into the system, a systems biology approach combining experimental data with mathematical modelling becomes necessary (Vera and Wolkenhauer, 2008).

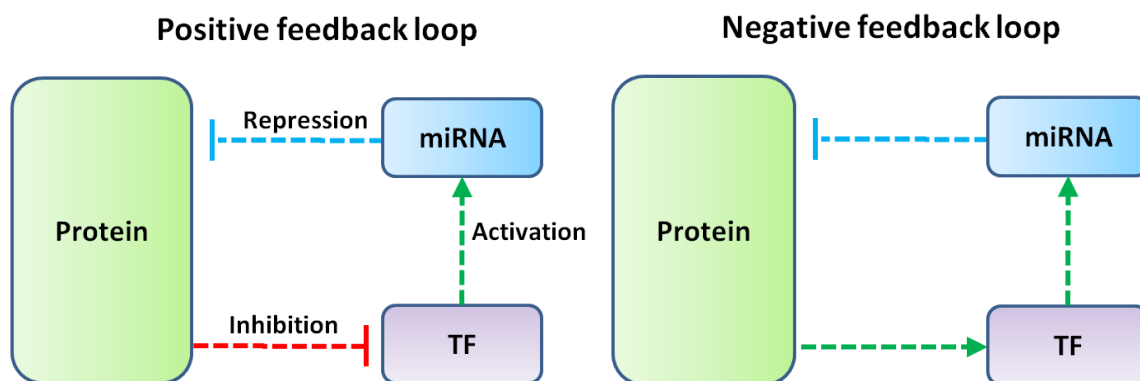


Figure 3.2: miRNA-mediated feedback loops. In biochemical systems, the complex interactions among TFs, miRNAs and signalling proteins make the generation of network motifs such as positive (left) and negative (right) feedback loops possible.

A recent study has proved that p53, the well-studied tumour suppressor protein, is involved in a positive feedback loop mediated by miR-34a (Figure 3.3). In this loop, miR-34a whose expression is transcriptionally promoted by p53 represses the production of SIRT1. SIRT1 can regulate apoptosis in response to oxidative and genotoxic stress by deacetylating p53 (Longo and Kennedy, 2006). Other than miR-34a, DBC1 has been found to be another negative regulator of SIRT1. DBC1 directly interacts with SIRT1 and inhibits SIRT1 deacetylation *in vitro* and *in vivo*, and therefore it can activate p53 and subsequently upregulate p53-mediated pathways (Kim *et al.*, 2008). Another key player in regulation of p53 is Mdm2, which forms a negative feedback loop with p53 (Freedman *et al.*, 1999; Juven-Gershon and Oren, 1999). On one hand, Mdm2 binding to p53 can repress the transcriptional function of p53 and lead to complete elimination of p53 through proteolytic degradation. On the other hand, p53 upregulates the expression of Mdm2 through transcriptional activation. p53 plays a key role in preventing the

development of cancer through tight regulation of the cell cycle arrest and/or apoptosis in response to genotoxic stress. Mutations that perturb p53 function, often observed in its DNA binding domain or disruptions to the upstream or downstream regulatory networks of p53, have been found in approximately half of human cancers (Rodier *et al.*, 2007; Riley *et al.*, 2008). Because of the central role of p53 in coordinating the cellular responses to a broad range of cellular stress factors, it is interesting to systematically investigate the dynamic properties of the p53/SIRT1 signalling pathway, which includes the newfound miR-34a mediated feedback loop.

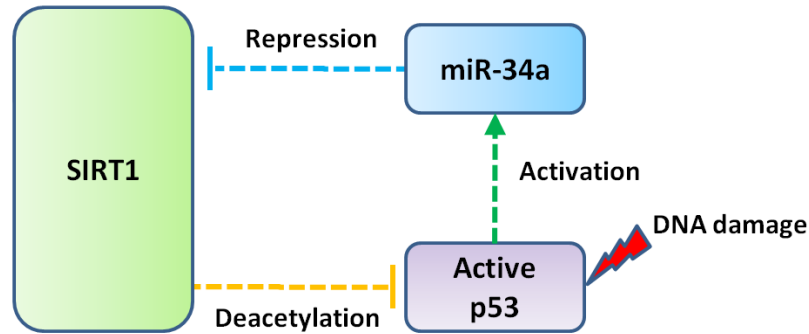


Figure 3.3: The positive feedback loop formed by active p53, SIRT1 and miR-34a. In response to DNA damage, the upregulation of active p53 promotes the synthesis of miR-34a. miR-34a can downregulate the expression of SIRT1 through interacting with the mRNA of SIRT1. SIRT1 can decrease the production of active p53 through deacetylation. These interactions make a positive feedback loop in the p53/SIRT1 signalling pathway.

3.2 Materials and methods

3.2.1 Model construction

For the investigation of the regulatory role of miR-34a in the p53/SIRT1 signalling pathway, we set up an ODE-based model using the power-law formalism. The model was composed of four parts (Figure 3.4): 1) the activation (acetylation) of p53 in response to a stress signal that can cause DNA damage and the deactivation (deacetylation) of p53 regulated by SIRT1 (Appella and Anderson, 2001; Vaziri *et al.*, 2001; Yamakuchi and Lowenstein, 2009), 2) the positive feedback loop integrated by p53, SIRT1 and miR-34a (Fujita *et al.*, 2008; Yamakuchi *et al.*, 2008; Kato *et al.*, 2009), 3) the upregulation of DBC1 induced by DNA damage and its inhibitory effect on SIRT1 (Kim *et al.*, 2008; Kwon and Ott, 2008; Zhao *et al.*, 2008; Cha *et al.*, 2009; Li *et*

al., 2009), and 4) the inconsistent regulation between Mdm2 and active p53 (Ramalingam *et al.*, 2007; Vera *et al.*, 2010).

The formulated differential equations accounted for the change of the concentrations of the signalling pathway components over time: Mdm2 (*Mdm2*; Equation (3.1)), non-active (deacetylated) p53 (*p53*; Equation (3.2)), active (acetylated) p53 (*p53**; Equation (3.3)), miR-34a (*miR34a*; Equation (3.4)), SIRT1 (*Sirt1*; Equation (3.5)), DBC1 (*DBC1*; Equation (3.6)). Additionally, an algebraic equation was formulated to account for the total amount of p53 (*p53_{total}*; Equation (3.7)).

$$\frac{dMdm2}{dt} = k_{syn1}^{mdm2} + k_{syn2}^{mdm2} \cdot p53^*(t - \tau_1) - k_{deg}^{mdm2} \cdot Mdm2 \quad (3.1)$$

$$\begin{aligned} \frac{dp53}{dt} = & k_{syn1}^{p53} + k_{syn2}^{p53} \cdot DD - k_{ace}^{p53} \cdot p53 \cdot DD + k_{dea}^{p53*} \cdot p53^* \cdot Sirt1 \cdot DBC1^{g_1} \\ & - k_{deg}^{p53} \cdot p53 \cdot Mdm2 \end{aligned} \quad (3.2)$$

$$\frac{dp53^*}{dt} = k_{ace}^{p53} \cdot p53 \cdot DD - k_{dea}^{p53*} \cdot p53^* \cdot Sirt1 \cdot DBC1^{g_1} - k_{deg}^{p53*} \cdot p53^* \cdot Mdm2 \quad (3.3)$$

$$\frac{dmiR34a}{dt} = k_{syn1}^{miR34a} + k_{syn2}^{miR34a} \cdot p53^*(t - \tau_2) - k_{deg}^{miR34a} \cdot miR34a \quad (3.4)$$

$$\frac{dSirt1}{dt} = k_{syn}^{Sirt1} \cdot miR34a(t - \tau_3)^{g_2} - k_{deg}^{Sirt1} \cdot Sirt1 \quad (3.5)$$

$$\frac{dDBC1}{dt} = k_{syn1}^{DBC1} + k_{syn2}^{DBC1} \cdot DD - k_{deg}^{DBC1} \cdot DBC1 \quad (3.6)$$

$$p53_{total} = p53 + p53^* \quad (3.7)$$

For p53, the model contained equations accounting for the basal synthesis of p53, the extra synthesis of p53 induced by DNA damage (*DD*), p53 activation (acetylation) mediated by *DD*, p53 deactivation (deacetylation) mediated by SIRT1 and its degradation mediated by Mdm2. For Mdm2, the equations that describe the basal synthesis of Mdm2, the extra synthesis of Mdm2 induced by active p53 (*p53**) and the degradation of Mdm2 were formulated. In case of miR-34a, the equations considered its basal synthesis, degradation and extra synthesis induced by *p53**. For SIRT1, the model accounted for its basal synthesis that is repressed by miR-34a and its degradation. For DBC1, the model included the equations that describe its basal synthesis and extra synthesis induced by *DD* as well as its degradation. The total amount of p53 is the sum of its non-active and active fractions. According to the definition of power-law model in **Chapter 2.1**, we assigned -1 to the kinetic orders g_1 and g_2 which were used to describe the DBC1-mediated inhibition of SIRT1 deacetylase activity and the repression of

SIRT1 by miR-34a, respectively. Besides, we introduced three biologically possible time delays: the time delay caused by the $p53^*$ -induced of Mdm2 (τ_1), the time delay attributed to the $p53^*$ -induced synthesis of miR-34a (τ_2) and the time delay associated with the repression of SIRT1 by miR-34a (τ_3).

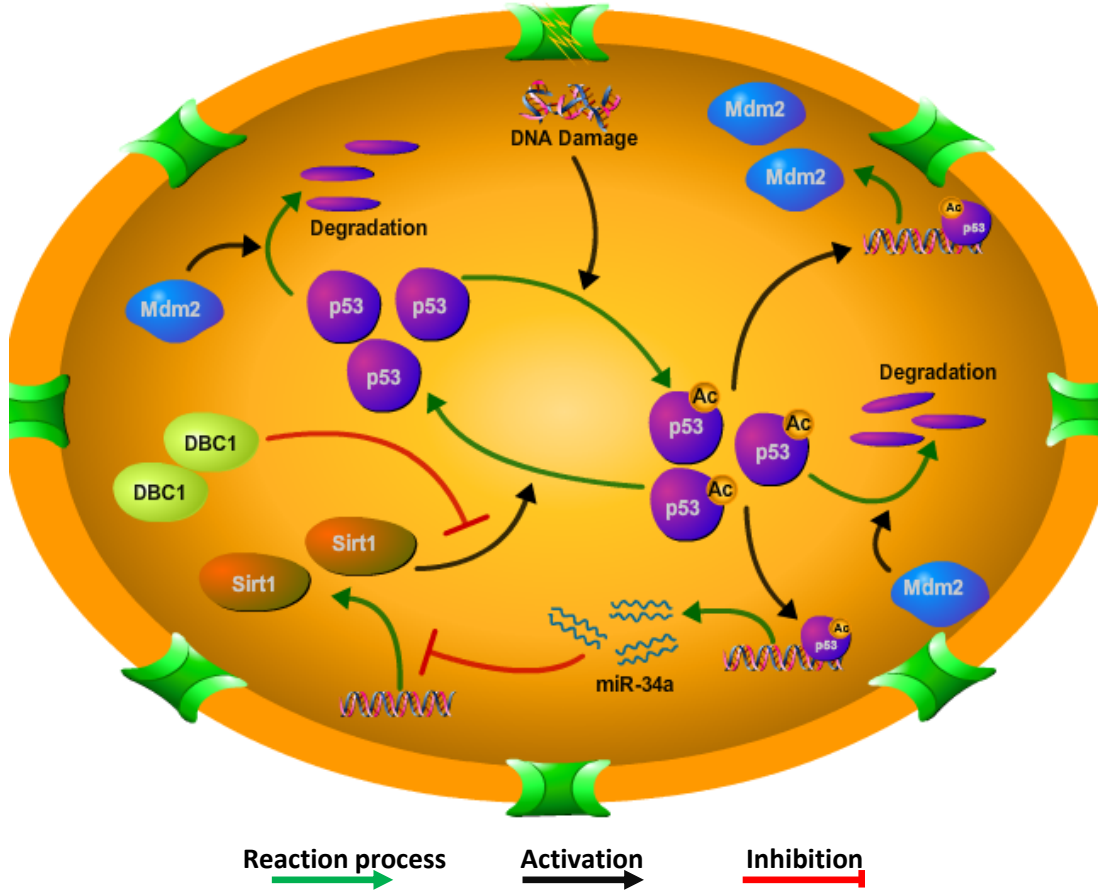


Figure 3.4: Scheme of the p53/Sirt signalling pathway. In the reaction processes, the molecules are converted from one form to another (e.g. $p53 \rightarrow \text{Ac-p53}$). In the activation or inhibition processes, the molecules activate or inhibit the corresponding processes but they are not consumed or converted to another form (e.g. $\text{DBC1} \rightarrow \text{SIRT1}$).

3.2.2 Model calibration

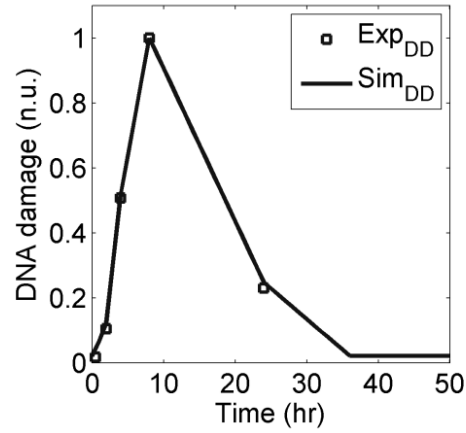
We calibrated the model with the following procedures: 1) the biological information concerning protein half-lives were used to characterise the degradation rate constants of some molecules (k_{deg}^{mdm2} , k_{deg}^{miR34a} , k_{deg}^{Sirt1} and k_{deg}^{DBC1}), 2) the measured exogenous DNA damage response was used to shape the dynamics of the input signal (DD) by using the MATLAB's build-in interpolation function (Figure 3.5A), and 3) the quantitative data published in Yamakuchi *et al.* (2008) were retrieved and normalised to estimate the

values of other unknown parameters (for the detailed process of parameter estimation, see **Chapter 2.2.1**). The data showed the dynamics of $p53_{total}$, $p53^*$, *Sirt1* and *miR34a* after treatment with doxorubicin, a genotoxic-stress inducing agent. Before running the parameter estimation, the initial parameter values and boundaries were defined within physically plausible ranges. The estimated parameter values as well as the initial concentrations of the state variables are summarised in Table 3.1. As shown in Figure 3.5B, there is a good agreement between the model simulations and the experimental data. More specifically, in response to DNA damage the concentrations of $p53_{total}$ and $p53^*$ increase and reach their peaks several hours after the stimulation. Upon accumulation of $p53^*$, upregulation of miR-34a is observed with several hours of delay due to the time (τ_2) that is needed for transcriptional induction by $p53^*$. Subsequently, with increasing level of miR-34a, concentration of SIRT1 starts to decline with a delay (τ_3). Because of the persistent inhibitory effect of miR-34a, the concentration of SIRT1 stays at low level until end of the simulation.

3.2.3 Model validation

To validate the model, we compared the model simulations with another independent experimental data set published by Yamakuchi *et al.* (2008). Within the work, the authors carried out experiments to measure active p53 ($p53^*$) expression levels in wild-type and p53-mutated human colorectal carcinoma cells (HCT116). Both types of cells were transfected with antisense oligonucleotides (AS-miR34a) that knockdown endogenous expression of miR-34 or scrambled oligonucleotide controls (AS-miRscr) that cannot affect endogenous miRNA expression at all. As shown in Figure 3.6, the model simulations are in a good agreement with these experimental data, which were not used for parameter estimation. Thus, we can conclude that the model is capable of making reliable predictions for the defined biochemical system.

A



B

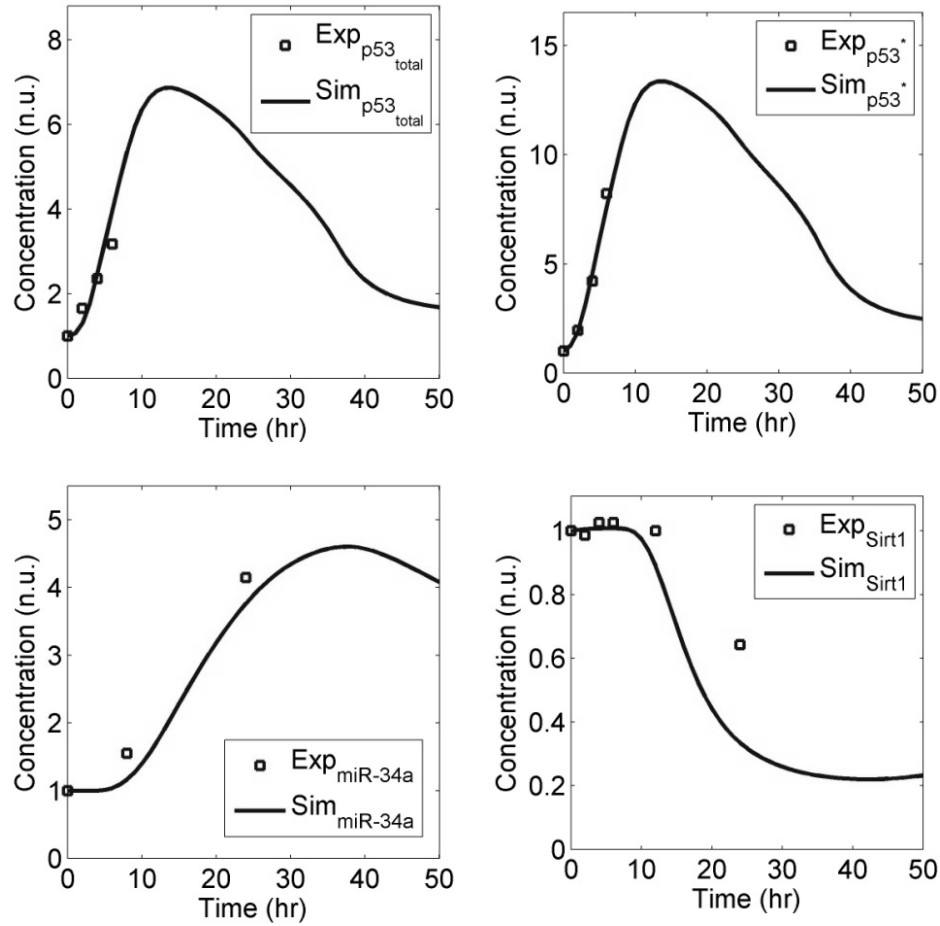


Figure 3.5: Comparison of model simulations and time-series data. **A:** The change of the exogenous DNA damage response in the defined time frame. **B:** The change of selected molecule concentrations, including total amount of p53 ($p53_{total}$), active p53 ($p53^*$), miR-34a ($miR34a$) and SIRT1 ($Sirt1$), in the defined time frame. The solid lines and square markers represent model simulation results (Sim) and experimental data (Exp) in normalised unit (n.u.), respectively.

Table 3.1: The model variables and parameters. The initial concentrations of model variables were assumed to 1, meaning the basal levels for the model variables are 1. Such an assumption was made based on experimental results such as western and northern blot, in which measured expression of proteins and RNAs are normalised to the initial (or control) measurement, to show down- (<1) and upregulation (>1) of the corresponding molecules. The parameter values were either fixed using available information from the literature (blue font) or estimated by using the experimental data. The time delays were all assumed to be 1 hr.

Variables	Description	Initial concentration (unit)
<i>Mdm2</i>	Mdm2	1 (n.u.)
<i>p53</i>	Deacetylated (non-active) p53	1 (n.u.)
<i>p53*</i>	Acetylated (active) p53	1 (n.u.)
<i>miR34a</i>	MicroRNA-34a	1 (n.u.)
<i>Sirt1</i>	SIRT1	1 (n.u.)
<i>DBC1</i>	DBC1	1 (n.u.)
Parameter	Description	Value (unit)
k_{syn1}^{mdm2}	Basal synthesis rate constant of Mdm2	1.317 (n.u. · hr ⁻¹)
k_{syn2}^{mdm2}	Extra synthesis rate constant of Mdm2 induced by active p53	0.068 (hr ⁻¹)
k_{deg}^{mdm2}	Degradation rate constant of Mdm2	1.386 (hr ⁻¹)
k_{syn}^{p53}	Basal synthesis rate constant of non-active p53	2.136 (n.u. · hr ⁻¹)
k_{syn2}^{p53}	Extra synthesis rate constant of non-active p53 induced by DNA damage	0.957 (hr ⁻¹)
k_{ace}^{p53}	Acetylating (activation) rate constant of non-active p53	0.282 (n.u. ⁻¹ · hr ⁻¹)
k_{deg}^{p53}	Degradation rate constant of non-active p53	2.079 (n.u. ⁻¹ · hr ⁻¹)
k_{dea}^{p53*}	Deacetylating (deactivation) rate constant of active p53	0.282 (hr ⁻¹)
k_{deg}^{p53*}	Degradation rate constant of active p53	0.078 (n.u. ⁻¹ · hr ⁻¹)
k_{syn1}^{miR34a}	Basal synthesis rate constant of miR-34a	0.010 (n.u. · hr ⁻¹)
k_{syn2}^{miR34a}	Extra synthesis rate constant of miR-34a induced by active p53	0.018 (hr ⁻¹)
k_{deg}^{miR34a}	Degradation rate constant of miR-34a	0.028 (hr ⁻¹)
k_{syn}^{Sirt1}	Basal synthesis rate constant of SIRT1	0.582 (n.u. ² · hr ⁻¹)
k_{deg}^{Sirt1}	Degradation rate constant of SIRT1	0.577 (hr ⁻¹)
k_{syn1}^{DBC1}	Basal synthesis rate constant of DBC1	0.023 (n.u. · hr ⁻¹)
k_{syn2}^{DBC1}	Extra synthesis rate constant of DBC1 induced by DNA damage	0.003 (hr ⁻¹)
k_{deg}^{DBC1}	Degradation rate constant of DBC1	0.023 (hr ⁻¹)
g_1	Kinetic order	-1
g_2	Kinetic order	-1
τ_1	Time delay	1 (hr)
τ_2	Time delay	1 (hr)
τ_3	Time delay	1 (hr)

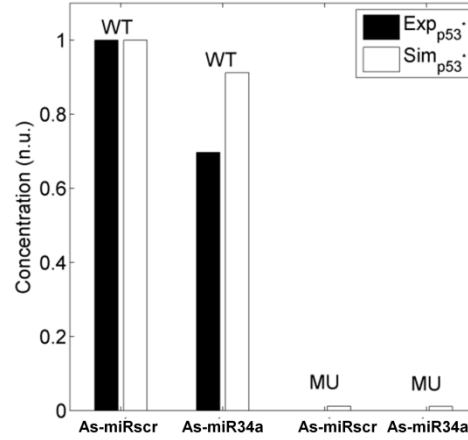


Figure 3.6: Effects of endogenous miR-34a knockdown on the concentration of active p53. The black bars represent the experimental data (Exp_{p53*}) and the white bars denote the model simulations (Sim_{p53*}). In Yamakuchi *et al.* (2008), the expression of active (acetylated) p53 was measured at 16 hr after treatment with 5-Fluorouracil (5-FU, a genotoxic stress-inducing agent) that can induce the activation of p53 in two different cells: wild type HCT116 (WT) and p53-mutated HCT116 (MU). The cells were further transfected with AS-miR34a or AS-miRscr, respectively.

3.3 Results

After model validation, we performed two groups of predictive simulations. First, we simulated and analysed different hypotheses concerning the mechanisms by which miR-34a represses SIRT1. Second, we used the model to investigate the dynamic features of the p53/SIRT1 signalling pathway.

3.3.1 The post-transcriptional repression of SIRT1 by miR-34a

As introduced in **Chapter 1.2.1**, there exist several mechanisms by which miRNAs can repress gene expression. A miRNA can induce mRNA cleavage if the mRNA target site exhibits extensive base complementarity to the miRNA, or it can cause destabilisation of the target mRNA by partially complementary binding. The destabilisation of the target mRNA can be implemented either through deadenylation of the target mRNA followed by degradation or through sequestration of the target mRNA into processing bodies (P-bodies) followed by degradation (Bartel, 2004; Filipowicz *et al.*, 2008).

Here, we combined the available quantitative data and model simulation to identify the mechanism by which miR-34a represses SIRT1. We formulated four hypotheses accounting for miR-34a repression mechanisms: 1) miR-34a enhances the degradation of the SIRT1 mRNA (Figure 3.7 mode 1), 2) miR-34a sequesters the SIRT1 mRNA into P-bodies which is followed by quicker degradation of the mRNA (Figure 3.7 mode 2), 3)

miR-34a represses SIRT1 translation (Figure 3.7 mode 3), and 4) miR-34a indirectly inhibits the synthesis of the SIRT1 mRNA (Figure 3.7 mode 4).

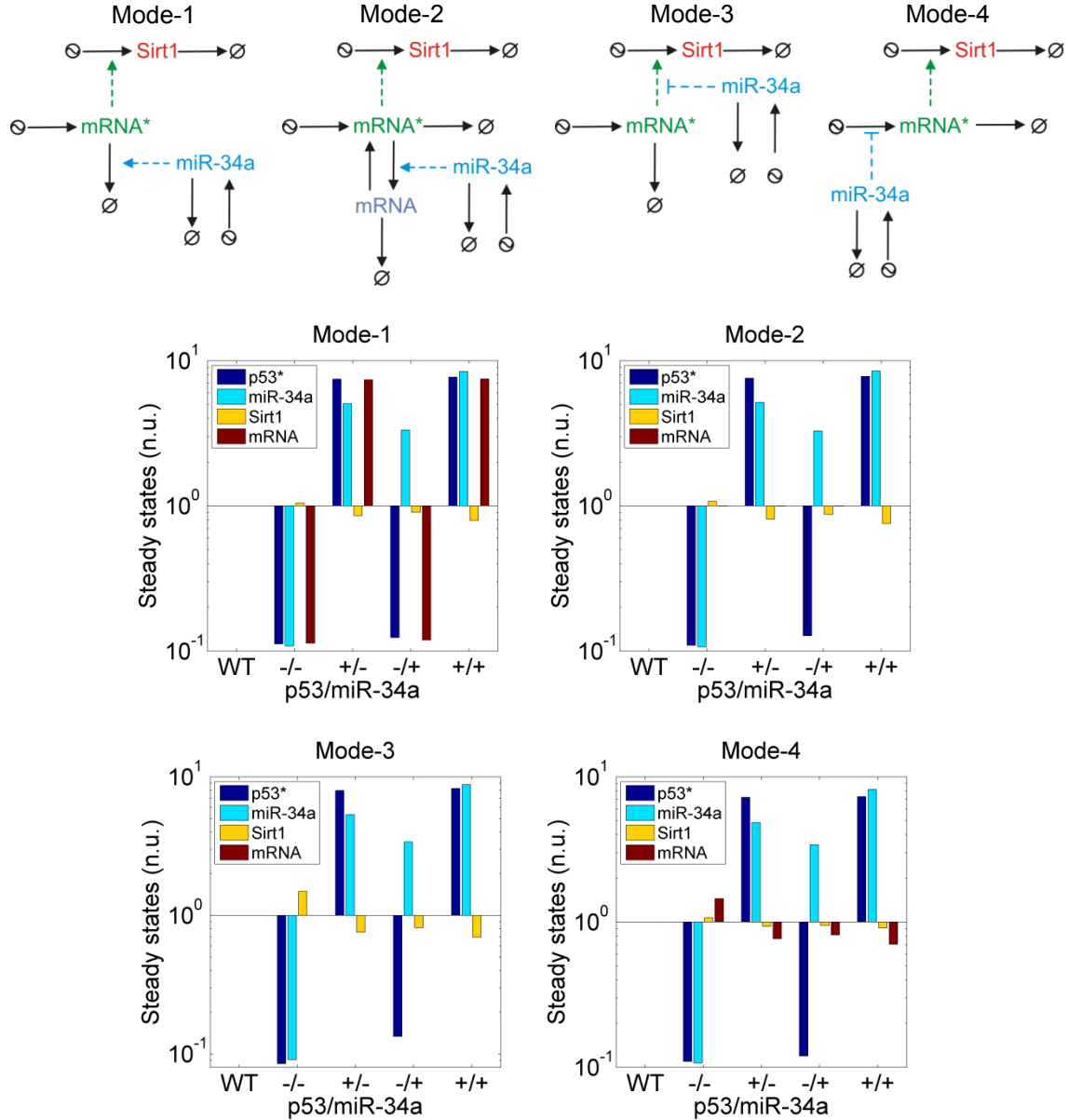


Figure 3.7: The hypothetical repression mechanisms of miR-34a. **Top:** The schemes of the four hypothetical repression mechanisms mediated by miR-34a. The dashed lines with arrow or blunted heads represent activation or inhibition. The solid lines represent synthesis when starting with \odot and degradation when finishing at \emptyset . Mode-1: the enhanced SIRT1 mRNA degradation mediated by miR-34a. Mode-2: the SIRT1 mRNA translocation followed by degradation in P-bodies. Mode-3: translation repression. Mode-4: indirect repression of the SIRT1 mRNA synthesis by miR-34a. **Bottom:** The predicted steady-state levels of active p53 (p53*), miR-34a (miR-34a), SIRT1 (Sirt1) and its mRNA (mRNA) for different experimental conditions: 1) wild-type (WT), 2) downregulation of p53 and miR-34a (-/-), 3) upregulation of p53 and downregulation of miR-34a (+/-), 4) downregulation of p53 and upregulation of miR-34a (-/+) and 5) upregulation of p53 and miR-34a (+/+).

We expanded our model according to these hypotheses accounting for the different mechanisms by which miR-34a represses SIRT1 (see **Appendix 6.1**) and simulated the steady-state levels of the selected molecules for five different experimental conditions (Figure 3.7 bottom): wild-type (WT), downregulation of p53 and miR-34a (-/-), upregulation of p53 and downregulation of miR-34a (+/-), downregulation of p53 and upregulation of miR-34a (-/+) and upregulation of both p53 and miR-34a (+/+). The aim of the simulations was to predict whether the experiments with such design can differentiate the different miR-34a repression mechanisms. For comparison, we converted the steady-state levels of the molecules into logarithmic scale and normalised them with the results obtained in the experiment of WT. Interestingly, we found that for all the mechanisms, the steady-state levels of p53 and miR-34a were the same; however, the steady state levels for SIRT1 and its mRNA were different. These results suggest that the proposed experimental design allows for differentiating modes 1/4 and modes 2/3; in modes 1/4 the steady-state levels of the SIRT1 mRNA were affected by the varied expression of p53 and miR-34a but such change were not observed in modes 2/3. Thus, such an experimental design will fail to differentiate modes 2/3, suggesting that additional experiments concerning the dynamics of the molecules are required for fully differentiating the hypothetical mechanisms.

To computationally identify the mechanism by which miR-34a represses SIRT1, we used time-series data of SIRT1 and its mRNA in wild-type and p53-mutated cell lines and compared the data with model predictions (Ford *et al.*, 2008). We found that the mechanisms encoded in modes 1/4 were not able to reproduce the dynamics of SIRT1. As shown in the Figure 6.1 (see **Appendix 6.1**), the expression of SIRT1 predicted by the model declined too slow compared to the experimental data, which were measured after the stimulation with 5-FU in wild-type cells (WT). Furthermore, the time-series data measured in p53-mutated cells (MU) could only be fitted by mode 3, which is the unique mechanism able to illustrate the stable expression level of SIRT1 after the p53-mutated cells were treated with 5-FU for 48 hr (Figure 3.8). Taken together, our analyses suggest that in the studied model miR-34a inhibits the expression of SIRT1 through translational repression (mode 3), the most common miRNA repression mechanism in animals (Bartel, 2004). Furthermore, this result is also in agreement with the conclusion

made by Yamakuchi *et al.* (2008), in which the authors conducted the experiments under similar conditions and proved that the repression of SIRT1 by miR-34a is achieved by translation repression.

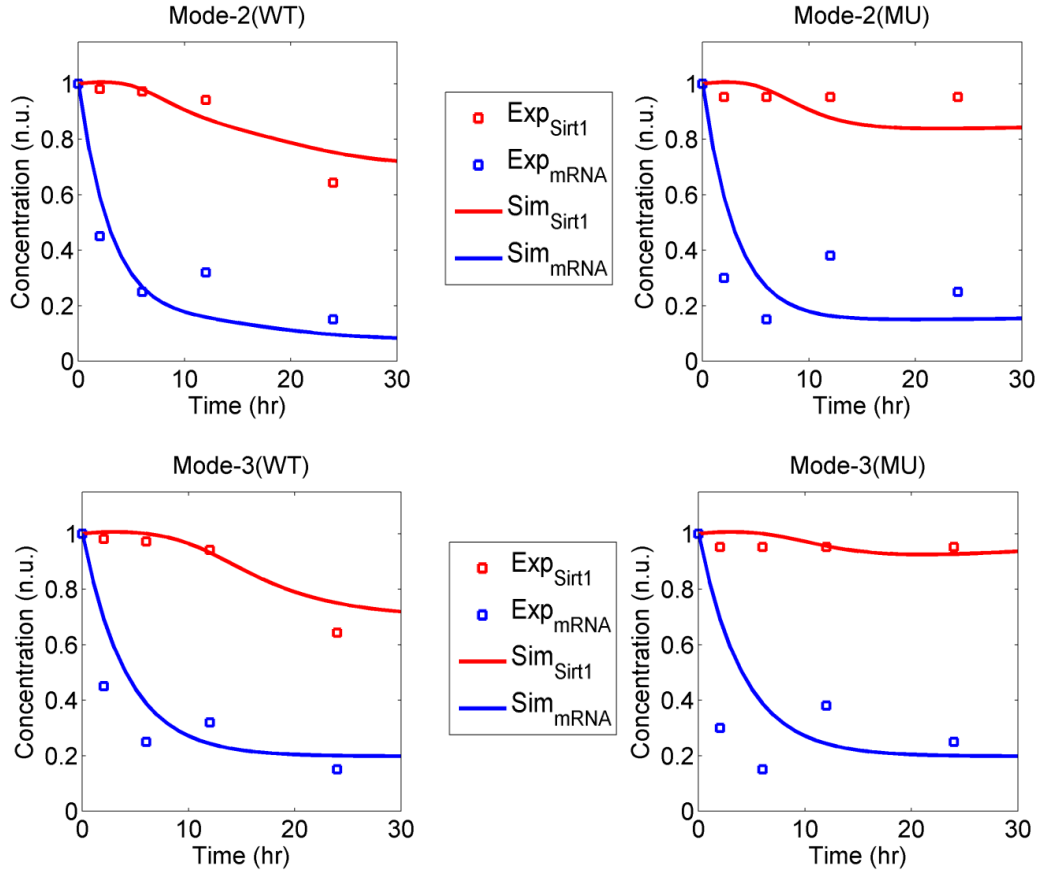


Figure 3.8: Identification of the mechanism by which miR-34a represses SIRT1. The plots of modes 2/3 are shown, and the plots of modes 1/4 can be found in **Appendix 6.1**. The square markers represent the time-series data of SIRT1 ($\text{Exp}_{\text{Sirt1}}$) and its mRNA (Exp_{mRNA}). The data were measured in wild-type (WT) and p53-mutated cells (MU) after the treatment with 5-FU for 48 hr. The solid lines represent the continuous concentrations of SIRT1 ($\text{Sim}_{\text{Sirt1}}$) and its mRNA (Sim_{mRNA}) predicted by the model.

3.3.2 The regulatory effect of miR-34a on the activation of p53

Within the p53/SIRT1 signalling pathway, there are two inhibitors for SIRT1, namely DBC1 and miR-34a. Both molecules can promote the activation (acetylation) of p53 but through different mechanisms: DBC1 can inhibit the decetylation function exerted by SIRT1 on p53 and miR-34a can repress the expression of SIRT1. Thus, it is interesting to compare their regulatory effects on the activation of p53. To do so, we modulated the parameters accounting for the concentrations of DBC1 and miR-34a in the interval $[10^{-1}, 10^1]$ and computed the steady-state levels of active p53 ($p53^*$). As shown in Figure 3.9,

the simulations indicated that repression of DBC1 and miR-34a strongly affects the steady-state levels of $p53^*$, reducing them to 15% of its basal level when both of DBC1 and miR-34a are extremely downregulated. Conversely, extreme upregulation of DBC1 and miR-34a increases the steady-state levels of $p53^*$ by nearly two-fold, showing their positive roles in the activation of p53. Interestingly, the simulations showed that although the concentration of DBC1 and miR-34a were modulated in the same normalised interval, changes in the concentration of DBC1 can induce bigger variations in the steady-state levels of $p53^*$ than the modulation of miR-34a, suggesting DBC1 is a stronger positive regulator for the activation of p53 than miR-34a.

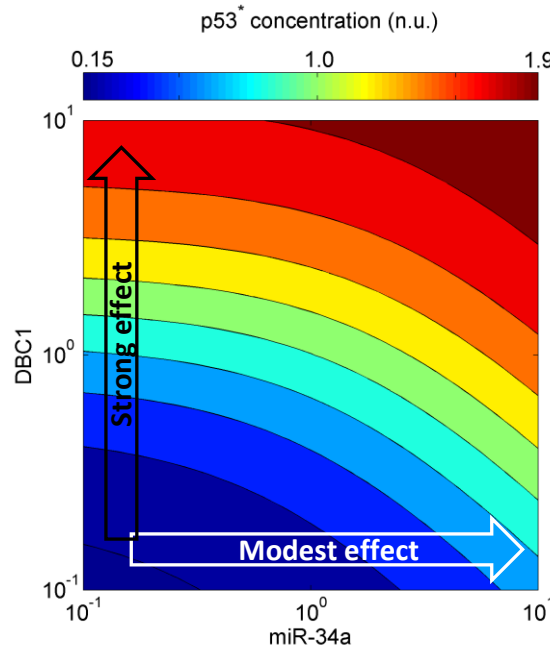


Figure 3.9: Regulatory effects of DBC1 and miR-34a on the activation of p53. Every point in the plot represents a steady-state level of $p53^*$ for given concentrations of miR-34a and DBC1 (10^0 accounts for the basal level), ranging from extreme downregulation (10^{-1}) to extreme upregulation (10^1).

Moreover, we investigated the ability of DBC1 and miR-34a to compensate the loss of $p53^*$ caused by aberrantly expressed of SIRT1. Such upregulation of SIRT1 can be observed in cancerous cells (Kwon and Ott, 2008). The simulation results showed that in case of an intermediate upregulation ($\sim 10^{0.5}$) of SIRT1 the loss of $p53^*$ can be compensated by upregulating either DBC1 or miR-34a (Figure 3.10). However, only the extreme upregulation (10^1) of DBC1 is able to compensate the loss of $p53^*$ due to the abnormal upregulation of SIRT1 (Figure 3.10 left). Taken together, the simulation

results predicted different regulatory effects on the activation of p53 by DBC1 and miR-34a. This could be caused not only by their different interactions with SIRT1 but also by their different regulatory routes in the signalling pathway; DBC1, which enhances the activation of p53 through a simple regulation (DBC1 \rightarrow SIRT1 \rightarrow p53^{*}), shows stronger regulatory effect than miR-34a, which enhances the activation of p53 through a positive feedback loop (p53^{*} \rightarrow miR-34a \rightarrow SIRT1 \rightarrow p53^{*}).

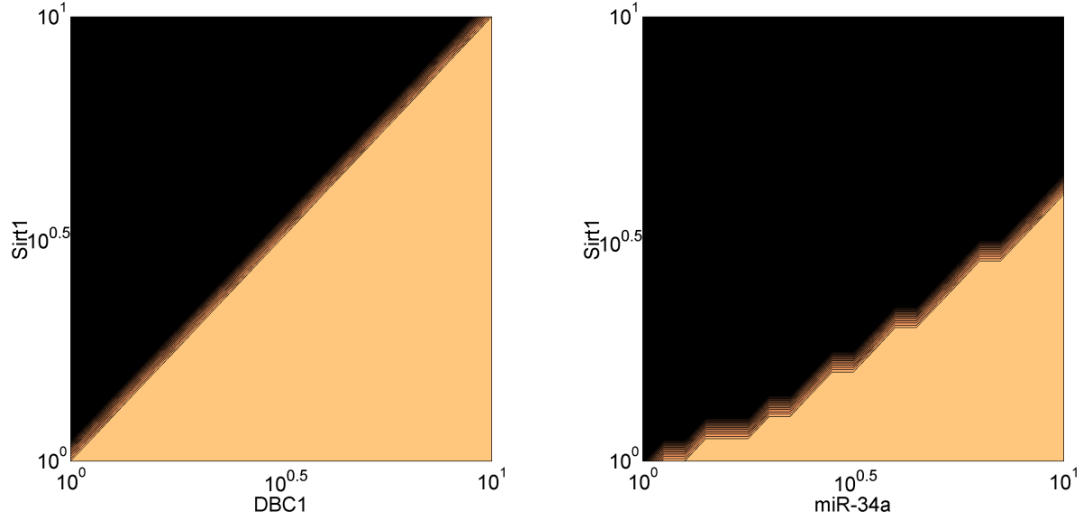


Figure 3.10: miR-34a and DBC1 can compensate the loss of active p53 induced by the abnormal upregulation of SIRT1. Dark coloured area: The steady-state levels of active p53 are not able to recover to the basal level by the upregulation of DBC1 (left) or miR-34a (right). Light coloured area: The steady-state levels of active p53 are able to recover to the basal level by the upregulation of DBC1 (left) or miR-34a (right).

3.4 Conclusion

We discussed and illustrated the utilisation of a systems biology approach for the analysis of the regulatory effect of miR-34a in the p53/SIRT1 signalling pathway. The rationale behind is that in complex biochemical systems involving feedback loops the integration of biological hypotheses and quantitative data through mathematical modelling becomes appealing to acquire a system-level understanding of the system.

The signalling system, which consists of the SIRT1-mediated deacetylation of p53, some other p53 regulators such as DBC1 and Mdm2 as well as its post-transcriptional regulator miR-34a, was constructed. Although the system does not consider all possible interactions associated with p53 (Vera *et al.*, 2010; Vera *et al.*, 2011), it is a good example of a complex regulatory system containing positive and negative feedback

loops. The system was translated into a power-law model, and the model was calibrated and validated by quantitative data.

The well-characterised model was used to investigate two main features of the system. We tested whether the model allows for identifying the mechanism by which miR-34a represses SIRT1. To do so, the model was expanded to account for the hypotheses about the mechanisms. Our analyses revealed that the basic experimental design, which measures the steady-state levels of the selected molecules in the model, can help us partially differentiate the hypothetical mechanisms; however, to completely differentiate them, more complicated experiments are needed. Thus, we further simulated the model to regenerate the experimental data, which shows the temporal dynamics of SIRT1 and its mRNA in distinctive p53 expression conditions. After comparing the model simulations with the data, only the candidate model, in which we hypothesized that miR-34a represses SIRT1 translation, can reproduce the experimental data. Thus, we excluded the possibility of the other miR-34a repression mechanisms in the defined system. In addition, a number of predictive simulations showed the different regulatory effects of DBC1 and miR-34a on the activation of p53.

Above all, our results concerning the p53/SIRT1 signalling pathway are far from giving a realistic and complete picture of the biochemical system related to p53. The primary goal, however, is to illustrate the application of the systems biology approach to investigate the regulatory roles of miRNAs in signalling pathways. Additionally, the function of miRNA is proved to be very often exerted together with a set of different miRNAs rather than isolated or unique ones. Thus, additional analysis can be carried out to investigate whether other miRNAs can intensify (in a summative or synergistic manner) the regulatory effect of miR-34a.

Chapter 4

Target Hub Gene Repression by Multiple and Cooperative MicroRNAs

miRNA target hubs are genes that can be simultaneously targeted by a comparatively large number of miRNAs. Although the details of target hub regulation remain poorly understood, recent experiments suggest that pairs of miRNAs can cooperate if their binding sites reside in close proximity. To test this and other hypotheses, I present a novel approach, which has been published in Lai *et al.* (2012b), to investigate mechanisms of collective miRNA repression. The approach combines TF and miRNA target prediction algorithms with data from the literature and databases to generate a regulatory map for a chosen target hub. By using this approach, a comprehensive regulatory map for p21 is constructed. Through analysing the map, the network motifs mediated by p21-targeting miRNAs are identified and discussed.

Furthermore, a kinetic model is derived from the p21 regulatory map. The model, validated by experimental data, is further used to investigate the mechanism by which p21 expression is regulated by a pair of cooperative miRNAs. Moreover, the model is used to study the effect of different miRNAs expression profiles in combination with their cooperativity on determining the p21 expression levels for different biological contexts.

4.1 Target hub gene regulation

Genes, combining several TFs in their promoter regions, are referred to as target hubs (Borneman *et al.*, 2006). Shalgi *et al.* (2007) defined the notion of miRNA target hub for genes that are regulated by at least 15 different miRNAs. Such kinds of genes are usually involved in complicated regulatory networks, which are composed of TFs, miRNAs and interacting proteins (Figure 4.1). The complexity of these networks implies important roles of target hub genes in determining cell responses and fates.

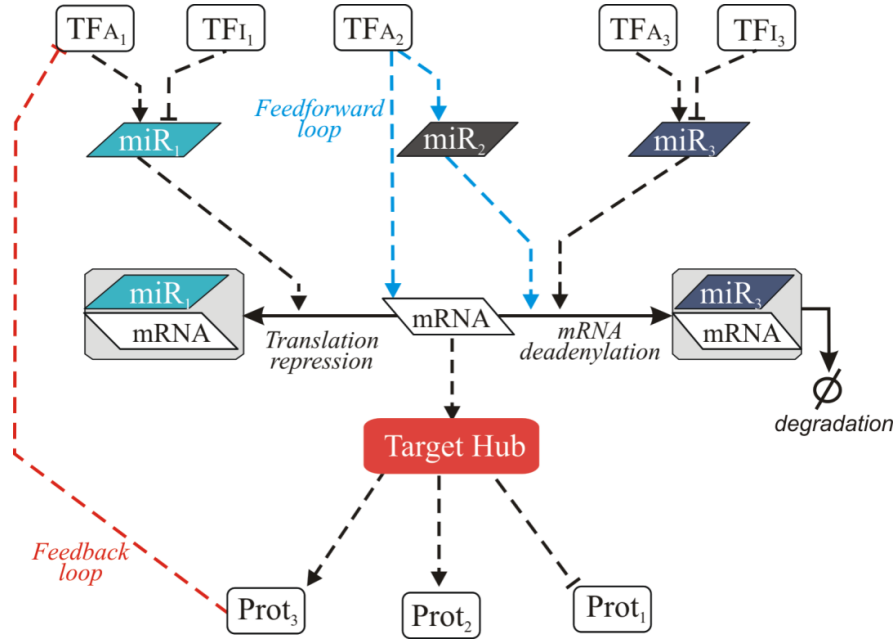


Figure 4.1: A miRNA target hub regulatory network. In such a network, TFs, miRNAs and interacting proteins are involved. TFs can either promote (TF_A) or inhibit (TF_I) the synthesis of the miRNAs and the target hub mRNA. Once transcribed, the target hub mRNA can be post-transcriptionally regulated by multiple miRNAs. These miRNAs can repress target gene expression through translational repression or mRNA deadenylation followed by degradation. Besides, the target hub is highly interconnected with other proteins. Due to the complex interactions among different regulators, such a target hub centred network may have many network motifs like feedback and feedforward loops.

In recent years, at least two groups experimentally proved that pairs of miRNAs, whose binding sites reside in close proximity or partially overlap, show cooperative effect on their targets (Doench and Sharp, 2004; Sætrom *et al.*, 2007). This property adds to the complexity of miRNA target regulation. Sætrom *et al.* (2007) proposed a limited range of 13-35 nt for the distance between the binding start sites for which the phenomenon appears. According to this experimental evidence, we assumed this kind of interaction as plausible and applied it in a kinetic model of the regulation of a miRNA target hub to investigate the dynamic and regulatory consequences of this feature.

p21 (also known as CDKN1A or Cip1/Waf1) is a well-known cell cycle regulator and tumour suppressor (Harper *et al.*, 1993). Specifically, p21 is involved in the G₁ phase cell cycle arrest in response to DNA damage provoked by stress signals. The expression of p21 is dependent on environmental conditions and is transcriptionally regulated through p53-dependent and -independent mechanisms (Gartel and Tyner, 1999). Recently, numerous miRNAs have been identified to regulate the expression of

p21. From 266 predicted miRNAs, Wu *et al.* (2010) validated the ability of a subset of 28 miRNAs to target p21 using a high-throughput luciferase reporter screen. Thus, p21, to our knowledge, is one of the first experimentally verified miRNA target hubs.

In this chapter, I present the research in which we investigate the structure and dynamics of p21-centred network including concerted miRNA-mediated repression of p21 by using a kinetic model. To do so, we make use of target prediction algorithms and data from the literature and databases to construct the regulatory map of p21. Using this map, we find potential 'housekeeping' miRNAs that are promoted by a few TFs but are associated with many distinct cellular functions and identify the feedback and feedforward loops underlying p21 regulation. Based on this map, we derive a quantitative data-driven model to test hypotheses about mechanisms of collective miRNA repression. We computationally detect several pairs of miRNAs that may cooperate in the repression of p21 and experimentally validate the cooperativity between miR-572 and miR-93. We further use these two miRNAs as an example to investigate three hypothetical target regulation mechanisms by multiple miRNAs. We find that one miRNA is sufficient to completely repress a target when highly expressed. However, the same effect can be achieved by two cooperating miRNAs, both of which are only expressed at an intermediate level. In addition, by using the model we predict p21 expression for nine cellular functions for which different miRNA profiles are configured. The model predicts high levels of p21 expression during DNA damage, DNA repair, senescence and migration, and low levels of p21 expression for cell proliferation and apoptosis.

4.2 Materials and methods

The aim of our analysis is to unravel the complex mechanisms by which gene regulatory networks are regulated by multiple miRNAs. We iteratively integrate data from the biomedical literature, high-throughput experiments and biological databases into a kinetic model of miRNA target hub regulation. The kinetic model is then used to formulate and test hypotheses about mechanisms of target regulation and cellular function-related variability. In short, the adopted methodology includes three modules (Figure 4.2): 1) data retrieval; 2) construction and analysis of the regulatory map; 3)

kinetic modelling and simulation of the regulatory map. These modules are discussed in the following sections.

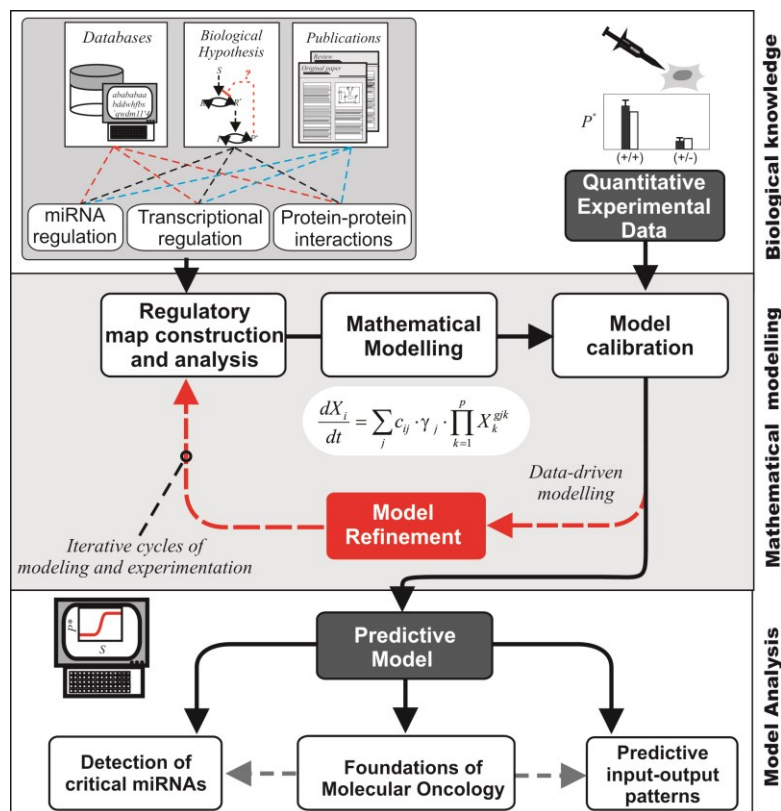


Figure 4.2: Overview of the methodology. Biological knowledge and quantitative data are collected and converted into a mathematical model which can describe the regulatory roles of miRNAs in gene regulatory networks. The adopted methodology considers data retrieval, iterative cycles of model construction, model calibration and simulations.

4.2.1 Data retrieval

Information about protein interactions was extracted from the Human Protein Reference Database (HPRD, release 9.0; Keshava Prasad *et al.*, 2009) and the database STRING (release 9.0; Szklarczyk *et al.*, 2011). A list of experimentally verified TFs for the considered target hub was generated from the literature. This list was complemented by putative TFs that are associated with conserved TF-binding sites (human, mouse and rat) residing in the 5 kilobase (kb) upstream region of the target gene. This information was extracted from the table of TFs with conserved binding sites in the genome browser developed by the University of Santa Cruz (UCSC; Karolchik *et al.*, 2003). Information about miRNA:target interactions can be extracted either from databases of validated interactions, e.g. miRecords (Xiao *et al.*, 2009), Tarbase (Sethupathy *et al.*, 2006) and

miRTarBase (Hsu *et al.*, 2011), or from predicted ones, which can be found in databases like miRWalk (Dweep *et al.*, 2011) and miRGen 2.0 (Alexiou *et al.*, 2010). In the case of p21, we used the information in Wu *et al.* (2010) where a list of predicted p21-regulating miRNAs was subjected to experimental validation. It is noteworthy that there exist other miRNAs than those included in our network that were experimentally confirmed as regulators of p21 expression (Wu *et al.*, 2010; Borgodoff *et al.*, 2010); however, in order to construct a kinetic model focusing on the regulation of p21 by its targeting miRNAs, we considered only those miRNAs for which there are consistent quantitative data describing their repression abilities on p21. A list of TFs controlling the expression of the miRNAs was constructed using information of experimentally proved TFs of miRNAs contained in TransmiR (release 1.0; Wang *et al.*, 2010). In addition, we generated a list of putative TFs of miRNAs with binding sites in the 10 kb upstream region of the miRNA genes using the information from the databases PuTmiR (release 1.0) and MIR@NT@N (version 1.2.1), and from the table of TFs with conserved binding sites in the UCSC genome browser (hg18; Bandyopadhyay and Bhattacharyya, 2010; Le Béchech *et al.*, 2011; Karolchik *et al.*, 2003;). We selected this region following the method in Shalgi *et al.* (2007), where the 10 kb upstream region is indicated as 'putative regulatory region of miRNAs'. For further investigation, we considered only the miRNA TFs that were experimentally verified or predicted in two out of three resources.

4.2.2 Construction and analysis of the p21 regulatory map

We first converted the information described in the previous section into a regulatory network map, which was implemented in SBGN-compliant notation in CellDesigner (Kitano *et al.*, 2005; Funahashi *et al.*, 2008). For assessing the reliability of the network structure, we computed a confidence score for each interaction included in the p21 regulatory map, similar to the procedure used in several interaction databases like STRING, iRefWeb or IntAct. The computed scores ranged between 0 (totally uncertain interaction) and 1 (most reliable interaction), and were established by integrating weighted scores for publications reporting an interaction, experimental method(s) used, interaction type and computational predictions. The scoring system was inspired by the one used in IntAct (Kerrien *et al.*, 2012). A detailed description of how the scores were

calculated is provided in **Appendix 6.2.1**. All the interactions (p21-protein, TF-p21, TF-miRNA and miRNA-p21) displayed in the map and their corresponding scores can be found in **Appendix Table 6.6**.

In our map, the network motifs including a TF that regulates p21 and a p21-targeting miRNA are considered as feedforward loops. Those, in which p21 is repressed by a TF and a miRNA, were classified as coherent feedforward loops. Those, in which p21 is activated by a TF and repressed by a miRNA, were classified as incoherent feedforward loops. Meanwhile, the network motifs including a TF that promotes a targeting miRNA and interacts with p21 were classified as feedback loops. Based on Gene Ontology (GO) terms, we derived tailored TF lists of p21 and its targeting miRNAs for different cellular functions including cell proliferation, apoptosis, immune response, inflammatory response, cell cycle control, DNA damage, cell senescence, DNA repair, cell motility and migration.

For identifying binding sites for the p21-targeting miRNAs we used results of two established target prediction algorithms, miRanda and RNA22 (John *et al.*, 2004; Miranda *et al.*, 2006). The results were filtered for binding sites with at least 7mer seed pairing (wobble pairs were allowed). Target sites are presented in **Appendix Table 6.5** along with their detailed binding motifs.

4.2.3 Model construction and calibration

Based on the regulatory map, a kinetic model was constructed using ODEs. Precisely, the kinetic model considered the mRNA ($mp21$; Equation (4.1)) and protein ($p21$; Equation (4.2)) of the miRNA target hub p21, the p21-targeting miRNAs considered (miR_i ; $i \in (1, \dots, 15)$; Equation (4.3)), and the complexes formed by targeted mRNA and miRNA, $[mp21|miR_i]$ (Equation (4.4)). Altogether, the model is constituted by 32 state variables and 64 parameters

$$\frac{dmp21}{dt} = k_{syn}^{mp21} \cdot f_{act}(TF_{mp21}) - mp21 \cdot (k_{deg}^{mp21} + \sum_i k_{ass}^{complex_i} \cdot miR_i), \quad (4.1)$$

$$\frac{d[mp21|miR_i]}{dt} = k_{ass}^{complex_i} \cdot mp21 \cdot miR_i - k_{deg}^{complex_i} \cdot [mp21|miR_i], \quad (4.2)$$

$$\frac{dmiR_i}{dt} = k_{syn}^{miR_i} \cdot f_{act}(TF_{miR_i}) - miR_i \cdot (k_{deg}^{miR_i} + k_{ass}^{complex_i} \cdot mp21), \quad (4.3)$$

$$\frac{dp21}{dt} = k_{syn}^{p21} \cdot mp21 + k_{deg}^{p21} \cdot p21, \quad (4.4)$$

$$mp21_{Total} = mp21 + \sum_i [mp21|miR_i]. \quad (4.5)$$

For $mp21$, processes considered in the model were its synthesis (k_{syn}^{mp21}) mediated by its TF ($f_{act}(TF_{mp21})$), its degradation (k_{deg}^{mp21}), and its association with a miRNA ($k_{ass}^{complex_i}$). For each miR_i , processes considered were its synthesis ($k_{syn}^{miR_i}$) mediated by its TF ($f_{act}(TF_{miR_i})$), its degradation ($k_{deg}^{miR_i}$) and its association with the p21 mRNA target ($k_{ass}^{complex_i}$). For each $[mp21|miR_i]$, processes considered were its formation by a miR_i and the p21 mRNA ($k_{ass}^{complex_i}$) and its degradation ($k_{deg}^{complex_i}$). For $p21$, processes considered were its synthesis (k_{syn}^{p21}) and degradation (k_{deg}^{p21}). An additional algebraic equation accounting for the total measurable amount of p21 mRNA ($mp21_{Total}$) was also included.

For calibrating the model, the parameter values and initial concentrations of the state variables were set and characterised using the following strategy. The initial concentrations of $mp21$ and $p21$ were set to 1, and this value was their basal expression level, meaning their expression levels stay at 1 when no miRNA repression occurs. The half-lives of the p21 protein and mRNA were used to characterise the values of their degradation rate constants (k_{deg}^{mp21} and k_{deg}^{p21}), and their synthesis rate constants values (k_{syn}^{mp21} and k_{syn}^{p21}) were fixed using the same value to ensure $mp21$ and $p21$ show their basal expression levels when no miRNAs are expressed. Recent reports indicated that miRNAs' half-lives vary under different cellular contexts (Bhattacharyya *et al.*, 2006; Hwang *et al.*, 2007; Krol *et al.*, 2010); however, due to the lack of experimental data measuring individual miRNA half-lives in different cellular contexts, we assumed the same degradation rate constant ($k_{deg}^{miR_i} = 0.0289 \text{ hr}^{-1}$ i.e. $t_{1/2}=24 \text{ hr}$) for all the miRNAs considered in the model. This assumption is supported by the evidence that miRNAs are rather stable molecules with half-lives of more than 24 hr (Kai and Pasquinelli, 2010).

As explained in **Chapter 1.2.1** miRNAs can repress gene expression through two main mechanisms in animals. During the modelling process, we made different assumptions that are specific for each mechanism. In case of translation repression, the

degradation rate constant of the mRNA of p21 is not affected by miRNA, and thus we assumed $k_{deg}^{complex_i} = k_{deg}^{mp21}$. In case of mRNA deadenylation followed by degradation, as in this mechanism miRNAs can promote the degradation of target mRNAs, we assumed $k_{deg}^{complex_i} > k_{deg}^{mp21}$. We extracted quantitative data from Wu *et al.* (2010), in which the p21 mRNA and protein levels were measured 48 hr after transfection of individual p21-targeting miRNAs into human embryonic kidney 293 cells. Depending on the repression mechanism of the transfected miRNA, we used these data to estimate $k_{ass}^{complex_i}$ or $k_{ass}^{complex_i}$ and $k_{deg}^{complex_i}$ for each $[mp21 | miR_i]$. Because of the large amount of transfected miRNAs, we assumed that the endogenous production of these miRNAs is negligible ($k_{syn}^{miR_i} = 0$) during parameter estimation. The parameters were estimated by using an iterative method combining global (particle swarm pattern search algorithm; Vaz and Vicent, 2007) and local (downhill simplex method in multidimensions; Press *et al.*, 2007) optimisation algorithms. For each miR_i considered in the model, the method minimises the distance between model simulations and experimental data using the following cost function

$$F_{cost}^{miR_i} = \frac{[mp21_{sim}^{miR_i}(t) - mp21_{exp}^{miR_i}(t)]^2}{(\delta_i^{mp21})^2} + \frac{[p21_{sim}^{miR_i}(t) - p21_{exp}^{miR_i}(t)]^2}{(\delta_i^{p21})^2}, i \in [1, \dots, 15] \quad (4.6)$$

where $mp21_{sim}^{miR_i}(t)$ and $mp21_{exp}^{miR_i}(t)$ represent the simulated p21 mRNA and protein expression levels for each miR_i at time point t . $p21_{sim}^{miR_i}(t)$ and $p21_{exp}^{miR_i}(t)$ represent the measured value for each miR_i at time point t , and their standard deviations are δ_i^{mp21} and δ_i^{p21} . Here, t is equal to 48 hr, at which the expression levels of the p21 protein and mRNA were measured after overexpression of the individual miRNAs in embryonic kidney 293 cells (Wu *et al.*, 2010). Furthermore, by using the profile likelihood analysis as introduced in **Chapter 2.2.2**, we calculated the 95% confidence interval for the estimated parameter values. As shown in **Appendix Table 6.2**, for most estimated parameters, their values have finite confidence intervals, meaning that they are identifiable. Only a few parameters show infinite upper bounds for their estimated values, meaning that they are practically unidentifiable. This could be caused by insufficiency or low quality of experimental data, which are used parameter estimation;

reducing the standard deviation or error of the experimental data can efficiently improve the identifiability of these parameters.

As shown in Figure 4.3, after model calibration the simulation results can correctly reproduce most of experimental data; however, in case of some miRNAs, namely miR-298, miR-208a, miR-132 and miR-28-5p, the agreements between model simulations and data are not as good as the other miRNAs. In these cases, the measured p21 mRNA expression after transfection of large amount of the corresponding miRNAs is higher than the control case, in which the p21 mRNA expression was measured without transfection of extra individual miRNAs. Given its structure, the model cannot capture this behaviour, which may be caused by experimental noise or unknown regulatory mechanisms. The characterised parameter values and the initial concentrations of the model variables can be found in **Appendix 6.2.2**.

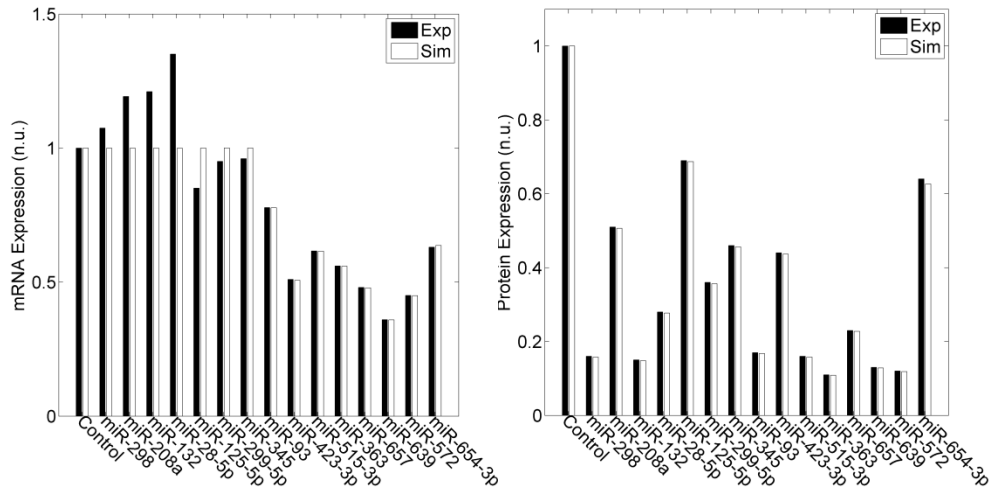


Figure 4.3: Fitting the model to the experimental data. The model parameters were numerically calculated using optimisation algorithms that minimise the distance between model simulations (Sim) and experimental data (Exp). The measured expression levels of the p21 mRNA (left) and protein (right) after overexpression of the indicated miRNAs was compared with the model simulations. The values were normalised to the scenario (Control) in which the expression levels of p21 protein and mRNA were measured when all the miRNAs were normally expressed (n.u.: normalised unit).

4.2.4 Experimental verification for microRNA cooperativity

For validating the kinetic model, we performed additional experiments. Precisely, SK-Mel-147 cells were transfected with mature miRNA mimics of miR-572 and miR-93. The miRNA mimics were transfected either individually at a concentration of 100 nM or in combination at 50 nM concentration. Cells were pulse-treated with 250 nM of the genotoxic substance doxorubicin and protein lysates were collected at 0, 2, 4, 6, 8, and

24 hr after treatment. Expression levels of p21 were measured using immunoblotting as explained in **Appendix 6.3**.

4.3 Results

4.3.1 Analysis of the p21 regulatory map

According to the approach described in the previous section, biomedical knowledge about p21 regulation retrieved from the literature and databases was integrated into a regulatory map (Figure 4.4; the high resolution map is available at www.sbi.uni-rostock.de/resources/software/target-hub). The map constructed in the software CellDesigner provides an up-to-date summary of information concerning the transcriptional and post-transcriptional regulation of p21. Using CellDesigner, the regulatory map is compliant with the Systems Biology Graphical Notation (SBGN; Le Novère *et al.*, 2009). In addition, the confidence score for each interaction in the map was calculated. These confidence measures were established integrating weighted scores for publications reporting an interaction, experimental method(s) used, interaction types and computational predictions (**Appendix Table 6.6**).

Overall, the map suggests a complex regulation of the miRNA target hub p21 at the transcriptional and post-transcriptional levels. According to our analysis, certain TFs, including EGR1 and SP1, promote the expression of groups of miRNAs regulating p21. This supports the hypothesis that miRNA cooperativity plays a role in the repression of p21. Further GO analysis shows that some of the cellular functions, in particular cell proliferation, apoptosis, immune response and cell cycle, are prominent in the regulation of the p21-targeting miRNAs by TFs (Table 4.1). We found that some miRNAs (e.g. miR-345) are regulated by a large number of TFs and associated with a small number of cellular functions, while others (e.g. miR-93) are regulated by a small number of TFs and associated with a large number of cellular functions.. This finding implies that miRNAs like miR-345 can be considered as 'housekeeping' miRNA and miRNAs like miR-93 can be considered as cellular function-specific miRNAs (Table 4.1). Moreover, distinctive regulation of p21 is implemented by the TFs associated with certain cellular functions such as inflammatory response or cell cycle. This suggests different degrees of p21 repression by miRNAs for different cellular functions (Table 4.1).

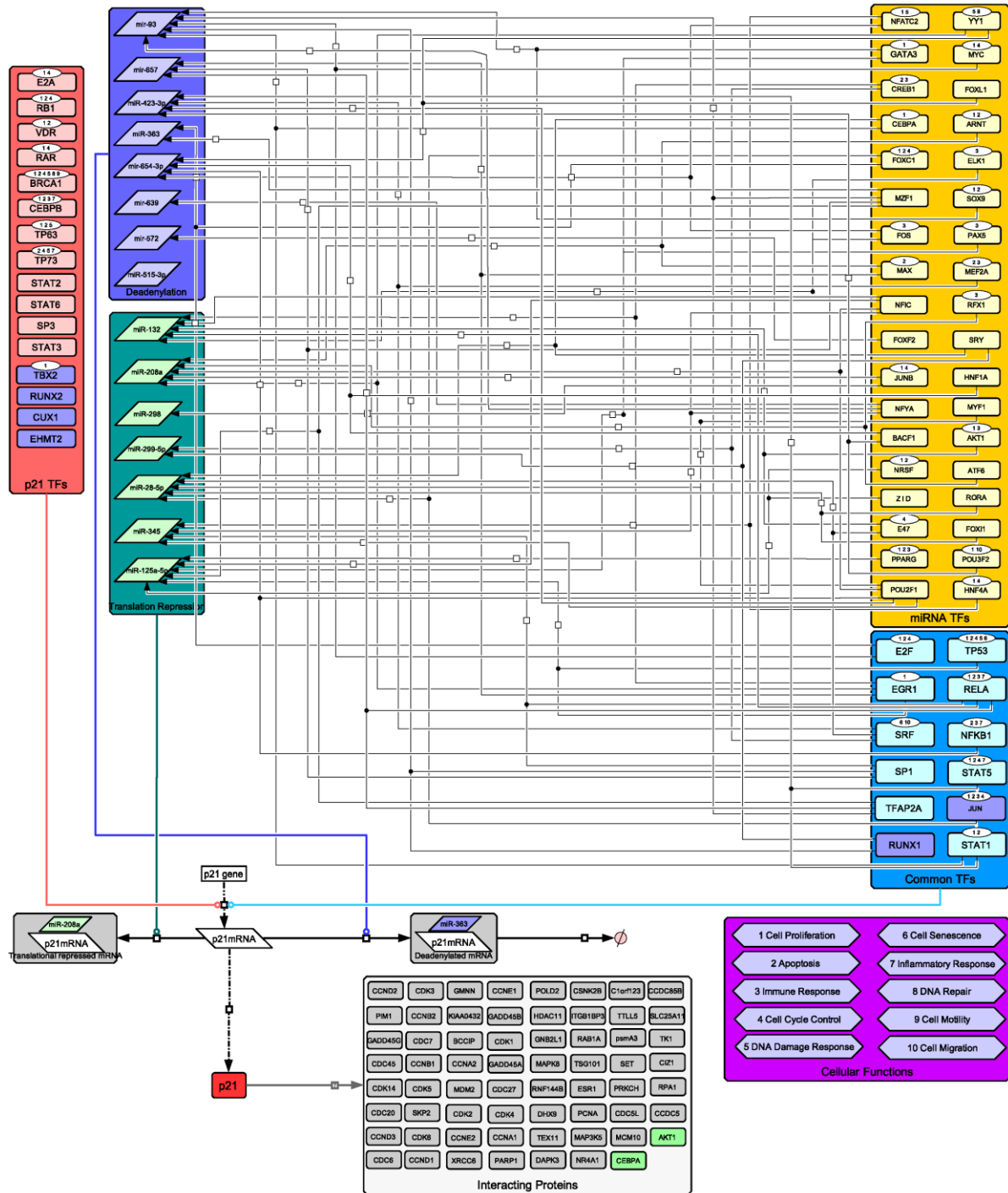


Figure 4.4: The p21 regulatory map. The map is composed of several big size blocks, and each of them represents a kind of molecules involved in the interactions (solid lines) derived from the literature and databases. In the big blocks, small blocks represent individual components. miRNAs were classified into two groups according to the mechanisms by which p21 is repressed: target mRNA deadenylation followed by degradation (dark blue box) and translation repression (green box). TFs were divided into three groups: p21's TFs (red), the p21-targeting miRNAs' TFs (yellow) and their common TFs (light blue). The TFs of p21 were further classified into two types: promoters and inhibitors (dark blue). The interacting proteins of p21 appear in grey boxes, and among them two small green boxes account for putative feedback loops (e.g. p21→AKT1→miR-132→p21). The purple boxes account for cellular functions, and the corresponding functions for TFs are specified by indexes above TF boxes.

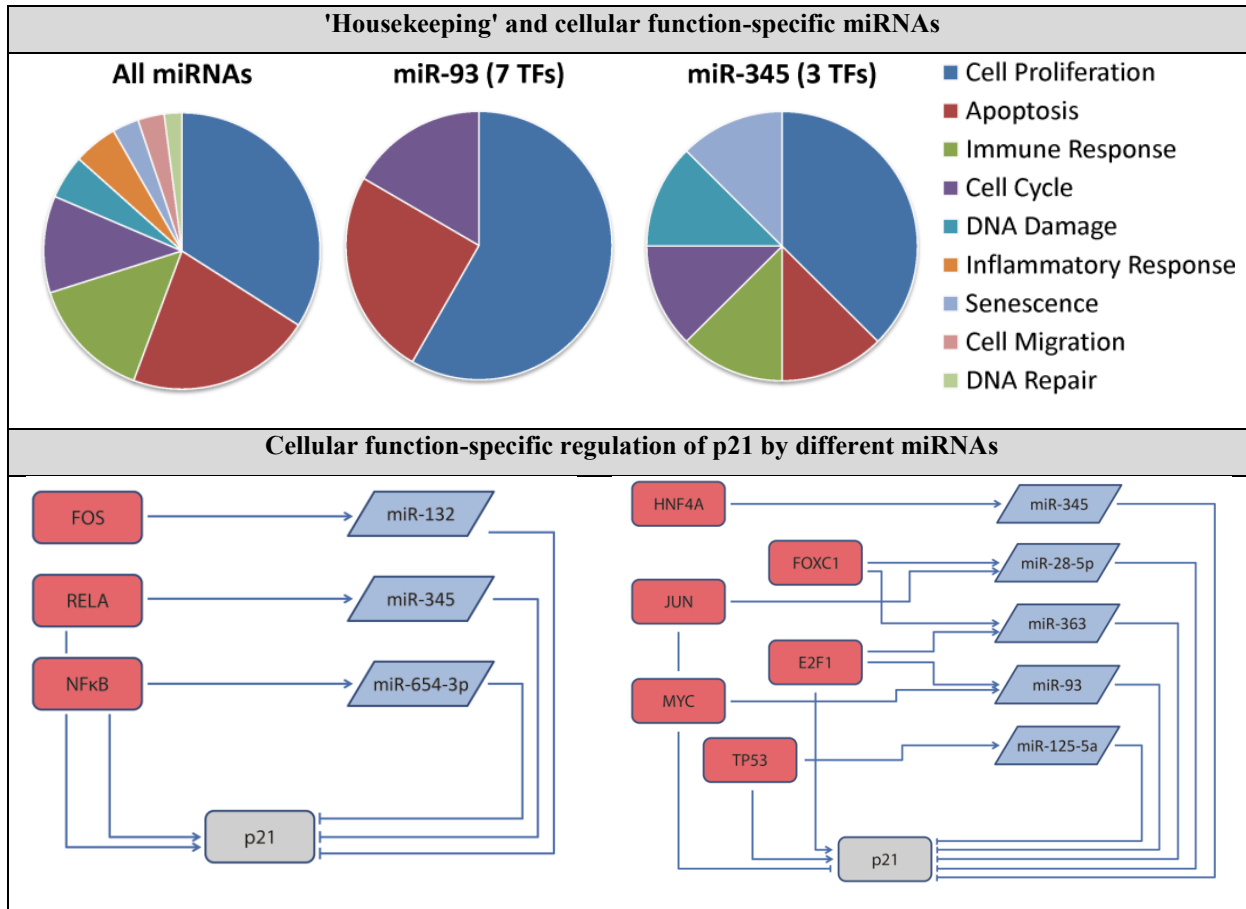


Table 4.1: GO analysis of the p21 regulatory map. Top: The cellular functions associated with the p21-targeting miRNAs were extracted from the GO terms of their corresponding TFs. For example, RELA was predicted to be a TF of miR-345 and its GO terms contained several cellular functions (e.g. cell proliferation, apoptosis, immune response and inflammatory response). Accordingly, miR-345 was considered to be associated with these cellular functions as well. The size of slices is scaled by the number times that the cellular functions appear in the TFs' GO terms. The number of the miRNAs' TFs was indicated in the brackets. **Bottom:** For different cellular functions such as inflammatory response (left) and cell cycle (right), different TFs regulate p21 directly and indirectly through different miRNAs.

4.3.2 Identification of network motifs

Different network motifs involving miRNAs, TFs and other signalling proteins were described in the literature (Shalgi *et al.*, 2007; Osella *et al.*, 2011; Tsang *et al.*, 2007). These motifs contain feedback loops, e.g. direct miRNA inhibition of its own TFs, and feedforward loops, e.g. a common target gene shared by a miRNA and its TF (Mangan and Alon, 2003). Our map reveals 30 network motifs in total. This includes 27 feedforward loops integrated by TFs that regulate the expression of p21 and its targeting miRNAs, which are summarised in Table 4.2. The feedforward loops were further categorised into 24 incoherent and 3 coherent feedforward loops. In a coherent feedforward loop, p21 is consistently regulated by a TF, which directly inhibits p21 and indirectly represses p21 by activating a p21-targeting miRNA (Table 4.2). This particular feedforward loop, where two inhibitors independently repress the target, is associated with a delay or extension in the target repression termination for transient stimuli (Mangan and Alon, 2003). Conversely, in an incoherent feedforward loop, p21 is oppositely regulated, e.g. when a TF directly activates p21 and indirectly represses it by activating its targeting miRNA (Table 4.2). This network motif can provoke acceleration in the target repression initiation; for the case of a step-like TF activation the system can generate a pulse response in p21 mRNA and protein levels (Mangan and Alon, 2003).

p21 has dual roles during the cell cycle process: under a non-stressed condition, p21 is expressed low and promotes cell cycle progression; under a stressful condition, like DNA damage is happening, p21 expression is increased through p53-dependent pathways and it becomes a cell cycle inhibitor (Jung *et al.*, 2010). Our results predict that the tumour suppressor p53 together with miR-125a could regulate p21 through an incoherent feedforward loop (Table 4.2). Besides, miR-125a-5p is downregulated in non-small lung cancer cells (Jiang *et al.*, 2010). This suggests that for some cancer-associated phenotypes the feedforward loop formed by p53, p21 and miR-125a-5p is deactivated. The model simulations suggest that the suppression of the feedforward loop can favour cancer progression by delaying the initiation of p21-triggered cell cycle arrest after responding to DNA damage (Table 4.2).

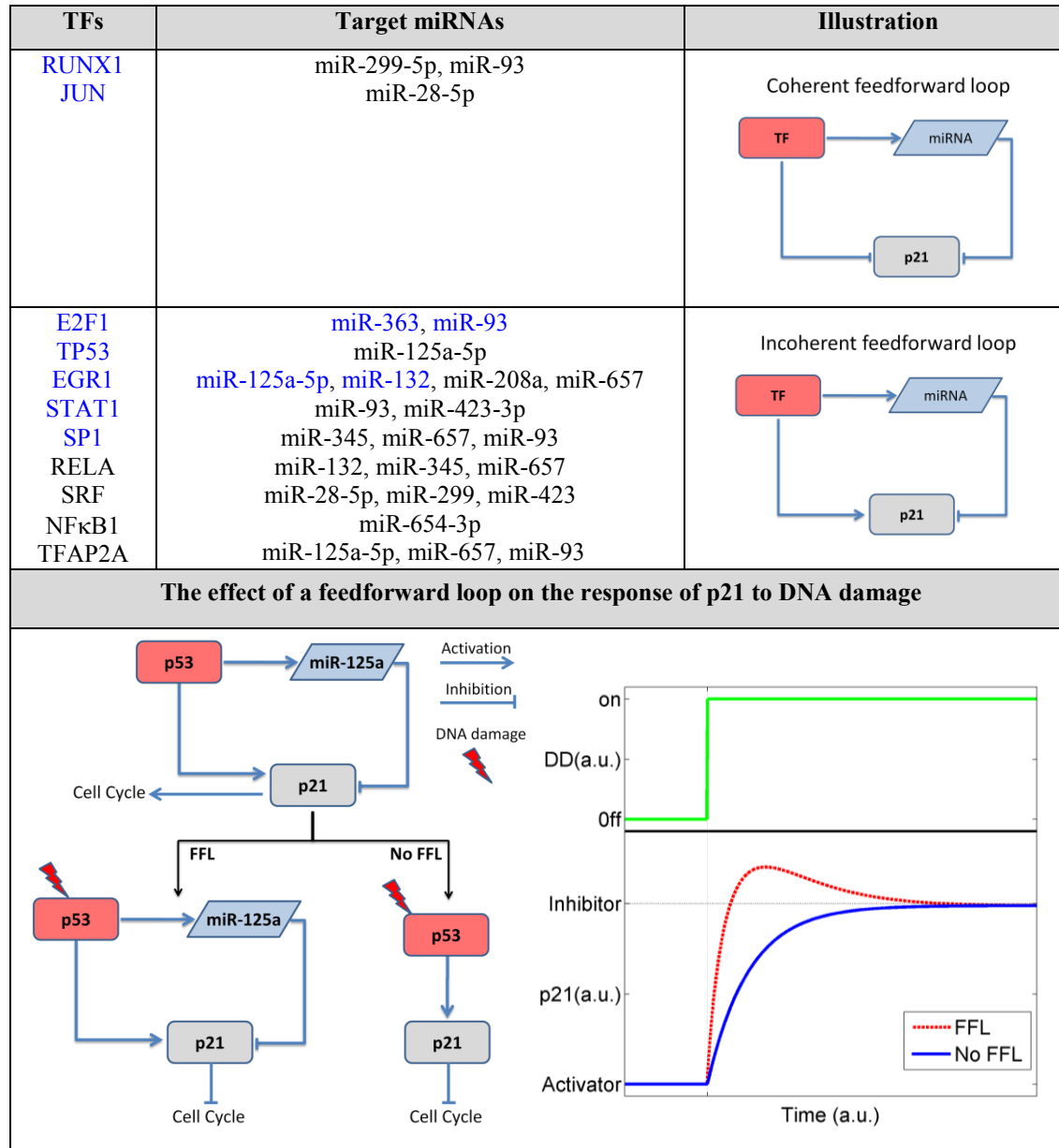


Table 4.2: Identification and analysis of miRNA-mediated network motifs. Top: Feedforward loops formed by p21, p21-targeting miRNAs and their common TFs. The TFs are either experimentally verified (blue) or predicted (black) to promote p21 expression. The miRNAs experimentally verified to be promoted by the TFs were coloured in blue, whereas coloured in black if predicted. The plots describe the dynamic characteristics of p21 in a feedforward loop (blue solid lines) and a simple regulation (dashed lines). In the simple regulation, only the interaction between the TF and p21 is reserved. **Bottom left:** Illustration of the dual roles of p21 during cell cycle. In response to DNA damage, the expression p53 is upregulated, and it promotes the expression of p21 and miR-125a-5p. The increasing expression of p21 makes it become an inhibitor from an activator for cell cycle. The different expression of miR-125a-5p can lead to different responses of p21 to DNA damage. In wild type cells miR-125a-5p is normally expressed, so the interactions among p53, p21 and miR-125a-5p form a feedforward loop (FFL). However, in non-small lung cancer cells, the feedforward loop cannot be formed due to the downregulation of miR-125a (No FFL). **Bottom right:** Model simulations for the response of p21 to DNA damage for FFL and No FFL. We used a step-like function to characterise the DNA damage response (DD). Compared to No FFL, the response of p21 to DNA damage was quicker and stronger for FFL.

4.3.3 Kinetic modelling of p21 regulation by multiple miRNAs

We derived a kinetic model with a structure suitable to investigate the hypothesis of enhanced miRNA repressive ability associated with miRNA binding sites in close proximity on the 3' UTR of the target mRNA. Enhanced repression in this context originates from a cooperative interaction between two miRNAs whose binding sites are in the optimal proximity range (13-35 nt; Sætrom *et al.*, 2007). To test the consequences of this hypothesis, we first predicted the binding sites of the p21-targeting miRNAs on the 3' UTR of the p21 mRNA; then, we derived a kinetic model to analyse mechanisms for pairs of miRNAs repressing p21. Figure 4.5 shows the matrix of potentially cooperating and non-cooperating miRNA pairs targeting p21. Our results indicate that several pairs of miRNAs targeting p21 meet the criteria as described in previous studies (Doench and Sharp 2004; Sætrom *et al.*, 2007), and thus can cause enhanced target repression. The only exception is miR-639 with a single binding site that does neither overlap nor is in close proximity to any other miRNA binding site.

Using the approach previously described in section 4.2.3 and based on the regulatory map, we derived a kinetic model using ODEs, which accounts for the dynamics of $p21$, $mp21$, miR_i and $[mp21|miR_i]$ over time. To substantiate the cooperative effect associated with the proximity of miRNA binding sites, we defined a group of new state variables ($[mp21|miR_i|miR_j]$), which account for the ternary complexes composed by the p21 mRNA and two putatively cooperating miRNAs (miR_i and miR_j). For these new variables, processes considered are the association of p21 mRNA with miR_i and miR_j into the complex ($k_{ass}^{co-complex_{i,j}}$) and their degradation ($k_{deg}^{co-complex_{i,j}}$). The corresponding ODEs, which complement the already established equations for the particular cases of miRNA cooperativity, are listed below

$$\begin{aligned} \frac{dmp21}{dt} = & k_{syn}^{mp21} \cdot f_{act}(TF_{mp21}) - mp21 \cdot (k_{deg}^{mp21} \\ & + \sum_i k_{ass}^{complex_i} \cdot miR_i + \sum_{i,j} k_{ass}^{co-complex_{i,j}} \cdot miR_i \cdot miR_j), \end{aligned} \quad (4.7)$$

$$\begin{aligned} \frac{d[mp21|miR_i|miR_j]}{dt} = & k_{ass}^{co-complex_{i,j}} \cdot mp21 \cdot miR_i \cdot miR_j \\ & - k_{deg}^{co-complex_{i,j}} \cdot [mp21|miR_i|miR_j]. \end{aligned} \quad (4.8)$$

Experimental results showed that a stronger repression of the target gene can happen when two miRNA binding sites on the target mRNA are in close proximity (Doench and Sharp, 2004; Saetrom *et al.*, 2007). Thus, we assumed a stronger association rate constant for the complex $[mp21|miR_i|miR_j]$ which is equal to the aggregation of their individual association rate constants ($k_{ass}^{co-complex_{i,j}} = k_{ass}^{complex_i} + k_{ass}^{complex_j}$). Similarly, the degradation rate of the complex $[mp21|miR_i|miR_j]$ was assumed to be the aggregation of degradation rate constants of single miRNA binding complexes ($k_{deg}^{co-complex_{i,j}} = k_{deg}^{complex_i} + k_{deg}^{complex_j}$). The corresponding parameter values for the putative miRNA cooperativity can be found in **Appendix Table 6.2**.

For validating the model and verifying the method used to predict miRNA cooperativity, we picked out a pair of putative cooperative miRNA namely miR-572 and miR-93 and carried out some experiments. These two miRNAs may cooperate to regulate p21 according to our analysis (the distance of their binding sites in p21 3' UTR is 24 nt). We transfected melanoma cells with the mature miRNA mimics of the two miRNAs either individually (100 nM) or in combination (50 nM each) and further treated the cells with doxorubicin, a genotoxic-stress inducing agent. The expression levels of p21 were measured by immunoblotting at different time points (0, 2, 4, 6, 8, 24 hr) after doxorubicin treatment. By doing so, we obtained the p21 response after genotoxic stress in four scenarios: 1. endogenous miRNA expression; 2. only miR-572 overexpressed (100 nM); 3. only miR-93 overexpressed (100 nM); and 4. both miRNAs partially overexpressed (50 nM for each miRNA). Finally, we simulated the model of seven ODEs by configuring it to the designed experiments and compared the model simulations with the experimental data (the set of ODEs and parameter values can be found in **Appendix 6.2.2**).

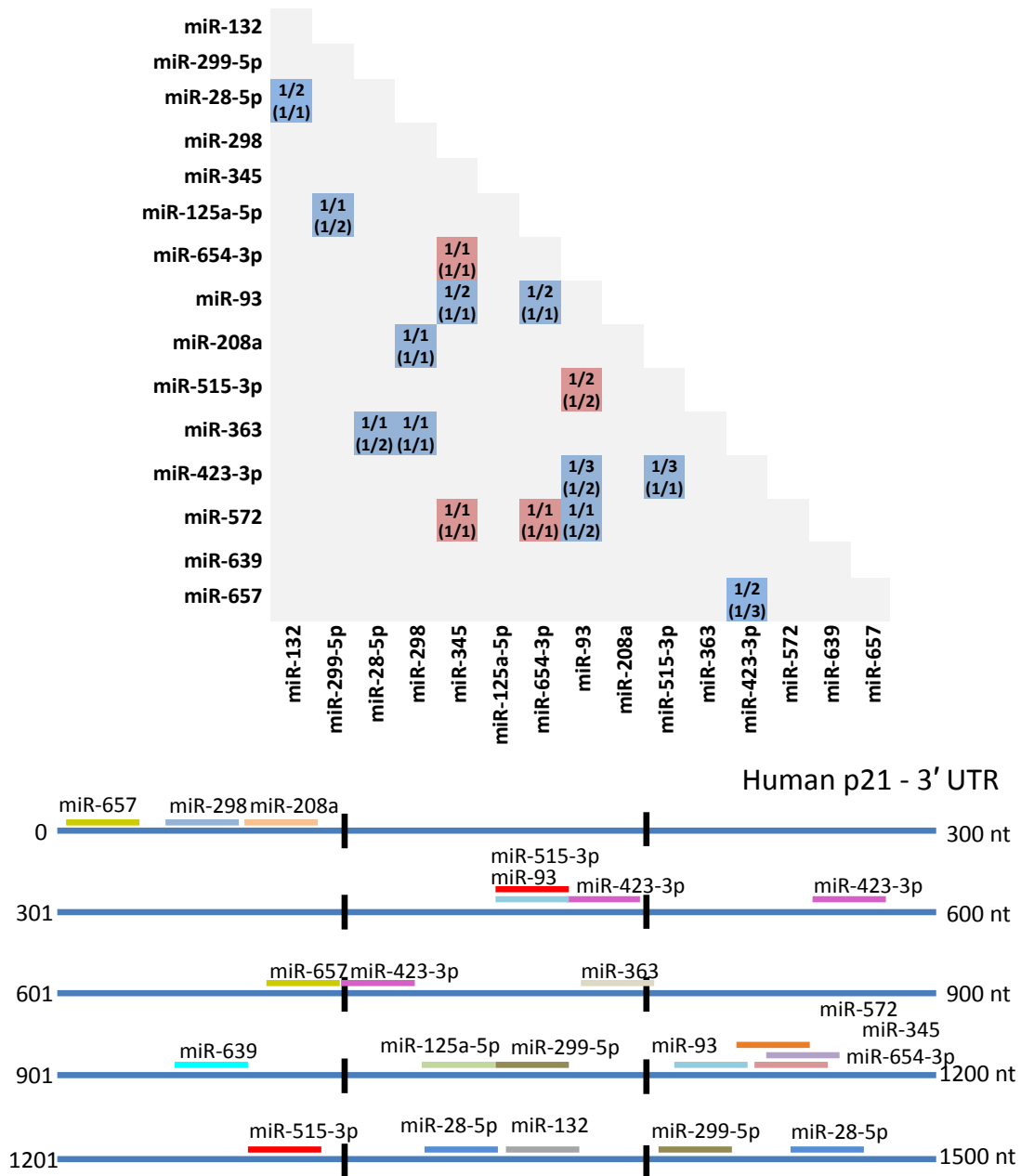


Figure 4.5: Identification of cooperative miRNA pairs for p21. **Top:** Matrix of putative cooperating miRNAs. The intersections of pairs of miRNAs denote their potential for cooperation. Gray cells indicate a non-interacting pair, blue cells denote potentially cooperating pairs based on binding site proximity range (13-35 nt) defined by Saetrom *et al.* (2007). Red cells, however, indicate that cooperation cannot be established due to binding sites with extensive overlap or miRNA pairs that share the same binding site. The figures inside the cells specify the fraction of binding sites interacting with the respective partner (the number of cooperative binding sites/the number of total binding sites). The figures outside and inside the brackets corresponds to the miRNAs on the y- and x-axis, respectively. **Bottom:** Binding sites of the miRNAs in the 3' UTR of the p21 mRNA. The detailed binding motifs for the p21-targeting miRNAs can be found in **Appendix Table 6.5**.

As shown in Figure 4.6 top, the model simulations are in good agreement with the experimental observations for p21 response after genotoxic stress. Overall, the overexpression of miR-572 or miR-93 is able to reduce the upregulation of p21 by genotoxic stress. The differences in p21 responses are due to the different repression efficiencies of the two miRNAs. Furthermore, the data indicates that the combined partial overexpression of both miRNAs induces stronger downregulation of the p21 response. These results verify the hypothesis of cooperativity for this pair of miRNAs. This not only validates the model but also proves the ability of our method to detect and characterise miRNA cooperativity.

To further test the predictive ability of the model, we used it to predict miRNA-mediated p21 expression patterns in different tissues. First, we extracted and normalised the tissue-specific miRNA expression profiles from the database miRNAmap (release 2.0; Hsu *et al.*, 2008). Second, for each miRNA expression profile obtained, we computed the steady-state levels of p21 by changing accordingly the initial concentrations of the corresponding miRNAs in our model. Finally, we retrieved the qualitative information about the p21 expression levels in different tissues from the database ArrayExpress (version as of January 2012; Brazma *et al.*, 2006). To make the simulation results and experimental data comparable, the tissue-specific p21 expression levels were discretised in two categories: low and high (see **Appendix 6.2.2** for detailed explanation). Assuming that epigenetic regulation exerted by miRNAs plays an important role for tissue-specific protein expressions, our model is able to correctly predict the relative p21 expression levels in 9 of 12 tissues (75%; Figure 4.6 bottom).

4.3.4 Computational analysis of miRNA cooperativity

Using the calibrated and validated model, we hypothesized three mechanisms for the target regulation conducted by pairs of miRNAs: i) **independent target regulation**, in this case the target site proximity does not produce an enhanced repression (represented by setting $k_{ass}^{co-complex_{i,j}} = 0$); ii) **interdependent target regulation**, in which the combined binding of both miRNAs is required to repress the target ($k_{ass}^{complex_i} = 0, k_{ass}^{complex_j} = 0$ and $k_{ass}^{co-complex_{i,j}} > 0$); and iii) **synergistic target regulation**, which is a combination of the previous two target regulation mechanisms ($k_{ass}^{complex_i} >$

$0, k_{ass}^{complex_j} > 0$ and $k_{ass}^{co-complex_{i,j}} > 0$). By using the cooperative miRNA pair miR-93 and miR-572 whose corresponding variables are miR_8 and miR_{14} in the model, we investigated the consequences of the three mechanisms for target repression. Figure 4.7 shows the course of the p21 protein expression levels for the three mechanisms upon different initial concentrations of the two miRNAs, $miR_8(0)$ and $miR_{14}(0) \in [10^{-1}, 10^2]$.

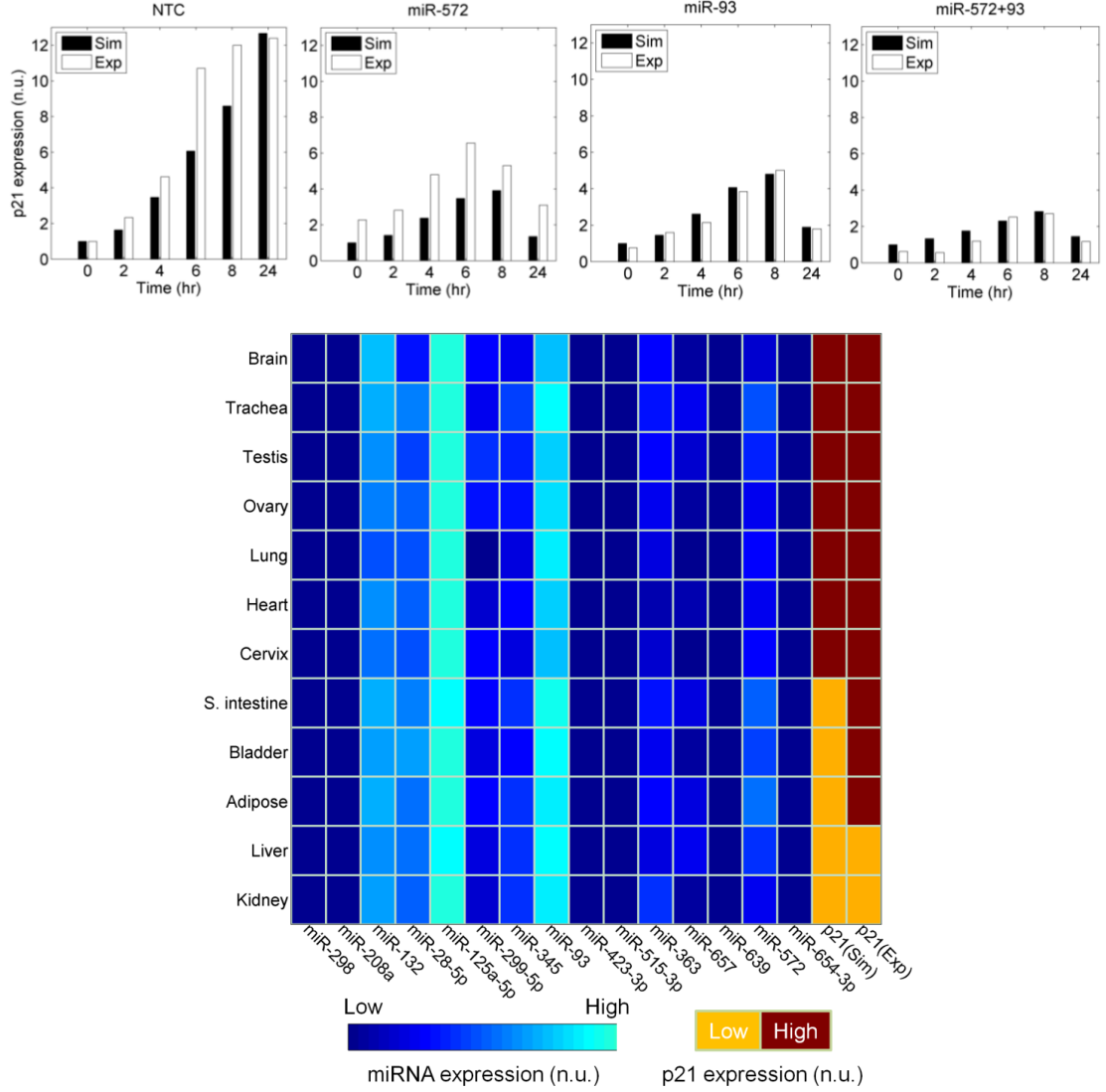


Figure 4.6: Model validation. **Top:** Reduction of the genotoxic-induced upregulation of p21 by miR-572 and miR-93. The experimental data of p21 protein expression levels in response to genotoxic stress (Exp) were compared with the model simulations (Sim) in four biological scenarios: 1) both miRNAs are normally expressed (NTC); 2) miR-572 is over expressed (miR-572); 3) miR-93 is over expressed (miR-93); 4) both miRNAs are over expressed (miR-572+93). **Bottom:** Tissue-specific p21 expression levels mediated by its targeting miRNAs. The model simulations (p21(Sim)) correctly predicted the p21 expression levels in 9 of 12 tissues as compared to the experimental data (p21(Exp)).

In case of independent target regulation (Figure 4.7 left), the model predicts that sufficient upregulation of one of the two miRNAs is able to induce the complete repression of p21. In combination with the upregulation of a second miRNA a reduced overall level of the miRNAs is required to silence p21 ($p21 = 0$ n.u.). In contrast, the simulations for interdependent target regulation suggest that effective gene silencing is possible only when both miRNAs are sufficiently upregulated. In other words, the overexpression of a single miRNA is not able to induce gene silencing, but rather results in a low miRNA-specific gene downregulation (Figure 4.7 middle). This mechanism may explain the relatively poor repression ability of some miRNAs when they are experimentally overexpressed alone (Selbach, 2008). Finally, in synergistic target regulation gene silencing can be achieved in two ways (Figure 4.7 right): i) high overexpression of any of the two miRNAs (at least 10^2 fold upregulation); or ii) combined modest upregulation of the two cooperative miRNAs, which reduces the amount of the miRNAs required for achieving gene silencing by at least one order of magnitude. Besides, through this mechanism, the system becomes more sensitive to miRNA expression changes both for individual as well as combined miRNA down- and upregulation.

Based on the previous results (Figure 4.6 top), we can say that synergistic target regulation is most likely the mechanism by which miR-572 and miR-93 regulate the expression of p21. Therefore, we further investigated this mechanism for different strengths of their cooperativity (named as K) and simulated four scenarios with different initial miRNA concentrations ($[miR_8(0), miR_{14}(0)]$): 1) both miRNAs are normally expressed ($[1,1]$); 2) miR-93 is normally expressed, miR-572 is overexpressed ($[1,10]$); 3) miR-93 is overexpressed, miR-572 is normally expressed ($[10,1]$); 4) both miRNAs are overexpressed ($[10,10]$). For each scenario, we defined an interval accounting for the strength of the miRNA cooperativity ($K = k_{ass}^{co-complex_{8,14}} \times [10^{-5}, 10^5]$). We simulated the model, assigning values to K in steps of $10^{0.25}$; and for every round of simulation, we computed the expression levels of p21 at 48 hr (Figure 4.8 top). According to the value of K , we divided the emerging simulation results into three regions: region I, in which the cooperative target repression induced by the pair of miRNAs is negligible when compared with the p21 repression by the independent

miRNAs; region III, in which the repression of p21 is mainly driven by the cooperative effect of the two miRNAs; and region II, in which independent and cooperative target regulation contribute equally.

When the value of K is very small (i.e. the miRNA cooperativity is weak; Figure 4.8 top, region I), miR-572 and miR-93 repress p21 gene expression independently; the strongest p21 repression is achieved when both miRNAs are overexpressed (purple triangles); overexpression of one of the two miRNAs leads to different levels of target repression due to their different repressive abilities; here, miR-572 induces stronger repression (red diamonds) compared to miR-93. For very big values of K (i.e. the miRNA cooperativity is strong; Figure 4.8 top, region III), the p21 repression saturates and enters into the interdependent target regulation mechanism in which the cooperative interaction overcomes the repression by individual miRNAs; p21 silencing is achieved when both miRNAs are overexpressed (purple triangles). For normal values of K (i.e. the miRNA cooperativity is moderate; Figure 4.8 top, region II), the performance of the target repression increases gradually; the most remarkable and steep decrease in p21 expression levels can be observed when both miRNAs are overexpressed (purple triangles). The results in region II suggest that active modulation of miRNA cooperativity can play an important role in determining the efficacy of target repression. In line with this, some RBPs like FMRP or PUF have been experimentally proved to enhance target repression by interacting with the miRISCs, while others (e.g. DND1 and HuR) have been reported to counteract miRNA-mediated repression (Krol *et al.*, 2010). Taken together, we hypothesized that the activity of those RBPs in combination with the repression by multiple miRNAs can induce a tunable-like target repression. According to this, the mechanism of synergistic target regulation could induce a sophisticated regulation of miRNA targets, in which the regulation by RBPs shifts the performance of target repression from one region to another (Figure 4.8 bottom).

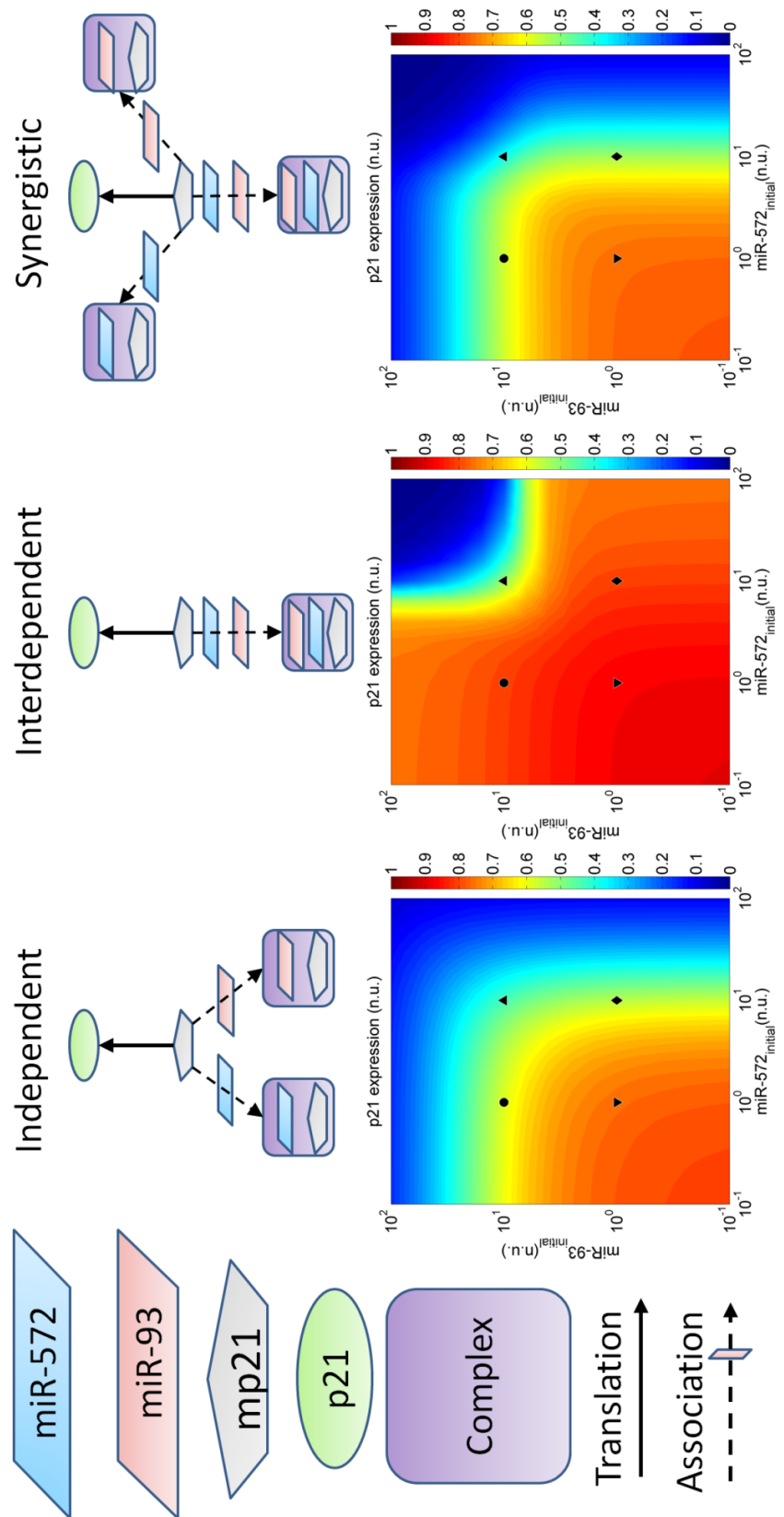


Figure 4.7: Computational analysis of the p21 regulation mechanisms by miR-572 and miR-93. For each depicted target regulation mechanism, the p21 expression level was computed for different combinations of the initial concentrations of miR-93 and miR-572. The black symbols stand for four different scenarios: both miRNAs are normally expressed ([1, 10], \blacktriangledown); miR-572 is overexpressed ([10, 1], \bullet); both miRNAs are overexpressed ([10, 10], \blacktriangle). To make our result comparable with the experimental results generated by Wu *et al.* (2010), we computed the expression level of p21 protein at 48 hr. The legend bar represents the p21 expression levels ranging from basal levels (1) to full repression (0).

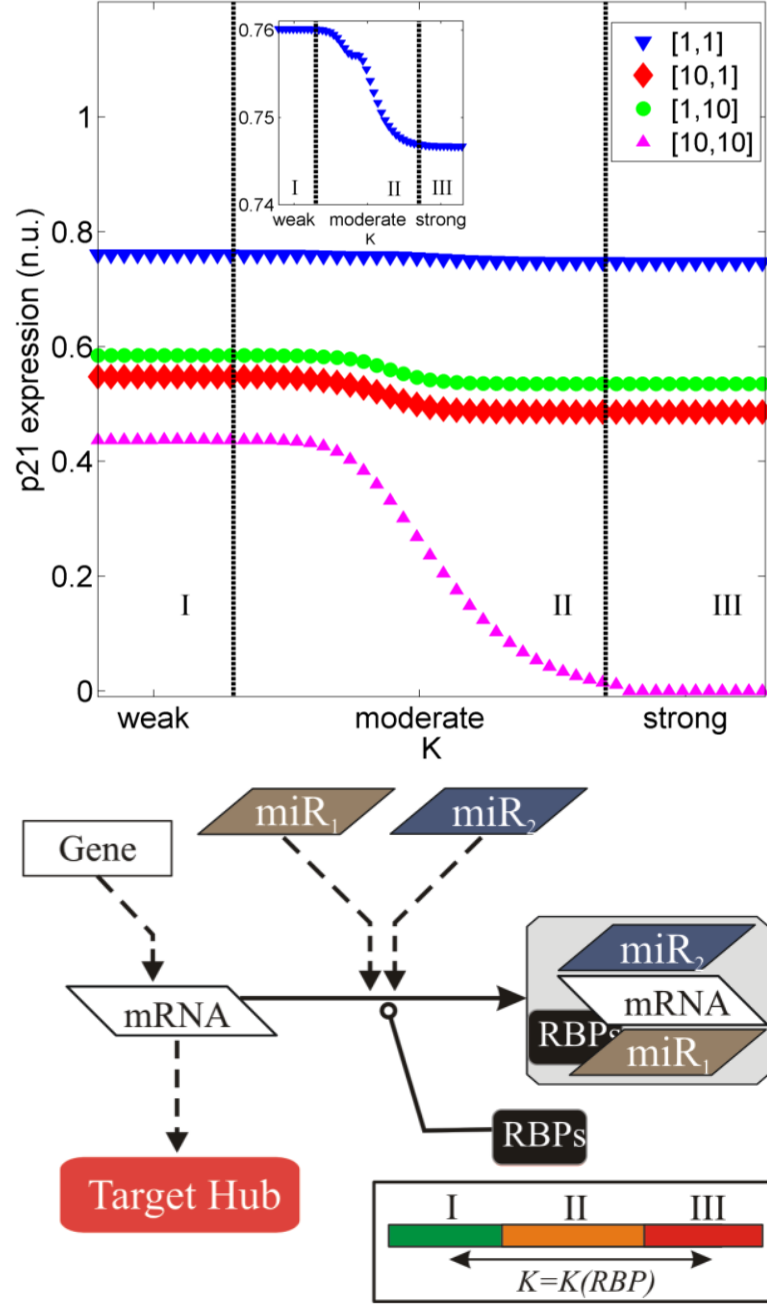


Figure 4.8: Computational analysis of miRNA cooperativity. **Top:** The p21 expression levels at different strengths of cooperativity (K) between miR-93 and miR-572. The dashed vertical lines represent the thresholds of K , for which the repression of p21 by the two miRNAs displays different behaviours. The different symbols correspond to different miRNA initial concentration scenarios: both miRNAs are normally expressed ($[1, 1]$, \blacktriangledown); miR-572 is overexpressed ($[1, 10]$, \blacklozenge); miR-93 is overexpressed ($[10, 1]$, \bullet); both miRNAs are overexpressed ($[10, 10]$, \blacktriangle). The small plot zooms in on the first scenario (denoted by \blacktriangledown) to illustrate the sigmoid shape of the expression levels of p21 at different K . **Bottom:** The role of RBPs in multiple miRNA-mediated target repression. Our analysis suggests the activity of RBPs in combination with the repression by multiple miRNAs can induce a tunable-like target repression.

4.3.5 The response of p21 to stimulus signals

We further investigated whether the combination of changes in miRNA abundance and the cooperativity between miRNAs can affect the features of p21 response (*p21*) to transient stimulations. In case of p21 such a stimulus signal could be a p53-mediated activation signal in response to DNA damage (Vera *et al.*, 2010). Subsequently, we defined a transient stimulus signal activating the synthesis of p21 mRNA (*mp21*) as a function of μ and τ , which represent the amplitude and duration of the signal, respectively (Figure 4.9 A). The stimulus signal ($S(\mu, \tau)$) was included into the model

$$\begin{aligned} \frac{dmp21}{dt} = & S(\mu, \tau) - mp21 \cdot (k_{deg}^{mp21} \\ & + \sum_i k_{ass}^{complex_i} \cdot miR_i + \sum_{i,j} k_{ass}^{co-complex_{i,j}} \cdot miR_i \cdot miR_j). \end{aligned} \quad (4.9)$$

In a series of simulations, we first modulated μ and τ and computed the peak of the p21 response (Figure 4.9A). Second, we simulated the p21 response for five different miRNA abundance scenarios: 1) no miRNA is expressed (**off**); 2) normal expression of all the miRNAs (**on**); 3) normal expression plus miRNA cooperativity (**on** + **C**); 4) overexpression of all the miRNAs (**on(x10)**); and 5) overexpression with miRNA cooperativity (**on(x10)** + **C**). Third, we computed the peaks of the p21 response to transient stimulation for different settings of stimulus signals (Figure 4.9B). Finally, we compared the dynamics of the p21 response when the synthesis of p21 mRNA is activated by long-lasting stimulus signals with low or high amplitude (Figure 4.9C). The detailed modelling process is described in **Appendix 6.2.2**.

For short stimulation (Figure 4.9B, $\tau = 1$ hr) the peak of p21 response is positively correlated with the amplitude of the stimulus signal, i.e. the stronger the stimulus signal the higher the peak. For the complete range ($[10^{-2}, 10^1]$) of the signal amplitude, the p21 response peak is negatively correlated with miRNA abundance. That means the p21 response peak is highest if miRNAs are not expressed, whereas p21 peak is gradually reduced with the increase of miRNA abundance (**off** > **on** > **on(x10)**). In addition, miRNA cooperativity further lowers the p21 response peak (**on** > **on** + **C**, **on(x10)** > **on(x10)** + **C**); however, with an increasing duration of the stimulus signal (Figure 4.9B, $\tau = 10$ and 24 hr), the p21 response peak pattern is distorted. For signals with low amplitude ($\mu < 1$) the p21 response peak maintains the same pattern (**off** > **on** > **on** + **C**

$> on(x10) > on(x10) + C$). In contrast, for higher amplitude ($\mu > 1$) the p21 response peaks in scenarios with miRNA expression and cooperativity gradually converge towards the situation in which the miRNAs are not expressed (*off*). This behaviour is caused by the consumption of the entire amount of available miRNAs. Interesting enough, higher peaks of p21 response are reached for $on(x10) + C$ than for $on(x10)$ when the amplitude and duration of the stimulus signal is intense and long ($\mu > 8$ and $\tau = 10$ hr or $\mu > 2$ and $\tau = 24$ hr). This result seems contradictory to our expectation of stronger p21 repression caused by miRNA cooperativity. However, simulations of miRNA consumptions over time indicate that under the condition of identical miRNA abundance, the model that considers miRNA cooperativity ($on(x10) + C$) shows quicker exhaustion of free miRNAs which in turn leads to higher peaks of p21 response (see **Appendix** Figure 6.3).

In addition, we defined a hypothetical threshold (10% of the basal p21 expression level) above which the p21 response peak is considered as significant. As shown in Figure 4.9B, the position in which the peak crosses the threshold accounts for the minimum signal amplitude required to obtain significant p21 response. The increasing miRNA abundance shifts the cross-point towards higher signal amplitudes required (Figure 4.9B, $\tau = 1$ hr). The inclusion of miRNA cooperativity further enhances this effect. On the other hand, the increasing duration of the signal reduces the amplitude required (Figure 4.9B, $\tau = 10$ and 24 hr). These results suggest that higher abundance of miRNAs as well as the phenomenon of cooperativity can enhance noise buffering by increasing the minimum TF activity level required to trigger significant target expression (Herranz and Cohen, 2010).

For long stimulus duration increasing abundance of the miRNAs and their cooperativity not only lower the p21 response peak, but also change the shape of the p21 temporal pattern (Figure 4.9C). For low stimulus amplitude ($\mu = 0.1$), the p21 response exhibits a rather flat activation, with values of p21 in the same interval for many hours, while for high signal amplitude ($\mu = 10$) the activation of p21 is delayed.

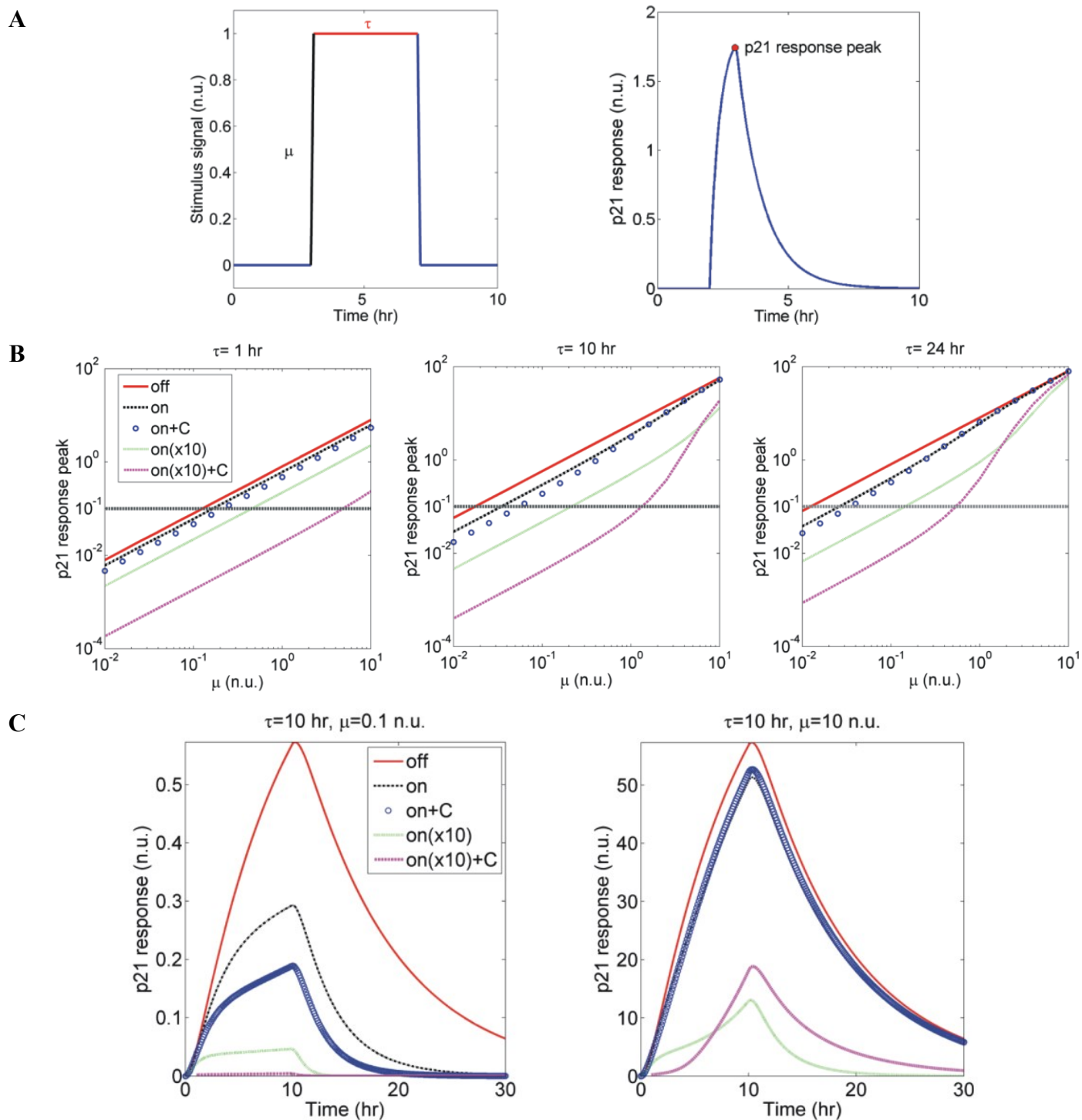


Figure 4.9: p21 responses to stimulus signals. **A:** The sketch of the stimulus signal computed (left) and the p21 response (right). The parameters μ and τ account for the amplitude and duration of the stimulus signal, respectively. **B:** The plots of p21 response peaks for different μ and τ for five defined miRNA abundance scenarios. The grey dashed lines represent the threshold, which is equal to 0.1. **C:** The time-series plots of the p21 response stimulated by stimulus signals with long duration ($\tau = 10$ hr) but different magnitude ($\mu = 0.1$ or 10 n.u.).

4.3.6 Cooperative miRNA regulation of p21 expression

To further analyse how miRNA cooperativity affects p21 expression levels in different cellular functions, we extracted a list of nine cellular functions which were obtained from the GO terms associated with the TFs of the miRNAs. The nine cellular functions include cell proliferation, cell apoptosis, immune response, inflammatory response, cell cycle control, DNA damage, cell senescence, DNA repair and cell migration. For each cellular function, we assumed that a miRNA is expressed when at least one of its TFs was associated with this cellular function, otherwise it is non-expressed. By doing so, we obtained the predicted expression profiles for the p21-targeting miRNAs for the nine cellular functions (Figure 4.10 left). In addition, we computed the p21 steady-state levels for two different conditions: considering the putative cooperative effect by the p21-targeting miRNAs versus regulation by multiple non-cooperative miRNAs (Figure 4.10 right). The detailed model description can be found in **Appendix 6.2.2**. The model predicts high levels of p21 expression during DNA damage, DNA repair, senescence and migration, while low levels are associated with cell proliferation, apoptosis and cell cycle. In some of the cellular functions the p21 steady-state levels are identical no matter miRNA cooperativity is considered or not. This can be explained by the fact that the miRNAs expressed under these scenarios do not have their binding sites in close proximity and therefore do not effectively cooperate (Figure 4.10; DNA repair, cell migration and DNA damage). In contrast, cooperating miRNAs are expressed in other scenarios, and thus differences appear in the p21 steady-state levels for the two conditions (Figure 4.10; senescence and immune response). Taken together, these results suggest that cooperating miRNAs can be selectively expressed for specific cellular functions.

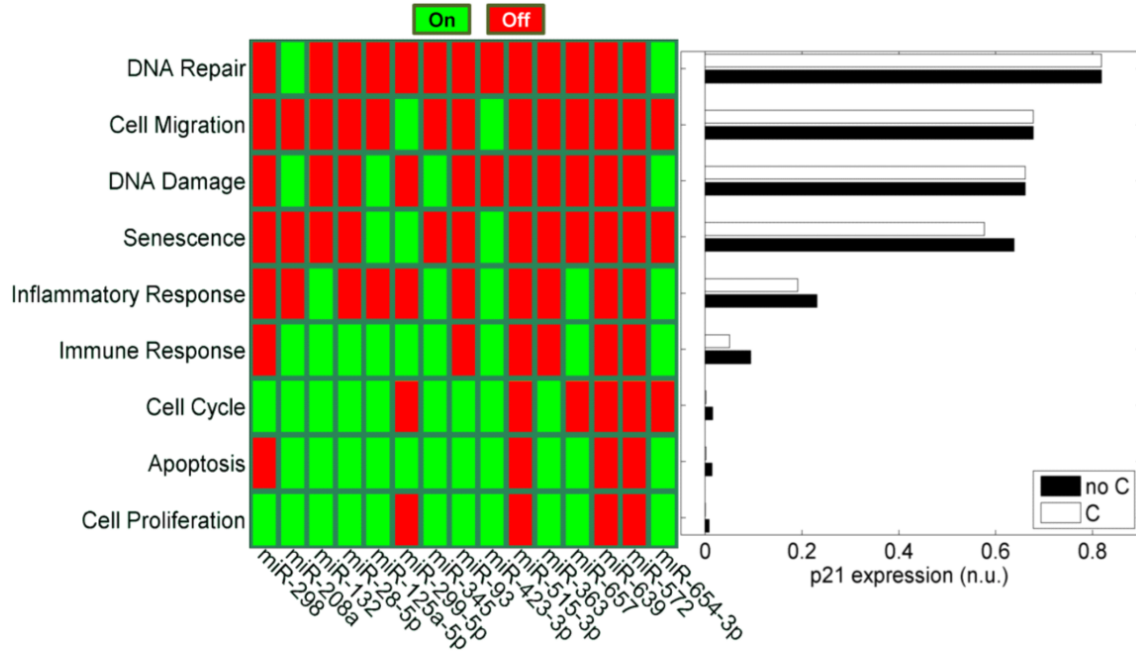


Figure 4.10: Cooperative miRNA regulation of p21 expression in different cellular functions. **Left:** The p21-targeting miRNAs expression profiles for the cellular functions as indicated. The states 'On' or 'Off' denote whether a miRNA is expressed or not in a cellular function. **Right:** The corresponding p21 steady-state levels were computed for each cellular function appearing in the left plot under two conditions: the putative cooperative effect by the p21-targeting miRNAs (C) versus regulation by multiple non-cooperative miRNAs (no C).

4.4 Conclusion

We integrated biological hypotheses and quantitative data through mathematical modelling to elucidate the mechanisms involved in the regulation of the miRNA target hub p21. Using the novel approach which combines TF and miRNA target prediction algorithms with data from the literature and databases, we constructed a map to depict the transcriptional and post-transcriptional regulation of p21. Given that the existence of up to 834 target hubs in *Homo sapiens* (Shalgi *et al.*, 2007), the novel approach developed for constructing the p21 regulatory map could provide guidance for constructing other miRNA target hub networks.

Based on the regulatory map of p21, we derived a kinetic model to test hypotheses concerning the mechanisms of collective miRNA repression. Using a distance of 13-35 nt between two miRNA binding site positions and the miRNA binding motifs as the criteria for allowing enhanced repression (Saetrom *et al.*, 2007), we computationally detected several pairs of miRNAs that may cooperate and experimentally verified the

cooperativity between miR-572 and miR-93. Our results suggested that these two miRNAs can induce cooperative effect to repress the expression of p21 via the mechanism of synergistic target regulation. In addition, by linking cellular functions to the activities of the p21-targeting miRNAs, we investigated tissue- and development-dependent patterns of p21 regulation. Our model predicted high levels of p21 expression during DNA damage, DNA repair, cell senescence and migration, while low levels of p21 were predicted to be associated with cell proliferation, apoptosis and cell cycle. Some of these predictions are also supported by the experiments describing p21 expression in the considered cellular functions. Borgdorff *et al.* (2010) identified a number of miRNAs targeting p21, whose endogenous upregulation can rescue cells from p21-mediated senescence. This finding is in line with the model predictions that the miRNA-mediated p21 repression is poor during senescence, but becomes strong when cells re-enter cell proliferation. In addition, it is known that one possible event triggering the initiation of apoptosis is the failure of mitosis, i.e. cells fail to properly arrest cell cycle (Vitale *et al.*, 2011). This phenomenon could result from insufficient expression of cell cycle arresters such as p21 and 14-3-3 σ (Chan *et al.*, 2000; Schultz *et al.*, 2009). Our simulation predicted the lower expression of p21 during apoptosis than in cell cycle, which is caused by the multiple and cooperative miRNAs, suggesting the potential role of the miRNAs in triggering the mitotic catastrophe. Taken together, the systems biology approach provides us with an efficient and systematic way to understand the regulation of target hub p21 that is accomplished by its targeting miRNAs, which can function independently and cooperatively.

Chapter 5

Conclusion and Discussion

Although miRNAs are physically small, they have been shown to play an important role in gene regulation. Currently, more and more studies are being carried out to advance the understanding of miRNA functions. However, purely experimental approaches have their limitations when dealing with complex biological systems composed of multiple layers of regulation such as the transcriptional and post-transcriptional regulation by TFs and miRNAs. Most experiments focus on the investigation of physiological consequences when perturbing miRNA expressions but are unsuitable to provide us with a system-level interpretation for observed phenomena. Therefore, the introduction of a systematic approach that can unravel the underlying mechanisms, by which miRNAs exert their functions, becomes increasingly appealing.

Within this thesis, a systems biology approach, combining biological data with mathematical modelling, is presented to investigate the cellular function of miRNAs. Such an approach provides a systematic and comprehensive understanding of the regulatory roles of miRNAs in signalling pathways and gene regulatory networks. The ODE-based models, which are calibrated and validated by means of experimental data relevant for the investigated biological problems, are accurate for predicting the time-series dynamics of molecule concentrations that are involved in biochemical systems. The model predictions can be used to uncover the dynamic behaviours of biochemical systems but also to obtain new insights into the systems and to formulate new biological hypotheses. The hypotheses can guide further experiments, and thus lead to the expansion of our current knowledge in the field of biology.

By using this systems biology approach, we constructed a kinetic model of the p53/SIRT1 signalling pathway. In the pathway, a newly identified regulator miR-34a was considered. After the translation of the signalling pathway into an ODE model, we calibrated and validated the model by using the quantitative data relevant to the defined

biochemical system. The data-driven model successfully reproduced the dynamics of the system which were experimentally measured. Furthermore, the model helped us to identify the mechanism by which miR-34a represses SIRT1. The model predicted different positive regulatory effects on p53 by DBC1 and miR-34a, which are caused by their distinct means of inhibition on SIRT1. Finally, the model showed the different ability of miR-34a and DBC1 to recover the loss of active p53 induced by the overexpression of SIRT1 usually found in cancerous cells. These results provided new insights into the p53 regulation by miR-34a for further experimentation.

Based on the experimental finding that miRNA target sites in close proximity can result in stronger repression of miRNA targets, we expanded this idea and applied it to the first experimentally verified miRNA target hub gene p21. We developed a novel approach, combining target prediction algorithms and experimental evidence, to construct the p21-centred regulatory map, which was composed by its TFs, targeting miRNAs and interacting proteins. For each interaction in the map, we assigned a confidence score which was calculated using a well-established approach applied in the published database, and such scores provided estimates for the reliability of the individual interactions. Analysis of the p21 regulatory map allowed the identification of miRNA-mediated feedback and feedforward loops and unravelled the miRNA-mediated regulation of p21 in a cell function-specific manner. Furthermore, we developed a kinetic model on the basis of the map to reproduce the experimental data which showed individual abilities of the p21-targeting miRNAs to repress p21. The model was validated by the quantitative immunoblotting data which confirmed the proposed cooperative effect on p21 by miR-572 and miR-93. The model also correctly predicted p21 expression based on the profiles of its targeting miRNAs in 9 of 12 tissues. With the help of the validated model, we showed the sophisticated mechanisms by which miR-572 and miR-93 co-regulate p21 expression independently and cooperatively. Further investigation of the p21 response to stimulus signals, e.g. the transcriptional activation from p53 after response to DNA damage, showed different responses of p21 when considering the putative cooperativity by the p21-targeting miRNAs versus regulation by multiple non-cooperative miRNAs. In addition, the predictive simulations regarding the p21 expression determined by the multiple and cooperative miRNAs provided a

plausible explanation for the distinct p21 expression levels for different cellular functions.

Although in this thesis I focused on the utilisation of ODE-based models, there exist other data-driven modelling frameworks that can be used for investigating biological problems. The right selection for specific biological problems depends largely on the mechanistic details desired in the model and the available experimental data (Kholodenko *et al.*, 2012). In comparison to ODE-based models, other modelling frameworks such as Bayesian and Boolean models provide less detailed descriptions of mechanisms of biological systems. For example, Bayesian models are helpful in the construction of connections in signalling networks and can reveal the most likely underlying structure of the network in a probabilistic manner; Boolean models use two discrete values (0 and 1) and logical gates (AND, NOT, and OR) to describe activities of network components and the information flow among them. After choosing the right modelling framework for the defined biological system, parameter estimation is the next crucial step to be considered. In some cases, insufficiency and low quality of experimental data can cause overfitting in parameter estimation. Such an issue usually results from too many estimated parameters and insufficient experimental data, and thus it can cause uncertainties in model predictions. With the development of molecular biology techniques, the generation of quantitative and sufficiently rich biological data becomes feasible and affordable. Therefore, the generation of large data sets in addition to making use of relevant qualitative data to improve the quality of a model can provide more reliable and accurate conclusions. As introduced in this thesis, local and global optimisation methods are widely used for estimating parameter values in systems biology. Each method has its pros and cons, and the most intuitive way to look for the global solution for a defined problem is the combination of both types of methods. This strategy not only increases the possibility to obtain the global solution but also improves the efficiency of the estimation process. It is noteworthy that given the difficulties in identifying the uniqueness of estimated parameters, models may remain limited concerning the mechanistic insight they provide and in their capability to predict system dynamics under unforeseen conditions. Thus, in order to better convert experiments into predictive models, the systems biology community needs to harmonise the experimental

and theoretical tools for data generation and analysis. Furthermore, hundreds of biological models have been published in online databases, but the reuse of these models is quite low due to the lack of the minimum information required for model annotation (Waltemath *et al.*, 2011). Moreover, using independent and incompatible software to construct and analyse a quantitative model increases the time and difficulties for researchers to communicate. Therefore, developing an integrated platform, which enables users to access data and knowledge from any stage in the systems biology workflow, would significantly improve the productivity and reduce errors in handling and analysis of complex data and models (Ghosh *et al.*, 2011).

In conclusion, although systems biology is still young, many studies have proved its ability to provide us with a better understanding how molecular mechanisms give rise to complex biological phenomena. With the continuous collaboration of researchers from different disciplines, I believe that systems biology will reach its full potential in revolutionising traditional experimental research, in establishing a better understanding of human diseases, and thus in accelerating the implementation of new medicine.

Appendix

6.1 Modelling SIRT1 repression by microRNA-34a

To characterise the hypothetical mechanistic processes of SIRT1 repression by miR-34a, we modified the model accordingly and obtained four candidate models (Table 6.1). The simulation results for mode 1/4 can be found in Figure 6.1.

Table 6.1: The expanded model equations of the four hypothetical miR-34a repression mechanisms. The model was accordingly modified to represent the hypothetical mechanisms shown in Figure 3.7.

<p>Mode-1</p> <p>miR-34a enhances the degradation of the SIRT1 mRNA</p> $mRNA_{Sirt1} = \frac{dmRNA^*}{dt} = k_{syn}^{mRNA^*} - k_{deg}^{mRNA^*} \cdot mRNA^* - k_{med}^{miR34a} \cdot mRNA^* \cdot miR34a(t - \tau_3)$ $\frac{dSirt1}{dt} = k_{syn}^{Sirt1} \cdot mRNA^* - k_{deg}^{Sirt1} \cdot Sirt1$
<p>Mode-2</p> <p>the translocation of the SIRT1 mRNA into P-bodies followed by quicker degradation</p> $\frac{dmRNA^*}{dt} = k_{syn}^{mRNA^*} - k_{deg}^{mRNA^*} \cdot mRNA^* - k_{trans}^{mRNA^*} \cdot mRNA^* \cdot miR34a(t - \tau_3) + k_{trans}^{mRNA} \cdot mRNA$ $\frac{dmRNA}{dt} = k_{trans}^{mRNA^*} \cdot mRNA^* \cdot miR34a(t - \tau_3) - k_{deg}^{mRNA} \cdot mRNA - k_{trans}^{mRNA} \cdot mRNA$ $\frac{dSirt1}{dt} = k_{syn}^{Sirt1} \cdot mRNA^* - k_{deg}^{Sirt1} \cdot Sirt1$ $mRNA_{Sirt1} = mRNA^* + mRNA$
<p>Mode-3</p> <p>miR-34a represses SIRT1 translation</p> $mRNA_{Sirt1} = \frac{dmRNA^*}{dt} = k_{syn}^{mRNA^*} - k_{deg}^{mRNA^*} \cdot mRNA^*$ $\frac{dSirt1}{dt} = \frac{k_{syn}^{Sirt1}}{miR34a(t - \tau_3)} - k_{deg}^{Sirt1} \cdot Sirt1$
<p>Mode-4</p> <p>miR-34a indirectly represses the synthesis of the SIRT1 mRNA</p> $mRNA_{Sirt1} = \frac{dmRNA^*}{dt} = \frac{k_{syn}^{mRNA^*}}{miR34a(t - \tau_3)} - k_{deg}^{mRNA^*} \cdot mRNA^*$ $\frac{dSirt1}{dt} = k_{syn}^{Sirt1} \cdot mRNA^* - k_{deg}^{Sirt1} \cdot Sirt1$

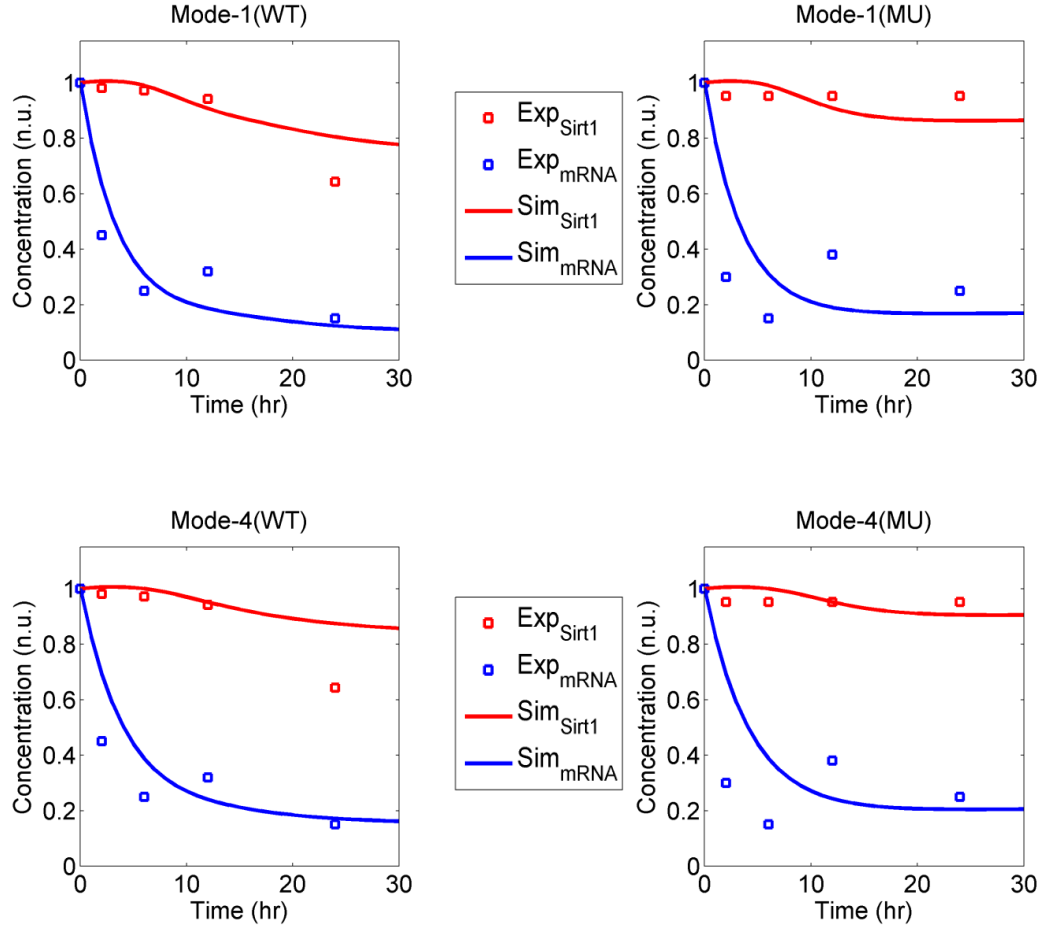


Figure 6.1: The hypothetical mechanisms (mode 1 and mode 4) by which miR-34a represses SIRT1. The solid lines represent the time courses of the concentrations (n.u.: normalised unit) of SIRT1 (Sim_{Sirt1}) and its mRNA (Sim_{mRNA}). The square markers represent the experimental data of SIRT1 (Exp_{Sirt1}) and its mRNA (Exp_{mRNA}).

6.2 MicroRNA target hub network analysis and model simulations

6.2.1 Confidence scores

For deriving confidence scores for the proposed interactions in the p21 regulatory map, we adopted the approach used by the database IntAct that is used to score molecular interactions (also known as MIscore; Kerrien *et al.*, 2012).

To assign appropriate weights for the features that were used to score interactions in the p21 regulatory map ($k_{<p,t,bs,r,cons,pred,m>}$) we carried out a survey. The survey was conducted within a small group of experts in network biology and gene regulation by miRNAs, experimentalists and modellers. Through the same survey we defined confidence scores for different methods applied in the validation of miRNA-target

interactions (S_m). We used these weights and scores in formulas to score different types of interactions (p21-protein, TF-p21, miRNA-p21, TF-miRNA). Confidence scores ranged between 0 and 1, where values towards 1 indicate higher confidence, whereas values towards 0 indicate lower confidence in a given interaction. The confidence score for each interaction of the regulatory map can be found in Table 6.6.

Protein-protein interactions

Experimentally validated interactions between p21 and other proteins were extracted from the databases HPRD (release 9.0; Keshava Prasad *et al.*, 2009) and STRING (release 9.0; Szklarczyk *et al.*, 2011). The union of the results obtained in the two databases were considered for further analysis. We scored these protein-protein interactions based on two criteria: the number of publications confirming these interactions (S_p) and their interaction types (S_t). The confidence scores for protein-protein interactions were calculated using the equation below

$$S_{PPI} = \frac{k_p \cdot S_p(n) + k_t \cdot S_t}{k_p + k_t}, \quad (6.1)$$

where $k_{<p,t>}$ denote the weights assigned to the scores for publications and interaction types ($k_p = 0.7$, $k_t = 0.9$).

Publication score. Values for the publication score were calculated as follows

$$S_p(n) = \log_{b+1}(n + 1), \quad (6.2)$$

where n denotes the number of publications reporting an interaction and b is a cut-off that represents the number of publications required for obtaining the maximum score of 1 (in this case $b = 6$).

Interaction type score. The score for the interaction type is a mean to favour direct interactions over indirect interactions or complexes. As we considered only direct interactions in the regulatory map, interaction type scores were all set to 1 ($S_t = 1$).

Transcriptional regulation of p21 expression (TF-p21 interactions)

Information about the transcriptional regulation of p21 by TFs was extracted from the literature. Similarly, we used the number of publications confirming this regulatory interaction as one criterion for the confidence score (see *publication score*, Equation (6.2)). The second criterion takes into account the way transcriptional regulation is

introduced. The third criterion is denoted by the number of binding sites reported for the individual TFs. The overall score for a putative p21 TF was derived by using the following equation

$$S_{Exp}^{TF} = \frac{k_p \cdot S_p(n) + k_r \cdot S_r + k_{bs} \cdot S_{bs}(m)}{k_p + k_r + k_{bs}}. \quad (6.3)$$

In the equation for the TF regulation confidence score the values for $k_{<p,r,bs>}$ denote the weights assigned to the scores for the number of publications, regulation types and the number of binding sites ($k_p = 0.7$, $k_r = 0.9$ and $k_{bs} = 0.9$). Similarly, the variables $S_{<p,r,bs>}$ represent individual scores for the three criteria.

We extended the list of p21 transcriptional regulators by five putative TFs that have conserved binding sites in the 5 kb upstream region of p21. This information was extracted using the table of conserved transcription factor binding sites (TFBSs) of the UCSC table browser (hg18; Karolchik *et al.*, 2003). These TFs were scored based on the normalised conservation score from UCSC and the number of predicted TFBSs ($k_{pred} = 0.3$ and $k_{bs} = 0.9$)

$$S_{Put}^{TF} = \frac{k_{cons} \cdot S_{cons} + k_{bs} \cdot S_{bs}(m)}{k_{pred} + k_{bs}}. \quad (6.4)$$

Binding sites score. Values for the binding sites score were calculated as follows

$$S_{bs}(m) = \log_{b+1}(m + 1), \quad (6.5)$$

where S_{bs} is the score for the number of binding sites (denoted by m) that a TF has in the upstream region of p21. For $m \geq b = 6$ the score S_{bs} equals 1.

Regulation type score. We differentiated the transcriptional regulations by TFs into three types: regulation through direct 'DNA binding' ($S_r = 1$), regulation realized by 'complex' formation ($S_r = 0.5$) and indirect regulation through a cofactor, namely 'mediated' ($S_r = 0.5$).

Conservation score. Values for the conservation score are determined by the criterion of whether the binding site is conserved ($S_{cons} = 1$) or not ($S_{cons} = 0$).

Post-transcriptional regulation of p21 expression (miRNA-p21 interactions)

The post-transcriptional regulation of p21 is realized by a set of miRNAs. The confidence score for miRNA-mediated p21 regulation incorporates three different criteria: the number of publications (n), the methods used to confirm this interaction and

the number of predicted binding sites. The score was calculated by the following equation

$$S_{miR} = \frac{k_p \cdot S_p(n) + k_m \cdot S_m(method) + k_{bs} \cdot S_{bs}(m)}{k_p + k_m + k_{bs}}, \quad (6.6)$$

where $k_{<p,m,bs>}$ denote the weights that were assigned to the scores $S_{<p,m,bs>}$ which account for the number of publications (see *publication score*, Equation (6.2)), detection method(s) and the number of predicted binding sites, respectively ($k_p = 0.7$, $k_m = 1$, $k_{bs} = 0.3$). The predicted binding sites score (S_{bs}) was calculated using modified Equation (6.5) in which $b = 3$, meaning $S_{bs} = 1$ when three or more binding sites were predicted.

Method score. The detection methods were scored with respect to their capability to detect true miRNA:target interactions. The values of this score were determined by our survey in the following table.

Method	Reporter assay	Western blot	QRT-PCR	Microarray
S_m	0.8	0.7	0.4	0.3

Transcriptional regulation of miRNA expression (TF-miRNA interactions)

For the confidence scores of TF-miRNA regulations we adopted the method used to score TF-p21 regulations. Since there is lack of experimental support for identifying TF-miRNA interactions, we used the help of predictions from diverse resources. In this manner, the score is composed of one term accounting for the number of publications which verify TF-miRNA regulations and the other term that considers the number of predictive binding sites. Thus, the TF-miRNA confidence score was calculated using the equation as follows

$$S_{TF:miR} = \frac{k_p \cdot S_p(n) + k_{pred} \cdot S_{pred}(m, bs)}{k_p + k_{pred}}, \quad (6.7)$$

where $k_{<p,pred>}$ are the weights for the publication and the prediction scores $S_{<p,pred>}$ respectively ($k_p = 0.8$ and $k_{pred} = 0.5$). Validated miRNA TFs were extracted from the database TransmiR (release 1.0) and the corresponding scores (S_p) were calculated using Equation (6.2). Predictive TFs were obtained from the resources MIR@NT@N (version 1.2.1; Béchec *et al.*, 2011), PuTmiR (release 1.0; Bandyopadhyay and Bhattacharyya, 2010) and the table of conserved TFBSs in the UCSC table browser (hg18; Karolchik *et al.*, 2003). The equation used to calculate prediction scores is as follows

$$S_{pred}(m, bs) = \frac{k_n \cdot \log_{(n_{max}+1)}(n+1) + k_{bs} \cdot \log_{(bs_{max}+1)}(bs+1)}{k_n + k_{bs}}, \quad (6.8)$$

where k_n and k_{bs} denote the number of algorithms predicting TF-miRNA interactions and the number of predictive binding sites respectively ($k_n = 1$ and $k_{bs} = 0.7$).

6.2.2 Model simulations

Modelling cooperative repression of p21 by miR-572 and miR-93

According to the experiments designed for verifying the cooperative effect on p21 repression by miR-572 and miR-93, we derived a corresponding model of seven ODEs.

$$\begin{aligned} \frac{dmp21}{dt} = & k_{syn}^{mp21} \cdot f_{act}(TF_{mp21}) - mp21 \cdot (k_{deg}^{mp21} + k_{ass}^{complex_8} \cdot miR_8 + k_{ass}^{complex_{14}} \\ & \cdot miR_{14} + k_{ass}^{co-complex_{8,14}} \cdot miR_8 \cdot miR_{14}) \end{aligned} \quad (6.9)$$

$$\frac{d[mp21|miR_8]}{dt} = k_{ass}^{complex_8} \cdot mp21 \cdot miR_8 - k_{deg}^{complex_8} \cdot [mp21|miR_8] \quad (6.10)$$

$$\frac{d[mp21|miR_{14}]}{dt} = k_{ass}^{complex_{14}} \cdot mp21 \cdot miR_{14} - k_{deg}^{complex_{14}} \cdot [mp21|miR_{14}] \quad (6.11)$$

$$\begin{aligned} \frac{d[mp21|miR_8|miR_{14}]}{dt} = & k_{ass}^{co-complex_{8,14}} \cdot mp21 \cdot miR_8 \cdot miR_{14} \\ & - k_{deg}^{co-complex_{8,14}} \cdot [mp21|miR_8|miR_{14}] \end{aligned} \quad (6.12)$$

$$\frac{dmiR_8}{dt} = k_{syn}^{miR_8} \cdot f_{act}(TF_{miR_8}) - miR_8 \cdot (k_{deg}^{miR_8} + k_{ass}^{complex_8} \cdot mp21) \quad (6.13)$$

$$\frac{dmiR_{14}}{dt} = k_{syn}^{miR_{14}} \cdot f_{act}(TF_{miR_{14}}) - miR_{14} \cdot (k_{deg}^{miR_{14}} + k_{ass}^{complex_{14}} \cdot mp21) \quad (6.14)$$

$$\frac{dp21}{dt} = k_{syn}^{p21} \cdot mp21 + k_{deg}^{p21} \cdot p21 \quad (6.15)$$

To mimic the four experimental settings (Figure 6.2 top), we configured the corresponding parameter values as follows

- 1) **Non-targeting control:** $miR_8(0) = miR_{14}(0) = 1$, $k_{syn}^{miR_8} = k_{deg}^{miR_8}$, $k_{syn}^{miR_{14}} = k_{deg}^{miR_{14}}$;
- 2) **miR-572:** $miR_8(0) = miR_{14}(0) = 1$, $k_{syn}^{miR_8} = k_{deg}^{miR_8}$, $k_{syn}^{miR_{14}} = 100 \cdot k_{deg}^{miR_{14}}$;
- 3) **miR-93:** $miR_8(0) = miR_{14}(0) = 1$, $k_{syn}^{miR_8} = 100 \cdot k_{deg}^{miR_8}$, $k_{syn}^{miR_{14}} = k_{deg}^{miR_{14}}$;
- 4) **miR-572+93:** $miR_8(0) = miR_{14}(0) = 1$, $k_{syn}^{miR_8} = 50 \cdot k_{deg}^{miR_8}$, $k_{syn}^{miR_{14}} = 50 \cdot k_{deg}^{miR_{14}}$,

and the other parameters were set as described in Table 6.2.

Subsequently, we characterised the function for the transcriptional activation of p21 ($f_{act}(TF_{mp21})$) by using the experimental data that describe the response of p53 after genotoxic stress induction (Figure 6.2 bottom). p53 is typically upregulated in response

to DNA damage and is known as a transcriptional activator of p21 (El-Deiry *et al.*, 1994; Sax and El-Deiry, 2003).

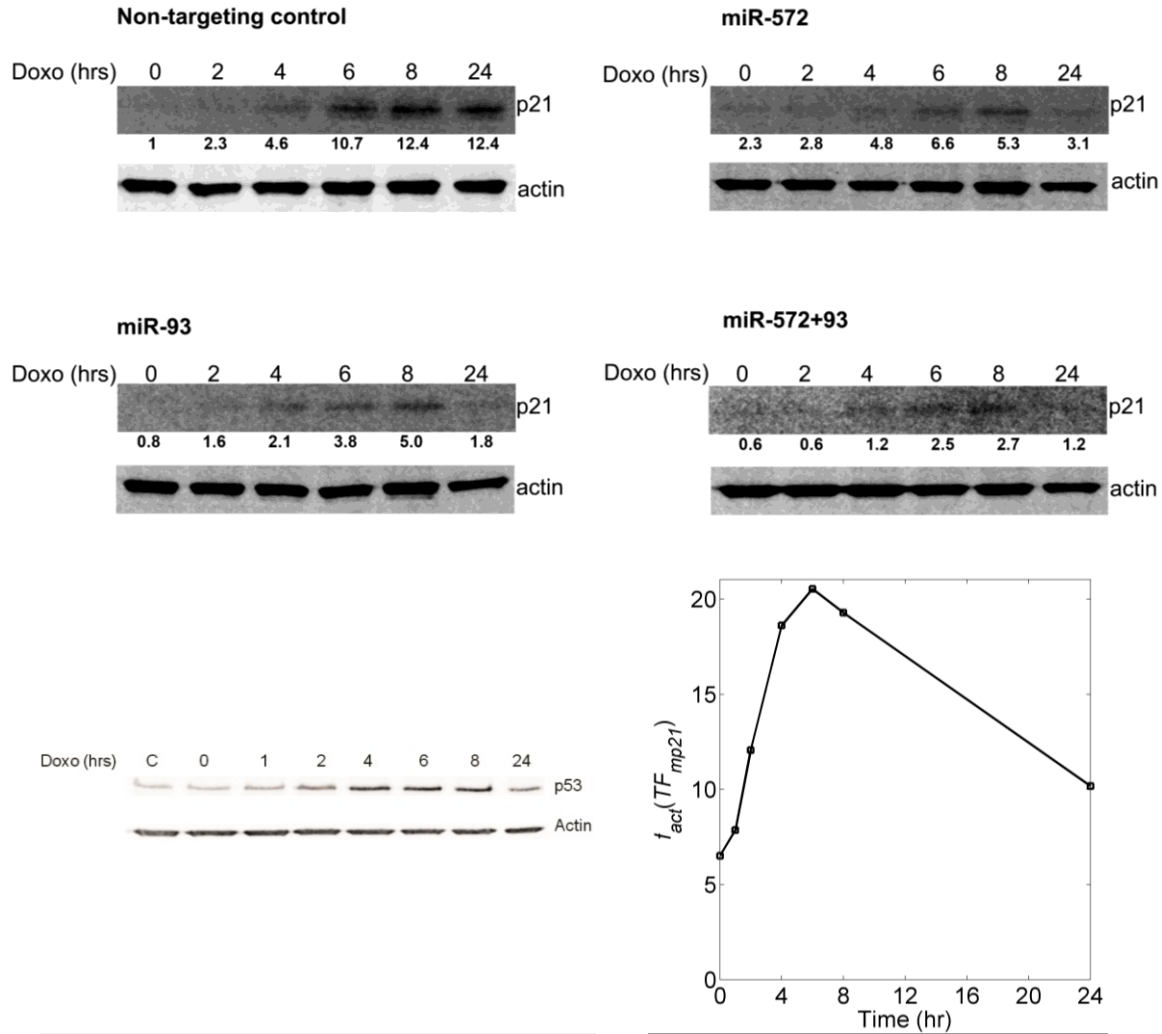


Figure 6.2: Regulation of p21 expression by miR-572 and miR-93. **Top:** The Western blots for p21 expression levels. p21 was measured after treatment with doxorubicin at the indicated time points for four scenarios: 1) endogenous miRNA expression (Non-targeting control); 2) miR-572 overexpressed (miR-572); 3) miR-93 overexpressed (miR-93); and 4) both miRNAs partially overexpressed (miR-572+93). **Bottom:** The Western blot for p53 expression levels. p53 was measured at the indicated time points (left). The data were used to characterise the transcriptional activation function of the p21 mRNA ($f_{act}(TF_{mp21})$; right).

Simulation of tissue-specific p21 expression in different tissues

We first extracted the miRNA expression levels in different tissues from the database miRNAmap (release 2.0; Hsu *et al.*, 2008) and normalised them according to the most abundant miRNA observed in each tissue. For example, in adipose the most abundant miRNA is miR-125a-5p. The expression of miR-125a-5p is normalised to 1 ($miR_5(0) =$

1), and accordingly other miRNA expression levels were rescaled. If a miRNA does not appear in a tissue expression profile its expression level is considered as 0 (Table 6.3). Next, for each tissue we computed the steady-state levels of p21 by changing the initial concentrations of the miRNAs according to their tissue-specific expression profiles, while other parameters were configured as described in Table 6.2. Then, we obtained the experimental data of p21 expression levels in different tissues from the ArrayExpress database (version as of January 2012; Brazma *et al.*, 2006). The tissue-specific p21 expression levels were categorised as low or high according to the experimental evidence from the database. For example, in adipose and kidney the p21 expression levels were observed to be over- and underexpressed respectively, so we can conclude that the p21 expression level in kidney is lower than in adipose. From 12 tissues, p21 was underexpressed in kidney and liver only. Thus, in kidney and liver the p21 expression levels were categorised as low while for the other tissues their p21 expression levels were categorised as high (Table 6.3). Similarly, the computed p21 expression levels were also categorised as low or high. To do so, we used the p21 expression level in kidney as a threshold. If the computed p21 expression level is smaller than this threshold, it was categorised as low; if not it was categorised as high. Finally, we compared the model simulations with the experimental data obtained from the database.

Simulation of the response of p21 to stimulus signals

We first defined a new term S for p21 stimulation by a transient stimulus signal. S is a function of the amplitude (μ) and duration (τ) of the stimulus signal. In our simulations, this term was added to the differential equation accounting for the p21 mRNA ($mp21$). Next, we further assumed non-basal synthesis for the p21 mRNA ($k_{syn}^{mp21} = 0$) and set initial concentrations $mp21(0) = 0$ and $p21(0) = 0$. In this manner, the p21 response ($p21$) was totally induced by the transient stimulus signal. Subsequently, in order to keep consistent with the experimental conditions of Wu *et al.* (2010) we assumed non-basal synthesis for each miRNA ($k_{syn}^{miR_{i=1...15}} = 0$). Then, we defined five miRNA abundance scenarios by setting the initial concentrations for the miRNAs and corresponding parameters accordingly

$$1) \text{ off: } miR_{i=1...15}(0) = 0, k_{ass}^{co-complex_{i,j}} = k_{deg}^{co-complex_{i,j}} = 0;$$

- 2) **on**: $miR_{i=1\dots 15}(0) = 1$, $k_{ass}^{co-complex_{i,j}} = k_{deg}^{co-complex_{i,j}} = 0$;
- 3) **on + C**: $miR_{i=1\dots 15}(0) = 1$, see Table 6.2 for $k_{ass}^{co-complex_{i,j}}$ and $k_{deg}^{co-complex_{i,j}}$;
- 4) **on(x10)**: $miR_{i=1\dots 15}(0) = 10$, $k_{ass}^{co-complex_{i,j}} = k_{deg}^{co-complex_{i,j}} = 0$;
- 5) **on(x10) + C**: $miR_{i=1\dots 15}(0) = 10$, see Table 6.2 for $k_{ass}^{co-complex_{i,j}}$ and $k_{deg}^{co-complex_{i,j}}$.

We also ran simulations to illustrate the consumption of the miRNAs for the scenario **on(x10)** and **on(x10) + C** when the stimulus signal is strong and long-lasting ($\mu=10$ n.u and $\tau=10$ hr; Figure 6.3).

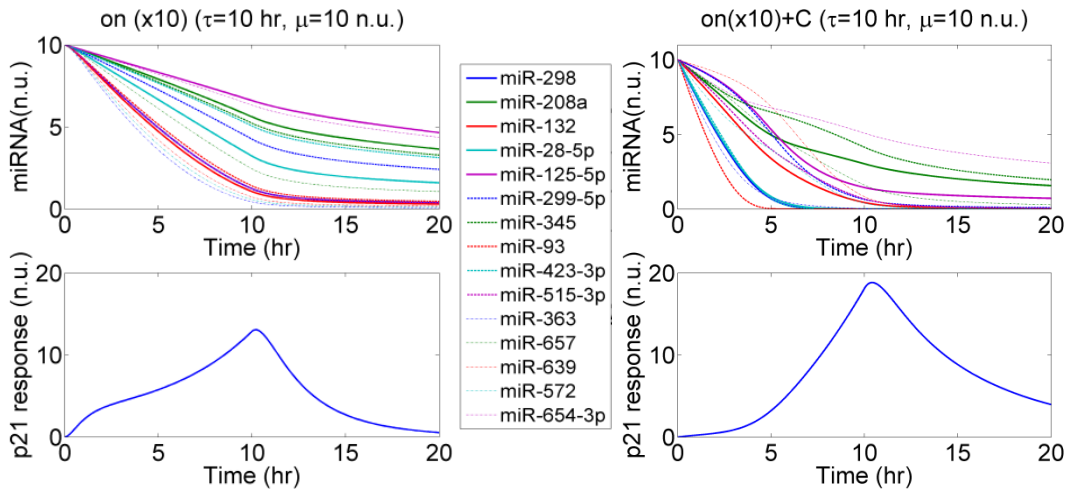


Figure 6.3: The response of p21 in different scenarios for specified signals. The plots describe the time-series of p21 responses and the p21-targeting miRNAs in two defined scenarios (left: *on (x10)*; right: *on (x10) + C*) for the stimulus signal with $\mu=10$ n.u. and $\tau=10$ hr.

Cooperative miRNA regulation of p21 expression in different cellular functions

We first extracted the list of GO terms associated with the miRNA TFs. For each cellular function, we assumed that a miRNA is expressed when at least one of its TFs is associated with the cellular function. For example, p53 is a TF for miR-125a-5p and it is associated with cell proliferation, so we assumed miR-125a-5p to be expressed ($miR_5(0) = 1$) when cells are proliferating. In contrast, we assumed miR-125a-5p to be non-expressed ($miR_5(0) = 0$) in DNA repair because none of its TFs is associated with this cellular function. By following this strategy, the miRNA expression profiles for the nine cellular functions were obtained (Table 6.4).

To compute the p21 steady-state levels for each cellular function, we set the following parameter values and initial concentrations for the model: 1) for each cellular

function, the corresponding initial concentrations of the miRNAs ($miR_{i=1...15}(0)$) were derived from Table 6.4, 2) the initial concentrations for p21 protein and mRNA were set to 1 ($p21(0) = 1$ and $mp21(0) = 1$) and the synthesis rate constant of each miRNA was set to 0 ($k_{syn}^{miR_{i=1...15}} = 0$), and 3) when considering miRNA cooperativity, the corresponding parameters values ($k_{ass}^{co-complex_{i,j}}$ and $k_{deg}^{co-complex_{i,j}}$) were assigned according to Table 6.2; for non-cooperative regulation by individual miRNAs these two parameters were set to 0.

6.3 Experimental methods

6.3.1 Small RNA transfection and doxorubicin treatment

Sk-Mel-147 cells were seeded in a six well plate. Mature miRNA mimics (miR-572 #C-300891-01-0005, miR-93 #C-300512-07-0005 or Mimic Negative Control #1-CN-001000-01-05; Thermo Scientific, Dharmacon RNAi Technologies) were transfected individually at a concentration of 100 nM or in combination at 50nM each using lipofectamine RNAimax reagent (Invitrogen, Karlsruhe, Schwerte, Germany). After 48 hr transfection, the cells were pulse treated with 250 nM doxorubicin-HCl (Sigma-Aldrich, Munich, Germany) for 1 hour after which normal growth medium was replenished. The protein lysates were collected at 0, 2, 4, 6, 8 and 24 hr post-doxorubicin treatment.

6.3.2 Immunoblotting

At indicated time points the cells were harvested in radioimmunoprecipitation buffer [50 mmol/l Tris-HCL (pH 7.4), 150 mmol/L NaCl, 1% NP-40, 0.5% deoxycholic acid, 0.1% SDS], supplemented with protease inhibitor mix (Roche Molecular Biochemicals, Mannheim, Germany). 20 µg of total protein extract was denatured in electrophoresis sample buffer for 5 min at 95°C, and subjected to SDS-polyacrylamide gel electrophoresis (PAGE). Gels were electroblotted onto nitrocellulose membranes (Highbond ECLTM, Amersham, Braunschweig, Germany). Immunodetection was performed using an anti-p21 mouse monoclonal Ab (sc-6246) and were re-probed with an anti-β-actin mouse monoclonal Ab (sc-5274) to verify equal loading of proteins (both the antibodies purchased from Santa Cruz Biotechnologies, Santa Cruz, CA, USA). The

Appendix

IRDye 800CW donkey anti-mouseIgG (926-32212) secondary antibody was used for immunodetection (LI-COR Biosciences, Bad Homburg, Germany). All the blots were processed in parallel and developed for 2 minutes. Immunodetection of p53 was performed using a mouse monoclonal antibody against p53 (#554293, BD Biosciences, Heidelberg, Germany) and the same secondary antibody as used for p21. The relative p21 protein expressions are represented as fold changes compared to the p21 expression in the non-targeting control at 0 hr time point. For detection and quantification of the band intensities we used LiCor Odyssey Western Blot detection system with integrated Image Studio software.

Table 6.2: Initial concentrations of model variables and model parameter values. Based on the experimental data, the p21-targeting miRNAs verified in Wu *et al.* (2010) were divided into two groups: the translation repression group (marked with asterisk) and the mRNA deadenylation group. A miRNA was classified into the mRNA deadenylation group if its overexpression can result in 20% or more downregulation of the p21 mRNA level (i.e. p21 mRNA level ≤ 0.8 ; the basal level is 1), otherwise it was classified into the translation repression group. For the translation repression group, only $k_{ass}^{complex_i}$ was estimated and $k_{deg}^{complex_i}$ was fixed, so only one corresponding confidence interval was calculated. For the other group both $k_{deg}^{complex_i}$ and $k_{ass}^{complex_i}$ were estimated, and both of their corresponding confidence intervals were calculated. The initial concentrations of *p21* and *mp21* were set to 1, and this value was used as their basal expression levels. During the parameter estimation, the initial concentrations of p21-targeting miRNAs were set to 100, because in Wu *et al.* (2010) the expression levels of *p21* and *mp21* were measured after the individual introduction of the p21-targeting miRNAs with amount of 100 nM. Due to the lack of biological information to characterise the transcriptional activation of p21 and its targeting miRNAs, the corresponding functions were assumed to 1 for simplicity.

Initial concentration of variables and TF functions					
Variable	Description		Initial concentration (n.u.)		
$p21$	p21 protein		1		
$mp21$	p21 mRNA		1		
$miR_{i=1 \dots 15}$	p21-targeting miRNAs		100		
$[mp21 \mid miR_{i=1 \dots 15}]$	Complexes formed by miR_i and $mp21$		0		
$f_{act}(TF_{mp21})$	p21's transcriptional activation function		1		
$f_{act}(TF_{miR_i \ (i=1 \dots 15)})$	The transcriptional activation function of miR_i		1		
Fixed parameter values					
Parameter	Description		Value	Comment	
k_{syn}^{mp21}	Synthesis rate constant of $mp21$		0.1155 hr ⁻¹	fixed	
k_{deg}^{mp21}	Degradation rate constant of $mp21$		0.1155 hr ⁻¹	Wang <i>et al.</i> , 2000	
$k_{syn}^{miR_i} \ (i=1 \dots 15)$	Synthesis rate constant of miR_i		0.0289 hr ⁻¹	fixed	
$k_{deg}^{miR_i} \ (i=1 \dots 15)$	Degradation rate constant of miR_i		0.0289 hr ⁻¹	Kai and Pasquinelli, 2010	
k_{syn}^{p21}	Synthesis rate constant of $p21$		1.3863 hr ⁻¹	fixed	
k_{deg}^{p21}	Degradation rate constant of $p21$		1.3863 hr ⁻¹	Maki and Howley, 1997	
Estimated parameter values and their confidence intervals					
miRNA	$k_{deg}^{complex_i}$ ($i = 1 \dots 15$) (hr ⁻¹)	$k_{ass}^{complex_i}$ ($i = 1 \dots 15$) (n.u. ⁻¹ · hr ⁻¹)	$F_{cost}^{miR_i}$ ($i = 1 \dots 15$)	Confidence interval [lower upper]	Experimental data of p21 (Protein, mRNA±SD)
miR-298 (miR_1) [*]	0.1155	0.0254	3.4e-004	[0.0243 0.0265]	(0.16, 1.074±0.025)
miR-208a (miR_2) [*]	0.1155	0.0041	2.0e-003	[0.0022 0.0076]	(0.51, 1.192±0.022)
miR-132 (miR_3) [*]	0.1155	0.0275	2.4e-003	[0.0222 0.0352]	(0.15, 1.21±0.147)
miR-28-5p (miR_4) [*]	0.1155	0.0119	5.9e-003	[0.0108 0.0132]	(0.28, 1.35±0.06)
miR-125-5p (miR_5) [*]	0.1155	0.0018	1.8e-003	[0.0013 0.0024]	(0.69, 0.85±0.051)
miR-299-5p (miR_6) [*]	0.1155	0.0080	1.8e-004	[0.0072 0.0088]	(0.36, 0.95±0.038)
miR-345 (miR_7) [*]	0.1155	0.0051	1.1e-004	[0.0045 0.0057]	(0.46, 0.96±0.039)

Table 6.2: Continued.

miR-93 (miR_8)	0.1564	0.0235	4.1e-014	[0.1434 1.7210] [0.0215 0.0259]	(0.17, 0.7776±0.03)
miR-423-3p (miR_9)	0.9118	0.0055	2.8e-009	[0.2136 Infinity] [0.0027 0.0131]	(0.44, 0.5102±0.11)
miR-515-3p (miR_{10})	0.2098	0.0253	1.2e-013	[0.1457 0.3811] [0.0221 0.0295]	(0.16, 0.616±0.037)
miR-363(miR_{11})	0.2261	0.0399	2.2e-014	[0.1384 0.6523] [0.0241 0.0900]	(0.11, 0.56±0.15)
mR-657 (miR_{12})	0.3465	0.0158	2.1e-014	[0.1828 Infinity] [0.0088 0.0353]	(0.23, 0.48±0.12)
miR-639 (miR_{13})	0.4305	0.0327	1.8e-017	[0.2540 1.6100] [0.0208 0.0634]	(0.13, 0.36±0.084)
miR-572 (miR_{14})	0.3039	0.0360	9.4e-023	[0.2427 0.4082] [0.0294 0.0456]	(0.12, 0.45±0.044)
miR-654-3p (miR_{15})	9.7485	0.0024	3.0e-014	[0.3491 Infinity] [0.0017 0.0036]	(0.64, 0.63±0.053)
The variables and parameters accounting for miRNA cooperativity					
Variable	$k_{ass}^{co-complex_{i,j}}$	$k_{deg}^{co-complex_{i,j}}$	Initial concentration (n.u.)		
$[mp2I miR_1 miR_2]$	$k_{ass}^{complex_1} + k_{ass}^{complex_2}$	$k_{deg}^{complex_1} + k_{deg}^{complex_2}$	0		
$[mp2I miR_1 miR_{11}]$	$k_{ass}^{complex_1} + k_{ass}^{complex_{11}}$	$k_{deg}^{complex_1} + k_{deg}^{complex_{11}}$	0		
$[mp2I miR_3 miR_4]$	$k_{ass}^{complex_3} + k_{ass}^{complex_4}$	$k_{deg}^{complex_3} + k_{deg}^{complex_4}$	0		
$[mp2I miR_4 miR_{11}]$	$k_{ass}^{complex_4} + k_{ass}^{complex_{11}}$	$k_{deg}^{complex_4} + k_{deg}^{complex_{11}}$	0		
$[mp2I miR_5 miR_6]$	$k_{ass}^{complex_5} + k_{ass}^{complex_6}$	$k_{deg}^{complex_5} + k_{deg}^{complex_6}$	0		
$[mp2I miR_7 miR_8]$	$k_{ass}^{complex_7} + k_{ass}^{complex_8}$	$k_{deg}^{complex_7} + k_{deg}^{complex_8}$	0		
$[mp2I miR_8 miR_9]$	$k_{ass}^{complex_8} + k_{ass}^{complex_9}$	$k_{deg}^{complex_8} + k_{deg}^{complex_9}$	0		
$[mp2I miR_8 miR_{15}]$	$k_{ass}^{complex_8} + k_{ass}^{complex_{15}}$	$k_{deg}^{complex_8} + k_{deg}^{complex_{15}}$	0		
$[mp2I miR_8 miR_{14}]$	$k_{ass}^{complex_8} + k_{ass}^{complex_{14}}$	$k_{deg}^{complex_8} + k_{deg}^{complex_{14}}$	0		
$[mp2I miR_9 miR_{10}]$	$k_{ass}^{complex_9} + k_{ass}^{complex_{10}}$	$k_{deg}^{complex_9} + k_{deg}^{complex_{10}}$	0		
$[mp2I miR_9 miR_{12}]$	$k_{ass}^{complex_9} + k_{ass}^{complex_{12}}$	$k_{deg}^{complex_9} + k_{deg}^{complex_{12}}$	0		

Appendix

Table 6.3: Normalised tissue-specific miRNA expression profiles. The miRNA expression levels were extracted from the database miRNAmap and normalised to the most abundance miRNA in the tissues. The p21 expression levels were extracted from the database ArrayExpress (p21(Exp)). Under: underexpression; Over: overexpression.

miRNA	kidney	liver	adipose	bladder	s. intestine	cervix	heart	lung	ovary	testis	trachea	brain
<i>miR₁</i>	0	0	0	0	0	0	0	0	0	0	0	0
<i>miR₂</i>	0	0	0	0	0	0	0	0	0	0	0	0
<i>miR₃</i>	0.0514	0.0333	0.0714	0.0533	0.0692	0.0177	0.04	0.0083	0.03	0.0333	0.07	0.1341
<i>miR₄</i>	0.0129	0.02	0.0214	0.05	0.0246	0.0082	0.015	0.0079	0.012	0.006	0.03	0.0022
<i>miR₅</i>	1	0.5	1	1	0.4615	1	1	1	1	1	0.9	1
<i>miR₆</i>	0.0005	0.0008	0.001	0.0007	0.0015	0.002	0.0005	0.0001	0.0023	0.0043	0.001	0.0017
<i>miR₇</i>	0.0051	0.005	0.0043	0.002	0.0038	0.0008	0.001	0.0008	0.0025	0.0027	0.007	0.001
<i>miR₈</i>	0.3142	0.4167	0.3571	0.4333	0.5769	0.1118	0.15	0.3021	0.275	0.1667	0.5	0.1037
<i>miR₉</i>	0	0	0	0	0	0	0	0	0	0	0	0
<i>miR₁₀</i>	0	0	0	0	0	0	0	0	0	0	0	0
<i>miR₁₁</i>	0.0049	0.0008	0.0014	0.001	0.0023	0.0006	0.0003	0.0008	0.0013	0.0013	0.0025	0.0013
<i>miR₁₂</i>	0.0002	0.0012	0.0009	0.0002	0.0007	0.0001	0.0003	0.0001	0.0002	0.0005	0.0012	0.0002
<i>miR₁₃</i>	0	0	0	0	0	0	0	0	0	0	0	0
<i>miR₁₄</i>	0.0011	0.005	0.0214	0.0063	0.0123	0.0017	0.001	0.0015	0.001	0.0027	0.011	0.0005
<i>miR₁₅</i>	0	0	0	0	0	0	0	0	0	0	0	0
p21 (Exp)	Under	Under	Over	Over	Over	Over	Over	Over	Over	Over	Over	Over

Table 6.4: p21-targeting miRNA expression profiles for the nine cellular functions. For each cellular function, according to the GO analysis as described in chapter if a miRNA expressed its expression level is set to 1 otherwise its expression level is 0.

miRNA	Cell Proliferation	Apoptosis	Cell Cycle	Immune Response	Inflammatory Response	Senescence	DNA Damage	Cell Migration
<i>miR₁</i>	1	0	1	0	0	0	0	0
<i>miR₂</i>	1	1	1	1	0	0	1	0
<i>miR₃</i>	1	1	1	1	1	0	0	0
<i>miR₄</i>	1	1	1	1	0	0	0	0
<i>miR₅</i>	1	1	1	1	0	1	1	0
<i>miR₆</i>	0	1	0	1	0	1	0	1
<i>miR₇</i>	1	1	1	1	1	0	1	0
<i>miR₈</i>	1	1	1	0	0	0	0	0
<i>miR₉</i>	1	1	1	1	1	1	0	1
<i>miR₁₀</i>	0	0	0	0	0	0	0	0
<i>miR₁₁</i>	1	1	1	0	0	0	0	0
<i>miR₁₂</i>	1	1	0	1	1	0	0	0
<i>miR₁₃</i>	0	0	0	0	0	0	0	0
<i>miR₁₄</i>	0	0	0	0	0	0	0	0
<i>miR₁₅</i>	1	1	0	1	1	0	1	0

Table 6.5: miRNA binding sites in the 3' UTR of p21. The detailed binding motifs of the p21-targeting miRNAs are predicted by the database miRanda or RNA22. '|' and ':' denote base and wobble pairs, respectively.

miRNA	Starting position	Predicted alignment	miRNA	Starting position	Predicted alignment
miR-208a	69	miRNA 3'-uguuucgaaAAACAGACGAAUA-5' :	miR-345	1157	miRNA 3'-cucggGACCUAGUCCUACAGUG-5' :
miR-298	40	miRNA 5'-agucucagUUUGUGUGUUAa-3 miRNA 3'-acccUCUGGAGGA---CGAAGACGa-5' :	miR-654-3p	1160	miRNA 5'-agcagCGGAACAAGGAGUCAGa-3' miRNA 3'-uuccacuaccagUC-GUCUGUAU-5' :
miR-299-5p	1404	miRNA 5'-ucaaaAGGCCCGUCUACAUUCUGGC-3' miRNA 3'-uacauacacccUGCCAUUUGU-5' :	miR-363	776	miRNA 5'-agcgaacaagGAGUCAGACAUu-3' miRNA 3'-au--GUCuACCuaUGGcACGUUA-5'
miR-299-5p	1049	miRNA 5'-ucuccaccuaGACUGUAACCU-3' miRNA 3'-TA-TATGATGGGGAGTAGATCT-5' :	miR-423-3p	470	miRNA 5'-tctcCAGcTGG--GCTcTGCAATT-3' miRNA 3' ugAC-UCCCCGGAGUGUGGUCUGa 5'
miR-515-3p	451	miRNA 5'-UACAUAC-ACCCUGCCAUUUGU-3' miRNA 3'-TGCAGGTTTCTTCCTGTAG-5' :		560	miRNA 5' ttTGAAGGGGCTC--ACCGAGTg 3' miRNA 3' ugACUC--CCCCGAGUCUGGUCUGa 5' :
miR-93	451	miRNA 5'-AAGT--AAACAGATGGCATT-3' miRNA 3' TGGACGT--GCTTGTCTGTAaa 5' : :	miR-423-3p	699	miRNA 5' agTGAGCACAGCCTAGGGCTGAGct 3' miRNA 3' ugACUCGCCG----GAGUC-UGGUCUGa 5' :
miR-93	1128	Target 5' AGAAGTAAACAGATGGCATT 3' miRNA 3'-gauGGACGUG-CUUGU--CGUGAAAc-5' 	miR-572	1152	miRNA 5' actGGGAGCCCGTCTCAGTCTTGAGCc 3' miRNA 3' acccggugggcUCGCCUg 5'
miR-125a-5p	1026	miRNA 5'-aucCCUCCCGAGUUAUUGCACUUUg-3 miRNA 3'-GTG--GGGTATCTCTGTGTTAGGGG-5' 	miR-639	944	miRNA 5' cactttgattagACGCGAa 3' miRNA 3' ugUCGCGAGCGGUUG---CGUCGUa 5' :
miR-132	1350	miRNA 5'-AGUGUCCAUAUUC-CAGAGUCCU-3' miRNA 3'-gcugguACCGACAUCUGACAAu-5' : :		2	miRNA 5' cuACCUCAGGGCAGCUCAAGCAGCGAc 3' miRNA 3' ggaucucucceacUCUUGGACGg 5' :
miR-28-5p	1456	miRNA 5'-acauacUGGC-CUGGACUGUUu-3' miRNA 3'-gaguuauucugacacUCGAGGAA-5' : : : :	miR-657	672	miRNA 5' aatccgccccacagGAGCCTGCa 3' miRNA 3' ggaucucucceacucUUGGACGg 5' :
miR-28-5p	1328	miRNA 5'-ucugugucuuuacacAGCUCCUc-3' miRNA 3'-gaGUUAUCU-GACACUCGAGGAAa-5' 			miRNA 5' cctcatggccctctGACCTGCa 3'
		miRNA 5'-ccCAA-ACACCUUCCAGCUCUc-3'			

Table 6.6: Confidence scores for the interactions considered in the p21 regulatory map. The p21 regulatory map consists of four types of interactions: miRNA-p21, TF-miRNA, TF-p21 and p21-protein. The corresponding scores for these interactions were calculated as described in **Appendix 6.2.1**.

miRNA - p21 interaction scores

miRNA	miR-125a-5p	miR-132	miR-208a	miR-28-5p	miR-298	miR-299-5p	miR-345	miR-363
Score	0.73	0.73	0.73	0.80	0.73	0.80	0.73	0.73
miRNA	miR-423-3p	miR-515-3p	miR-572	miR-639	miR-654-3p	miR-657	miR-93	
Score	0.85	0.73	0.73	0.73	0.73	0.80	0.95	

TF - miRNA interaction scores

miR-208	Score	miR-132	Score	miR-657	Score	miR-125a-5p	Score	miR-28-5p	Score	miR-93	Score
MAX	0.27	EGR1	0.93	TFAP2A	0.34	EGR1	0.86	MZF1	0.28	TFAP2A	0.34
EGR1	0.29	CREB1	0.86	SP1	0.34	PAX5	0.24	E47	0.27	SOX9	0.24
ARNT	0.27	AREB6	0.27	MZF1	0.34	NRSF	0.24	FOXCI	0.31	GATA3	0.27
RFX1	0.24	E47	0.24	MAX	0.29	ZID	0.24	FOXI1	0.24	MZF1	0.31
ATF6	0.24	ELK1	0.27	USF1	0.27	PPARG	0.27	SRY	0.27	SP1	0.34
YY1	0.27	EGR2	0.29	EGR1	0.34	GATA3	0.34	JUN	0.29	POU2F1	0.24
JUNB	0.24	FOS	0.24	RELA	0.29	MZF1	0.34	POU2F1	0.24	EGR1	0.29
POU2F1	0.24	NFIC	0.24	miR-654-3p	Score	TP53	0.34	SRY	0.27	CEBPA	0.24
NFIC	0.27	RELA	0.27	YY1	0.27	NFIC	0.34	CEBPA	0.29	NFYA	0.24
miR-345	Score	miR-423-3p	Score	BACH1	0.24	miR-299-5p	Score	RORA	0.24	RUNX1	0.24
SP1	0.34	BACH1	0.27	FOX1	0.29	CREB1	0.24	miR-363	Score	STAT1	0.24
RELA	0.27	STAT1	0.27	SRY	0.24	SRY	0.27	E2F1	0.62	E2F1	0.85
NFATC2	0.24	POU3F2	0.24	NFATC2	0.24	SRY	0.29	FOXCI	0.33	MYC	0.84
HNF4A	0.31	STAT5A	0.27	FOS	0.24	RUNX1	0.27	MZF1	0.34	miR-298	Score
NFYA	0.24	SRY	0.27	POU2F1	0.27	miR-572	Score	miR-639	Score	JUNB	0.31
POU2F1	0.24	MEF2A	0.27	NFkB1	0.24	FOXF2	0.24	NFYA	0.24		
NFIC	0.31	POU2F1	0.24	HNF1A	0.24						

TF - p21 interaction scores

TF (verified)	SP1	SP3	E2F1	Runx1	Runx2	STAT1	E2A	STAT5	TP53	TP63	TP73
Score	1.00	1.00	0.77	0.77	0.77	0.72	0.72	0.67	0.67	0.67	0.67
TF (verified)	STAT3	CUX1	TFAP2A	BRC1	VDR	RARA	C/EBPα	C/EBPβ	RB1	Tbx2	EHMT2
Score	0.66	0.66	0.60	0.60	0.60	0.60	0.60	0.60	0.60	0.60	0.60
TF (putative)	NFkB1	RELA	STAT2	STAT6	SRY						
Score	0.44	0.44	0.44	0.44	0.43						

p21 - protein interaction scores

Protein	TP53	PCNA	CASP3	CCNA1	CCND1	BCCIP	CCNA2	CCND2	CCNE2	AKT1	C1orf123	CCDC85B	CCNB1	CCNB2	CCND3
Score	1.00	0.92	0.87	0.87	0.87	0.81	0.81	0.81	0.81	0.72	0.72	0.72	0.72	0.72	0.72
Protein	CCNE1	CDC45	CDC5L	CDC6	CDC7	CDK14	CDK2	CDK3	CDK4	CDK6	CEBPA	CIZ1	CSNK2A1	CSNK2B	DAPK3
Score	0.72	0.72	0.72	0.72	0.72	0.72	0.72	0.72	0.72	0.72	0.72	0.72	0.72	0.72	0.72
Protein	ESR1	GADD45A	GADD45B	GADD45G	GMNN	GNB2L1	ITGB1BP3	MAP3K5	MAPK8	MCM10	PARP1	PIM1	POLD2	PSMA3	RAB1A
Score	0.72	0.72	0.72	0.72	0.72	0.72	0.72	0.72	0.72	0.72	0.72	0.72	0.72	0.72	0.72
Protein	SET	SLC25A11	STAT3	TEX11	TK1	TSG101	XRCC6	CDC20	CDC27	CDK5	DHX9	MDM2	NR4A1	PRKCH	RPA1
Score	0.72	0.72	0.72	0.72	0.72	0.72	0.72	0.56	0.56	0.56	0.56	0.56	0.56	0.56	0.56

Bibliography

The references are listed in alphabetical order:

Aguda, B. D., Kim, Y., Piper-Hunter, M. G., Friedman, A. & Marsh, C. B. MicroRNA regulation of a cancer network: consequences of the feedback loops involving miR-17-92, E2F, and Myc. *Proc. Natl. Acad. Sci. U.S.A.* **105**, 19678–19683 (2008).

Akao, Y., Nakagawa, Y. & Naoe, T. let-7 microRNA functions as a potential growth suppressor in human colon cancer cells. *Biol. Pharm. Bull.* **29**, 903–906 (2006).

Aldridge, B. B., Burke, J. M., Lauffenburger, D. A. & Sorger, P. K. Physicochemical modelling of cell signalling pathways. *Nat. Cell Biol.* **8**, 1195–1203 (2006).

Alexiou, P. *et al.* miRGen 2.0: a database of microRNA genomic information and regulation. *Nucleic Acids Res.* **38**, D137–141 (2010).

Alves, R., Vilaprinyo, E., Hernández-Bermejo, B. & Sorribas, A. Mathematical formalisms based on approximated kinetic representations for modeling genetic and metabolic pathways. *Biotechnol. Genet. Eng. Rev.* **25**, 1–40 (2008).

Andronov, A. A., Vitt, A. A. & Khaikin, S. É. *Theory of oscillators*. (Pergamon Press: 1966).

Angeli, D., Ferrell, J. E., Jr & Sontag, E. D. Detection of multistability, bifurcations, and hysteresis in a large class of biological positive-feedback systems. *Proc. Natl. Acad. Sci. U.S.A.* **101**, 1822–1827 (2004).

Appella, E. & Anderson, C. W. Post-translational modifications and activation of p53 by genotoxic stresses. *Eur. J. Biochem.* **268**, 2764–2772 (2001).

Ashyraliyev, M., Fomekong-Nanfack, Y., Kaandorp, J. A. & Blom, J. G. Systems biology: parameter estimation for biochemical models. *FEBS J.* **276**, 886–902 (2009).

Balsa-Canto, E., Alonso, A. A. & Banga, J. R. An iterative identification procedure for dynamic modeling of biochemical networks. *BMC Syst. Biol.* **4**, 11 (2010).

Bandyopadhyay, S. & Bhattacharyya, M. PuTmiR: a database for extracting neighboring transcription factors of human microRNAs. *BMC Bioinformatics* **11**, 190 (2010).

Bartel, D. P. MicroRNAs: genomics, biogenesis, mechanism, and function. *Cell* **116**, 281–297 (2004).

Bartel, D. P. MicroRNAs: target recognition and regulatory functions. *Cell* **136**, 215–233 (2009).

Berezikov, E. Evolution of microRNA diversity and regulation in animals. *Nat. Rev. Genet.* **12**, 846–860 (2011).

Bhattacharyya, S. N., Habermacher, R., Martine, U., Closs, E. I. & Filipowicz, W. Relief of microRNA-mediated translational repression in human cells subjected to stress. *Cell* **125**, 1111–1124 (2006).

Bibliography

- Borgdorff, V. *et al.* Multiple microRNAs rescue from Ras-induced senescence by inhibiting p21(Waf1/Cip1). *Oncogene* **29**, 2262–2271 (2010).
- Borneman, A. R. *et al.* Target hub proteins serve as master regulators of development in yeast. *Genes Dev.* **20**, 435–448 (2006).
- Brazma, A., Kapushesky, M., Parkinson, H., Sarkans, U. & Shojatalab, M. Data storage and analysis in ArrayExpress. *Meth. Enzymol.* **411**, 370–386 (2006).
- Brosh, R. *et al.* p53-Repressed miRNAs are involved with E2F in a feed-forward loop promoting proliferation. *Mol. Syst. Biol.* **4**, 229 (2008).
- Bueno, M. J., Pérez de Castro, I. & Malumbres, M. Control of cell proliferation pathways by microRNAs. *Cell Cycle* **7**, 3143–3148 (2008).
- Burke, J. V. & Ferris, M. C. A Gauss—Newton method for convex composite optimization. *Math. Program.* **71**, 179–194 (1995).
- Cacuci, D. G. & Ionescu-Bujor, M. K. *A Comparative Review of Sensitivity and Uncertainty Analysis of Large-Scale Systems - II: Statistical Methods.* *Nucl. Sci. Eng.* **147**, 204–217 (2004).
- Cha, E. J. *et al.* Expression of DBC1 and SIRT1 is associated with poor prognosis of gastric carcinoma. *Clin. Cancer Res.* **15**, 4453–4459 (2009).
- Chan, J. A., Krichevsky, A. M. & Kosik, K. S. MicroRNA-21 is an antiapoptotic factor in human glioblastoma cells. *Cancer Res.* **65**, 6029–6033 (2005).
- Chan, T. A., Hwang, P. M., Hermeking, H., Kinzler, K. W. & Vogelstein, B. Cooperative effects of genes controlling the G(2)/M checkpoint. *Genes Dev.* **14**, 1584–1588 (2000).
- Chendrimada, T. P. *et al.* MicroRNA silencing through RISC recruitment of eIF6. *Nature* **447**, 823–828 (2007).
- Cloutier, M. & Wang, E. Dynamic modeling and analysis of cancer cellular network motifs. *Integr. Biol. (Camb)* **3**, 724–732 (2011).
- Crampin, E. J., Schnell, S. & McSharry, P. E. Mathematical and computational techniques to deduce complex biochemical reaction mechanisms. *Prog. Biophys. Mol. Biol.* **86**, 77–112 (2004).
- Demin, O. & Goryanin, I. *Kinetic Modelling in Systems Biology.* (Chapman and Hall/CRC: 2008).
- Doench, J. G. & Sharp, P. A. Specificity of microRNA target selection in translational repression. *Genes Dev.* **18**, 504–511 (2004).
- Dweep, H., Sticht, C., Pandey, P. & Gretz, N. miRWalk--database: prediction of possible miRNA binding sites by ‘walking’ the genes of three genomes. *J. Biomed Inform.* **44**, 839–847 (2011).
- El-Deiry, W. S. *et al.* WAF1/CIP1 is induced in p53-mediated G1 arrest and apoptosis. *Cancer Res.* **54**, 1169–1174 (1994).
- Fabian, M. R., Sonenberg, N. & Filipowicz, W. Regulation of mRNA translation and stability by microRNAs. *Annu. Rev. Biochem.* **79**, 351–379 (2010).
- Feng, Y., Chen, X. & Gao, L. Knockdown of miR-21 as a novel approach for leukemia therapy. *J. Formos. Med. Assoc.* **109**, 621–623 (2010).

Bibliography

- Fell, D. *Understanding the Control of Metabolism*. (Portland Press: 1997).
- Ferrell, J. E., Jr & Machleder, E. M. The biochemical basis of an all-or-none cell fate switch in *Xenopus* oocytes. *Science* **280**, 895–898 (1998).
- Filipowicz, W., Bhattacharyya, S. N. & Sonenberg, N. Mechanisms of post-transcriptional regulation by microRNAs: are the answers in sight? *Nat. Rev. Genet.* **9**, 102–114 (2008).
- Ford, J., Ahmed, S., Allison, S., Jiang, M. & Milner, J. JNK2-dependent regulation of SIRT1 protein stability. *Cell Cycle* **7**, 3091–3097 (2008).
- Freedman, D. A., Wu, L. & Levine, A. J. Functions of the MDM2 oncoprotein. *Cell. Mol. Life Sci.* **55**, 96–107 (1999).
- Frey, H. C. & Patil, S. R. Identification and review of sensitivity analysis methods. *Risk Anal.* **22**, 553–578 (2002).
- Friedman, R. C., Farh, K. K.-H., Burge, C. B. & Bartel, D. P. Most mammalian mRNAs are conserved targets of microRNAs. *Genome Res.* **19**, 92–105 (2009).
- Fujita, Y. *et al.* Effects of miR-34a on cell growth and chemoresistance in prostate cancer PC3 cells. *Biochem. Biophys. Res. Commun.* **377**, 114–119 (2008).
- Funahashi, A. *et al.* CellDesigner 3.5: A Versatile Modeling Tool for Biochemical Networks. *P. IEEE* **96**, 1254–1265 (2008).
- Gardner, T. S., Cantor, C. R. & Collins, J. J. Construction of a genetic toggle switch in *Escherichia coli*. *Nature* **403**, 339–342 (2000).
- Gartel, A. L. & Tyner, A. L. Transcriptional regulation of the p21 (WAF1/CIP1) gene. *Exp. Cell Res.* **246**, 280–289 (1999).
- Ghosh, S., Matsuoka, Y., Asai, Y., Hsin, K.-Y. & Kitano, H. Software for systems biology: from tools to integrated platforms. *Nat. Rev. Genet.* **12**, 821–832 (2011).
- Goldbeter, A. Biological Rhythms as Temporal Dissipative Structures. *Special Volume in Memory of Ilya Prigogine: Advances in Chemical Physics* **135**, 253–295 (2007).
- Gomperts, B. D., Tatham, P. E. R. & Kramer, I. M. *Signal Transduction*. (Academic Press: 2002).
- Ha, T. Y. MicroRNAs in Human Diseases: From Lung, Liver and Kidney Diseases to Infectious Disease, Sickle Cell Disease and Endometrium Disease. *Immune Netw.* **11**, 309–323 (2011).
- Harper, J. W., Adami, G. R., Wei, N., Keyomarsi, K. & Elledge, S. J. The p21 Cdk-interacting protein Cip1 is a potent inhibitor of G1 cyclin-dependent kinases. *Cell* **75**, 805–816 (1993).
- Hill, A. The possible effects of the aggregation of the molecules of haemoglobin on its dissociation curves. *J. Physiol.* **40**, iv–vii (1910).
- Hsu, S. D. *et al.* miRNAmap 2.0: genomic maps of microRNAs in metazoan genomes. *Nucleic Acids Res.* **36**, D165–169 (2008).
- Hsu, S. D. *et al.* miRTarBase: a database curates experimentally validated microRNA-target interactions. *Nucleic Acids Res.* **39**, D163–169 (2011).

Bibliography

- Hübner, K., Sahle, S. & Kummer, U. Applications and trends in systems biology in biochemistry. *FEBS J.* **278**, 2767–2857 (2011).
- Hwang, H. W., Wentzel, E. A. & Mendell, J. T. A hexanucleotide element directs microRNA nuclear import. *Science* **315**, 97–100 (2007).
- Hwang, H. W. & Mendell, J. T. MicroRNAs in cell proliferation, cell death, and tumorigenesis. *Br. J. Cancer* **94**, 776–780 (2006).
- Ingalls, B. Sensitivity analysis: from model parameters to system behaviour. *Essays in Biochemistry: Systems Biology* **45**, 177–193 (2008).
- Iorio, M. V. *et al.* MicroRNA gene expression deregulation in human breast cancer. *Cancer Res.* **65**, 7065–7070 (2005).
- Jiang, L. *et al.* Hsa-miR-125a-3p and hsa-miR-125a-5p are downregulated in non-small cell lung cancer and have inverse effects on invasion and migration of lung cancer cells. *BMC Cancer* **10**, 318 (2010).
- John, B. *et al.* Human MicroRNA targets. *PLoS Biol.* **2**, e363 (2004).
- Johnson, S. M. *et al.* RAS is regulated by the let-7 microRNA family. *Cell* **120**, 635–647 (2005).
- Jones, D. R., Perttunen, C. D. & Stuckman, B. E. Lipschitzian optimization without the Lipschitz constant. *J. Optim. Theory Appl.* **79**, 157–181 (1993).
- Jung, Y.-S., Qian, Y. & Chen, X. Examination of the expanding pathways for the regulation of p21 expression and activity. *Cell. Signal.* **22**, 1003–1012 (2010).
- Juven-Gershon, T. & Oren, M. Mdm2: the ups and downs. *Mol. Med.* **5**, 71–83 (1999).
- Kai, Z. S. & Pasquinelli, A. E. MicroRNA assassins: factors that regulate the disappearance of miRNAs. *Nat. Struct. Mol. Biol.* **17**, 5–10 (2010).
- Karolchik, D. *et al.* The UCSC Genome Browser Database. *Nucleic Acids Res.* **31**, 51–54 (2003).
- Kasinski, A. L. & Slack, F. J. Epigenetics and genetics. MicroRNAs en route to the clinic: progress in validating and targeting microRNAs for cancer therapy. *Nat. Rev. Cancer* **11**, 849–864 (2011).
- Kato, M. *et al.* The mir-34 microRNA is required for the DNA damage response in vivo in *C. elegans* and in vitro in human breast cancer cells. *Oncogene* **28**, 2419–2424 (2009).
- Kerrien, S. *et al.* The IntAct molecular interaction database in 2012. *Nucleic Acids Res.* **40**, D841–846 (2012).
- Keshava Prasad, T. S. *et al.* Human Protein Reference Database--2009 update. *Nucleic Acids Res.* **37**, D767–772 (2009).
- Khanin, R. & Vinciotti, V. Computational modeling of post-transcriptional gene regulation by microRNAs. *J. Comput. Biol.* **15**, 305–316 (2008).
- Kholodenko, B., Yaffe, M. B. & Kolch, W. Computational approaches for analyzing information flow in biological networks. *Sci. Signal.* **5**, re1 (2012).
- Kim, J. E., Chen, J. & Lou, Z. DBC1 is a negative regulator of SIRT1. *Nature* **451**, 583–586 (2008).

Bibliography

- Kim, V. N. MicroRNA biogenesis: coordinated cropping and dicing. *Nat. Rev. Mol. Cell Biol.* **6**, 376–385 (2005).
- Kitano, H. Systems biology: a brief overview. *Science* **295**, 1662–1664 (2002a).
- Kitano, H. Computational systems biology. *Nature* **420**, 206–210 (2002b).
- Kitano, H., Funahashi, A., Matsuoka, Y. & Oda, K. Using process diagrams for the graphical representation of biological networks. *Nat. Biotechnol.* **23**, 961–966 (2005).
- Kozomara, A. & Griffiths-Jones, S. miRBase: integrating microRNA annotation and deep-sequencing data. *Nucleic Acids Res.* **39**, D152–157 (2011).
- Krol, J., Loedige, I. & Filipowicz, W. The widespread regulation of microRNA biogenesis, function and decay. *Nat. Rev. Genet.* **11**, 597–610 (2010).
- Kwon, H.-S. & Ott, M. The ups and downs of SIRT1. *Trends Biochem. Sci.* **33**, 517–525 (2008).
- Lai, X., Nikolov, S., Wolkenhauer, O. & Vera, J. A multi-level model accounting for the effects of JAK2-STAT5 signal modulation in erythropoiesis. *Comput. Biol. Chem.* **33**, 312–324 (2009).
- Lai, X., Wolkenhauer, O., Vera, J. Modelling miRNA regulation in cancer signalling systems: miR-34a regulation of the p53/SIRT1 signalling module. *Computational Modeling of Signaling Networks* **880**, 87–108 (2012a).
- Lai, X. U. Schmitz, S.K. Gupta, A. Bhattacharya, M. Kunz, O. Wolkenhauer, J. Vera. Computational analysis of target hub gene repression regulated by multiple and cooperative miRNAs. *Nucleic Acids Res.* **40**, 8818–34 (2012b).
- Le Novère, N. *et al.* The Systems Biology Graphical Notation. *Nat. Biotechnol.* **27**, 735–741 (2009).
- Levine, E., Ben Jacob, E. & Levine, H. Target-specific and global effectors in gene regulation by MicroRNA. *Biophys. J.* **93**, L52–54 (2007).
- Li, Z. *et al.* Inhibition of SUV39H1 methyltransferase activity by DBC1. *J. Biol. Chem.* **284**, 10361–10366 (2009).
- Liu, Y. *et al.* A multiscale computational approach to dissect early events in the Erb family receptor mediated activation, differential signaling, and relevance to oncogenic transformations. *Ann. Biomed. Eng.* **35**, 1012–1025 (2007).
- Longo, V. D. & Kennedy, B. K. Sirtuins in aging and age-related disease. *Cell* **126**, 257–268 (2006).
- Lytle, J. R., Yario, T. A. & Steitz, J. A. Target mRNAs are repressed as efficiently by microRNA-binding sites in the 5' UTR as in the 3' UTR. *Proc. Natl. Acad. Sci. U.S.A.* **104**, 9667–9672 (2007).
- Machado, D. *et al.* Modeling formalisms in Systems Biology. *AMB Express* **1**, 45 (2011).
- Maki, C. G. & Howley, P. M. Ubiquitination of p53 and p21 is differentially affected by ionizing and UV radiation. *Mol. Cell. Biol.* **17**, 355–363 (1997).
- Mangan, S. & Alon, U. Structure and function of the feed-forward loop network motif. *Proc. Natl. Acad. Sci. U.S.A.* **100**, 11980–11985 (2003).

Bibliography

- Martinez, N. J. & Walhout, A. J. M. The interplay between transcription factors and microRNAs in genome-scale regulatory networks. *Bioessays* **31**, 435–445 (2009).
- Milo, R., Jorgensen, P., Moran, U., Weber, G. & Springer, M. BioNumbers--the database of key numbers in molecular and cell biology. *Nucleic Acids Res.* **38**, D750–753 (2010).
- Miranda, K. C. *et al.* A pattern-based method for the identification of MicroRNA binding sites and their corresponding heteroduplexes. *Cell* **126**, 1203–1217 (2006).
- Mishra, P. J. & Merlino, G. MicroRNA reexpression as differentiation therapy in cancer. *J. Clin. Invest.* **119**, 2119–2123 (2009).
- Miyoshi, K., Miyoshi, T. & Siomi, H. Many ways to generate microRNA-like small RNAs: non-canonical pathways for microRNA production. *Mol. Genet. Genomics* **284**, 95–103 (2010).
- Nelson, D. E. *et al.* Oscillations in NF-kappaB signaling control the dynamics of gene expression. *Science* **306**, 704–708 (2004).
- Nikolov, S., Lai, X., Liebal, U. W., Wolkenhauer, O. & Vera, J. Integration of sensitivity and bifurcation analysis to detect critical processes in a model combining signalling and cell population dynamics. *Intern. J. Syst. Sci.* **41**, 81–105 (2010).
- Nissan, T. & Parker, R. Computational analysis of miRNA-mediated repression of translation: implications for models of translation initiation inhibition. *RNA* **14**, 1480–1491 (2008).
- Oglesby, I. K., McElvaney, N. G. & Greene, C. M. MicroRNAs in inflammatory lung disease--master regulators or target practice? *Respir. Res.* **11**, 148 (2010).
- Ono, K., Kuwabara, Y. & Han, J. MicroRNAs and cardiovascular diseases. *FEBS J.* **278**, 1619–1633 (2011).
- Ørom, U. A., Nielsen, F. C. & Lund, A. H. MicroRNA-10a binds the 5'UTR of ribosomal protein mRNAs and enhances their translation. *Mol. Cell* **30**, 460–471 (2008).
- Osella, M., Bosia, C., Corá, D. & Caselle, M. The role of incoherent microRNA-mediated feedforward loops in noise buffering. *PLoS Comput. Biol.* **7**, e1001101 (2011).
- Pastori G., Simons V. & Bogaert M. Systems biology in the European research. www.erasysbio.net, (2008).
- Press, W. H. *Numerical Recipes: The Art of Scientific Computing*. (Cambridge University Press: 2007).
- Purvis, J., Ilango, V. & Radhakrishnan, R. Role of network branching in eliciting differential short-term signaling responses in the hypersensitive epidermal growth factor receptor mutants implicated in lung cancer. *Biotechnol. Prog.* **24**, 540–553 (2008).
- Ramalingam, S. *et al.* Quantitative assessment of the p53-Mdm2 feedback loop using protein lysate microarrays. *Cancer Res.* **67**, 6247–6252 (2007).
- Raue, A. *et al.* Structural and practical identifiability analysis of partially observed dynamical models by exploiting the profile likelihood. *Bioinformatics* **25**, 1923–1929 (2009).
- Riley, T., Sontag, E., Chen, P. & Levine, A. Transcriptional control of human p53-regulated genes. *Nat. Rev. Mol. Cell Biol.* **9**, 402–412 (2008).

Bibliography

- Rodier, F., Campisi, J. & Bhaumik, D. Two faces of p53: aging and tumor suppression. *Nucleic Acids Res.* **35**, 7475–7484 (2007).
- Rossi, J. J. New hope for a microRNA therapy for liver cancer. *Cell* **137**, 990–992 (2009).
- Ruby, J. G., Jan, C. H. & Bartel, D. P. Intronic microRNA precursors that bypass Drosha processing. *Nature* **448**, 83–86 (2007).
- Saetrom, P. *et al.* Distance constraints between microRNA target sites dictate efficacy and cooperativity. *Nucleic Acids Res.* **35**, 2333–2342 (2007).
- Saltelli, A., Chan, K. & Scott, E. M. *Sensitivity Analysis*. (John Wiley & Sons: 2009).
- Sanga, S. *et al.* Predictive oncology: a review of multidisciplinary, multiscale in silico modeling linking phenotype, morphology and growth. *Neuroimage* **1**, 120–134 (2007).
- Savageau, M.A. A critique of the enzymologist's test tube. *Fundamentals of Medical Cell Biology* **3a**, 45–108 (1992).
- Savageau, M.A. Biochemical systems analysis. I. Some mathematical properties of the rate for the design law for the component enzymatic reactions. *J. Theor. Biol.* **25**, 365–369 (1969a).
- Savageau, M. A. Biochemical systems analysis. II. The steady-state solutions for an n-pool for the design system using a power-law approximation. *J. Theor. Biol.* **25**, 370–379 (1969a).
- Sax, J. K. & El-Deiry, W. S. p53 downstream targets and chemosensitivity. *Cell Death Differ.* **10**, 413–417 (2003).
- Schoeberl, B. *et al.* Therapeutically targeting ErbB3: a key node in ligand-induced activation of the ErbB receptor-PI3K axis. *Sci. Signal.* **2**, ra31 (2009).
- Schultz, J., Ibrahim, S. M., Vera, J. & Kunz, M. 14-3-3sigma gene silencing during melanoma progression and its role in cell cycle control and cellular senescence. *Mol. Cancer* **8**, 53 (2009).
- Schultz, J., Lorenz, P., Gross, G., Ibrahim, S. & Kunz, M. MicroRNA let-7b targets important cell cycle molecules in malignant melanoma cells and interferes with anchorage-independent growth. *Cell Res.* **18**, 549–557 (2008).
- Selbach, M. *et al.* Widespread changes in protein synthesis induced by microRNAs. *Nature* **455**, 58–63 (2008).
- Sethupathy, P., Corda, B. & Hatzigeorgiou, A. G. TarBase: A comprehensive database of experimentally supported animal microRNA targets. *RNA* **12**, 192–197 (2006).
- Sha, W. *et al.* Hysteresis drives cell-cycle transitions in *Xenopus laevis* egg extracts. *Proc. Natl. Acad. Sci. U.S.A.* **100**, 975–980 (2003).
- Shalgi, R., Lieber, D., Oren, M. & Pilpel, Y. Global and local architecture of the mammalian microRNA-transcription factor regulatory network. *PLoS Comput. Biol.* **3**, e131 (2007).
- Shenouda, S. K. & Alahari, S. K. MicroRNA function in cancer: oncogene or a tumor suppressor? *Cancer Metastasis Rev.* **28**, 369–378 (2009).
- Sinha, A. U., Kaimal, V., Chen, J. & Jegga, A. G. Dissecting microregulation of a master regulatory network. *BMC Genomics* **9**, 88 (2008).

Bibliography

- Strogatz, S. *Nonlinear Dynamics and Chaos: With Applications to Physics, Biology, Chemistry and Engineering*. (Westview Press: 2000).
- Szklarczyk, D. *et al.* The STRING database in 2011: functional interaction networks of proteins, globally integrated and scored. *Nucleic Acids Res.* **39**, D561–568 (2011).
- Tang, B. Orthogonal Array-Based Latin Hypercubes. *J. Am. Stat. Assoc.* **88**, 1392–1397 (1993).
- Takamizawa, J. *et al.* Reduced expression of the let-7 microRNAs in human lung cancers in association with shortened postoperative survival. *Cancer Res.* **64**, 3753–3756 (2004).
- Tsang, J., Zhu, J. & van Oudenaarden, A. MicroRNA-mediated feedback and feedforward loops are recurrent network motifs in mammals. *Mol. Cell* **26**, 753–767 (2007).
- Tyson, J. J., Chen, K. C. & Novak, B. Sniffers, buzzers, toggles and blinkers: dynamics of regulatory and signaling pathways in the cell. *Curr. Opin. Cell Biol.* **15**, 221–231 (2003).
- Vaziri, H. *et al.* hSIR2(SIRT1) functions as an NAD-dependent p53 deacetylase. *Cell* **107**, 149–159 (2001).
- Vera, J., Nikolov, S., Lai, X., Singh, A. & Wolkenhauer, O. Model-based investigation of the transcriptional activity of p53 and its feedback loop regulation via 14-3-3 σ . *IET Syst. Biol.* **5**, 293–307 (2011).
- Vera, J., Balsa-Canto, E., Wellstead, P., Banga, J. R. & Wolkenhauer, O. Power-law models of signal transduction pathways. *Cellular Signalling* **19**, 1531–1541 (2007).
- Vera, J. *et al.* Dynamical effects of epigenetic silencing of 14-3-3sigma expression. *Mol. Biosyst.* **6**, 264–273 (2010).
- Vera, J. & Wolkenhauer, O. A system biology approach to understand functional activity of cell communication systems. *Methods Cell Biol.* **90**, 399–415 (2008).
- Vitale, I., Galluzzi, L., Castedo, M. & Kroemer, G. Mitotic catastrophe: a mechanism for avoiding genomic instability. *Nat. Rev. Mol. Cell Biol.* **12**, 385–392 (2011).
- Vohradsky, J., Panek, J. & Vomastek, T. Numerical modelling of microRNA-mediated mRNA decay identifies novel mechanism of microRNA controlled mRNA downregulation. *Nucleic Acids Res.* **38**, 4579–4585 (2010).
- Voit, E. O. *Computational Analysis of Biochemical Systems: A Practical Guide for Biochemists and Molecular Biologists*. (Cambridge University Press: 2000).
- Waltemath, D. *et al.* Minimum information about a simulation experiment (MIASE). *PLoS Comput. Biol.* **7**, e1001122 (2011).
- Wang, J., Lu, M., Qiu, C. & Cui, Q. TransmiR: a transcription factor-microRNA regulation database. *Nucleic Acids Res.* **38**, D119–122 (2010).
- Wang, W. *et al.* HuR regulates p21 mRNA stabilization by UV light. *Mol. Cell. Biol.* **20**, 760–769 (2000).
- Whichard, Z. L., Motter, A. E., Stein, P. J. & Corey, S. J. Slowly produced microRNAs control protein levels. *J. Biol. Chem.* **286**, 4742–4748 (2011).

Bibliography

- Wittig, U. *et al.* SABIO-RK--database for biochemical reaction kinetics. *Nucleic Acids Res.* **40**, D790–796 (2012).
- Wolkenhauer, O., Ullah, M., Wellstead, P. & Cho, K.-H. The dynamic systems approach to control and regulation of intracellular networks. *FEBS Lett.* **579**, 1846–1853 (2005).
- Wu, S. *et al.* Multiple microRNAs modulate p21Cip1/Waf1 expression by directly targeting its 3' untranslated region. *Oncogene* **29**, 2302–2308 (2010).
- Xiao, F. *et al.* miRecords: an integrated resource for microRNA-target interactions. *Nucleic Acids Res.* **37**, D105–110 (2009).
- Xie, Z.-R., Yang, H.-T., Liu, W.-C. & Hwang, M.-J. The role of microRNA in the delayed negative feedback regulation of gene expression. *Biochem. Biophys. Res. Commun.* **358**, 722–726 (2007).
- Xiong, W. & Ferrell, J. E., Jr A positive-feedback-based bistable 'memory module' that governs a cell fate decision. *Nature* **426**, 460–465 (2003).
- Xu, F., Liu, Z., Shen, J. & Wang, R. Dynamics of microRNA-mediated motifs. *IET Syst. Biol.* **3**, 496–504 (2009).
- Yagil, G. & Yagil, E. On the Relation between Effector Concentration and the Rate of Induced Enzyme Synthesis. *Biophys. J.* **11**, 11–27 (1971).
- Yamakuchi, M., Ferlito, M. & Lowenstein, C. J. miR-34a repression of SIRT1 regulates apoptosis. *Proc. Natl. Acad. Sci. U.S.A.* **105**, 13421–13426 (2008).
- Yamakuchi, M. & Lowenstein, C. J. MiR-34, SIRT1 and p53: the feedback loop. *Cell Cycle* **8**, 712–715 (2009).
- Zhao, W. *et al.* Negative regulation of the deacetylase SIRT1 by DBC1. *Nature* **451**, 587–590 (2008).

Scientific contributions

Publications directly related to the topics of microRNAs:

- **X. Lai**, O. Wolkenhauer, J. Vera. Modelling miRNA regulation in cancer signalling systems: miR-34a regulation of the p53/SIRT1 signalling module. *Computational Modeling of Signaling Networks*, X. Liu and M. Betterton (eds.), Humana, 2012, ISBN: 9781617798230, doi:10.1007/978-1-61779-833-7_6.

Author contributions: XL designed the study and set up the mathematical model. XL performed the simulations. Model analyses were performed by XL and JV. All the authors drafted the manuscript.

- **X. Lai**^{*}, U. Schmitz^{*}, S.K. Gupta, A. Bhattacharya, M. Kunz, O. Wolkenhauer, J. Vera. Computational analysis of target hub gene repression regulated by multiple and cooperative miRNAs. *Nucleic Acids Research*, 40(18), 8818-34, 2012, doi:10.1093/nar/gks657.

^{*}These authors equally contributed to this work.

Author contributions: The original idea was developed by JV, US and XL. Mathematical model was derived by JV and XL. Numerical simulations and model analyses were implemented and performed by XL. Bioinformatics analyses were performed by SKG, US and XL. The experiments were carried out by AB and MK. XL, JV, US and OW drafted the manuscript.

Journal Publications

- J. Vera, S. Nikolov, **X. Lai**, A. Singh, O. Wolkenhauer. A model-based investigation of the transcriptional activity of p53 and its feedback loop regulation via 14-3-3 σ . *IET Systems Biology*, 5(5), 293-307, 2011, doi:10.1049/iet-syb.2010.0080.

Author contributions: The initial idea for the investigation comes from JV, SN and OW. The model was derived, computed and simulated by JV and XL. AS retrieved data. Stability and bifurcation analysis was performed by SN. The manuscript was drafted by JV, SN and OW.

- S. K. Gupta, S.K. Gupta, S. Smita, M. Srivastava, **X. Lai**, U. Schmitz, Q. Rahman, O. Wolkenhauer, J. Vera. Computational analysis and modeling the effectiveness of ‘Zanamivir’ targeting neuraminidase protein in pandemic H1N1 strains. *Infection, Genetics and Evolution*, 11(5), 1072-1082, 2011, doi:10.1016/j.meegid.2011.03.018.

Author contributions: XL performed the simulations and model analyses.

- **X. Lai**, S. Nikolov, O. Wolkenhauer, J. Vera. A multi-level model accounting for the effects of JAK2-STAT5 signal modulation in erythropoiesis. *Computational Biology and Chemistry*, 33(4), 312-324, 2009, doi:10.1016/j.compbiolchem.2009.07.003.

Author contributions: JV, XL and SN designed the study and set up the mathematical model. XL performed the calculations concerning the predictive simulations. Model analyses were performed by XL and JV. Finally, all the authors drafted the manuscript.

- S. Nikolov*, **X. Lai***, O. Wolkenhauer, J. Vera. Time delay and protein modulation analysis in a model of RNA silencing. *Communications of SIWN*, 6, 111-117, 2009, sai:cosiwn.2009.04.027.

*These authors equally contributed to this work.

Author contributions: XL, JV and SN designed the study and set up the mathematical model. XL performed the sensitivity analysis and the simulations. SN performed the bifurcation analysis. All the authors drafted the manuscript.

- S. Nikolov, **X. Lai**, U. W. Liebal, O. Wolkenhauer, J. Vera. Integration of Sensitivity and Bifurcation Analysis to Detect Critical Processes in a Model Combining Signaling and Cell Population Dynamics. *International Journal of Systems Science*, 41(1), 81-105, 2009, doi:10.1080/00207720903147746.

Author contributions: JV, XL and SN designed the study and derived the equations of the model. XL performed the sensitivity analysis with the support of UL. XL and SN performed the bifurcation analysis. XL performed the model simulations. Model analyses were performed by XL and JV. All the authors drafted the manuscript.

Book chapter

- J. Vera, **X. Lai**, U. Schmitz, O. Wolkenhauer. MicroRNA-regulated networks: the perfect storm for classical molecular biology, the ideal scenario for systems biology. *miRNA Cancer Regulation: Advanced Concepts, Bioinformatics and Systems Biology Tools*, J. Vera and U. Schmitz (eds.), Springer, 2012, ISBN: 9789400755895.

Encyclopaedia Essays

- **X. Lai**, J. Vera. miRNA feed forward loops. *Encyclopaedia of Systems Biology*, W. Dubitzky, O. Wolkenhauer, H. Yokata, K.H. Cho (eds.), Springer, 2012, ISBN: 9781441998620.
- **X. Lai**, J. Vera. miRNA clusters. *Encyclopaedia of Systems Biology*, W. Dubitzky, O. Wolkenhauer, H. Yokata, K.H. Cho (eds.), Springer, 2012, ISBN: 9781441998620.

- **X. Lai, J. Vera.** miRNA target hub. *Encyclopaedia of Systems Biology*, W. Dubitzky, O. Wolkenhauer, H. Yokata, K.H. Cho (eds.), Springer, 2012, ISBN: 9781441998620.

Conference Talks

- **Time delay and protein modulation analysis in a model of RNA silencing.** *The 2nd SIWN Congress- the 2nd International Conference on Bioinformatics and Systems Biology* (BSB 2009), Leipzig, Germany.
- **Integration of sensitivity and bifurcation analysis to detect critical processes in a model combining signalling and cell population dynamics.** *The 6th computational Methods in Systems Biology* (CMSB2008), Rostock, Germany (Short talk).

Conference Posters

- **A systems biology approach to study the cellular function of microRNAs.** *International Workshop on Small RNA in Cancer, Inflammation, and Aging*, Copenhagen, Denmark, 2012.
- **The role of microRNA regulation in the early inflammatory response: miR-146a and NFκB signalling in lung inflammation.** *Symposium on Remodeling, Repair and Regeneration in Lung Diseases*, Marburg, Germany, 2012 (**Best poster award**).
- **On the regulation of microRNA target hubs: a Systems Biology perspective.** *The 12th International Conference on Systems Biology* (ICSB2011), Heidelberg/Mannheim, Germany, 2011.
- **The role of microRNA regulation in the early inflammatory response: miR-146a and NFκB signalling in lung inflammation.** *The 12th International Conference on Systems Biology* (ICSB2011), Heidelberg/Mannheim, Germany, 2011.
- **Modelling miRNA regulation in signalling networks: miR-34a regulation of p53/SIRT1 module.** *The 3rd Conference on Systems Biology of Mammalian Cells* (SBMC2010), Freiburg, Germany, 2010.
- **A multi-level model accounting for the effects of JAK2- STAT5 signal modulation in erythropoiesis.** *The 2009 International Workshop on 'Computational and Integrative Biology'* (CIB 2009), Hangzhou, China, 2009.
- **Mathematical modelling of p53/miR-34a pathway.** *Transatlantic Summer School on Cancer Systems Biology* (CaSysBio), Rostock, Germany, 2009.
- **Use of sensitivity analysis to detect critical biochemical processes in a mathematical model linking intracellular and cell population dynamics in erythropoiesis.** *Systems Biology for Medical Applications Summer School 2008*, Tenerife, Spain, 2008.



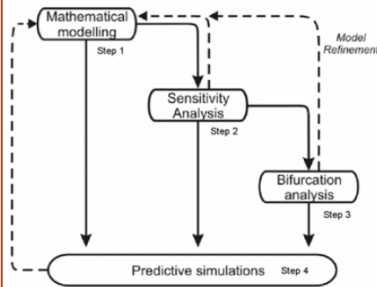
Integration of sensitivity and bifurcation analysis to detect critical processes in cell signalling pathways

X. Lai¹, S. Nikolov², U. Liebal¹, O. Wolkenhauer¹ and J. Vera¹

¹University of Rostock, Systems Biology and Bioinformatics Group (Germany)

²Institute of Mechanics and Biomechanics-BAS, Bulgarian Academy of Sciences (Sofia, Bulgaria)

Scheme of our Methodology



1. Mathematical modelling:

Set up the mathematical model using ordinary differential equations.

2. Sensitivity analysis:

Rank model parameters according to their sensitivity indices.

3. Qualitative bifurcation analysis:

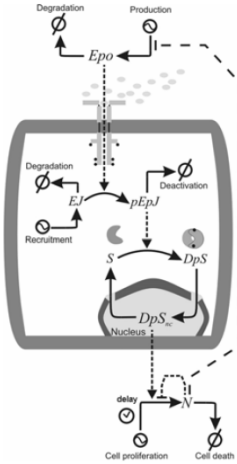
Determine the bifurcation points and stability Regions by using qualitative bifurcation analysis.

4. Predictive simulations:

Simulation of critical dynamic properties when we change the values of selected model parameters.

Case Study

1. Mathematical Model

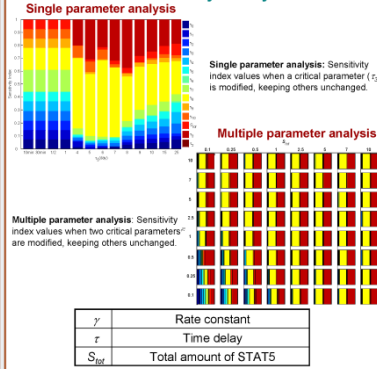


Mathematical model composed of JAK2-STAT5 signalling pathway and proliferation model of red blood cells. For details of the model see [1].

References

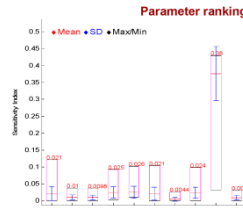
- [1] J. Vera et al. (2008): A systems biology approach to analyse amplification in the JAK2-STAT5 signalling pathway. *BMC Systems Biology*, 2:38.
- [2] S. Nikolov. (2008): Stability and bifurcation behavior of genetic regulatory systems with two delays. *Comptes rendus de l'Académie bulgare des Sciences*, 61(5), 585-594.
- [3] H. Schmitt et al. (2006): Systems Biology Toolbox for MATLAB: A computational platform for research in Systems Biology. *Bioinformatics*, 22(4), 514-515.

3. Sensitivity Analysis



After the above analysis, we get the following critical parameter ranking list:

$$SARK = \{\tau_3, \gamma_6, \gamma_{10}, S_{tot}, \gamma_3, \gamma_4, \gamma_7, \gamma_5, \gamma_8\}$$



3. Qualitative Bifurcation Analysis

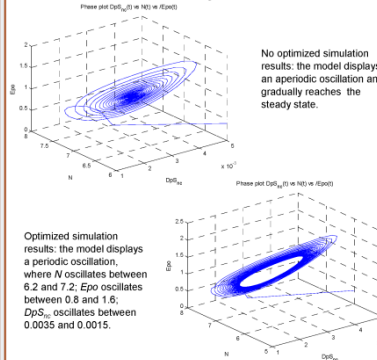
Based on the biological information we have another parameter ranking list:

$$BFRK = \{\gamma_0, \gamma_2, S_{tot}, \gamma_6, \tau_3, \gamma_{10}, \gamma_8\}$$

The intersection of the two sets are:

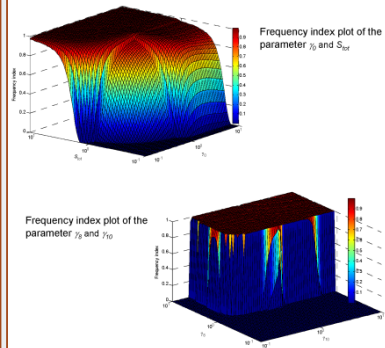
$$SARK \cap BFRK = \{\gamma_0, S_{tot}, \tau_3, \gamma_{10}, \gamma_6\}$$

Then we use bifurcation analysis to investigate the modulation of parameter τ_3 .



4. Predictive Simulations

In this part we investigate how the dynamic property of the model changes when the values of pairs of critical parameters ($\gamma_0 \cdot S_{tot}$ and $\gamma_6 \cdot \gamma_{10}$) are modified in an interval of biologically relevant values.



From the above two figures, we get three conclusions of the dynamic property of the model changes with the modified critical parameter values as follows:

1. Blue area (Frequency index less than 0.1): the oscillation of the model weakens very fast to the steady state.
2. Red area (Frequency index greater than 0.9): the model can display the stable periodic oscillation.
3. Transition area (Frequency index between 0.1 and 0.9): the model displays aperiodic oscillation, which weakens much slower than the red area, the smaller the value of frequency index is, faster the oscillation weakens.

Summary

We developed a methodology, combining sensitivity and bifurcation analysis.

We performed systematic simulations changing the value of critical parameters, observing their influence on the dynamics.

The method succeeded in detecting critical processes in sub-cellular dynamics.

The whole procedure validates the feasibility of our methodology. The next step is to develop a software package for general use.

Acknowledgements

Founded through CALSYS
(Investigating the Cancer and Aging Link through Systems Biology)



Contact

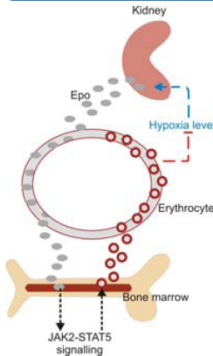
Xin Lai
FORSYS Junior Research Group CALSYS
Systems Biology and Bioinformatics
University of Rostock
Albert Einstein Str. 21
18059 Rostock, Germany
Email: xin.lai@uni-rostock.de
Website: www.sbi.uni-rostock.de

A multi-level model accounting for the effects of JAK2-STAT5 signal modulation in erythropoiesis

Xin Lai^a, Svetoslav Nikolov^b, Olaf Wolkenhauer^a, Julio Vera^a

^aSystems Biology and Bioinformatics Group, University of Rostock, Germany, ^bInstitute of Mechanics and Biomechanics-BAS, Sofia, Bulgaria

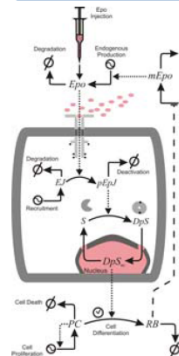
Abstract



We develop a multi-level model, in ordinary differential equations, based on quantitative experimental data, accounting for murine erythropoiesis. At the sub-cellular level, the model includes a description of the regulation of red blood cell differentiation through Epo-stimulated JAK2-STAT5 signalling activation, while at the cell population level the model describes the dynamics of (STAT5-mediated) red blood cell differentiation from their progenitors. Furthermore, the model also includes equations depicting the hypoxia mediated regulation of hormone erythropoietin blood levels (Fig. 1). Based on the model, we investigate the effect of deregulation of specified proteins involved in the JAK2-STAT5 signalling pathway on red blood cells. Our results suggest that down-regulation in any of the three signalling proteins considerably affects the hematocrit levels. In addition, our analysis predicts that exogenous Epo injection (an already existing treatment for several blood diseases) may compensate the effects of either single down-regulation of Epo hormone level, STAT5 or EpoR/JAK2 expression level, but it may be insufficient to counteract a combined down-regulation for both of them (the results have been published in Lai et al. 2009).

Figure 1 Scheme depicting the multi-level feedback loop controlling red blood cell differentiation/proliferation through the modulation of hypoxia levels, hormone erythropoietin production/delivery and JAK2-STAT5 signalling pathway.

Modelling



The model represented in the following ODEs accounts for three modules: 1. the molecular processes involved in the activation of the signalling pathway JAK2-STAT5 (Eqs. 1-4). 2. Dynamics of proliferation and differentiation of erythrocyte (Eqs. 5, 6). 3. Dynamics of the hormone Epo, for which we consider both endogenous synthesis and exogenous Epo injection (Eqs. 7, 8), (Fig. 2).

$$\begin{aligned} \frac{d}{dt} EJ &= \gamma_{EJ} - \gamma_{EJ} \cdot EJ \cdot (Epo + Epo_{inj}) - \gamma_{EJ} \cdot EJ & (1) \\ \frac{d}{dt} pEpoJ &= \gamma_{EJ} \cdot EJ \cdot (Epo + Epo_{inj}) - \gamma_{EJ} \cdot pEpoJ & (2) \\ \frac{d}{dt} DpS &= \gamma_{DpS} \cdot (S_{Hb} - 2 \cdot DpS - 2 \cdot DpS_{in}) - pEpoJ \cdot DpS & (3) \\ \frac{d}{dt} DpS_{in} &= \gamma_{DpS_{in}} \cdot DpS - \gamma_{DpS_{in}} \cdot DpS_{in} & (4) \\ \frac{d}{dt} PC &= \gamma_{PC} \cdot PC - \gamma_{PC} \cdot PC \cdot DpS_{in} - \gamma_{PC} \cdot PC^{-1} & (5) \\ \frac{d}{dt} RB &= \gamma_{RB} \cdot PC \cdot (1 - \tau) \cdot DpS_{in} - \gamma_{RB} \cdot RB & (6) \\ \frac{d}{dt} mEpo &= \frac{\gamma_{mEpo}}{RB} - \gamma_{mEpo} \cdot mEpo & (7) \\ \frac{d}{dt} Epo &= \gamma_{Epo} \cdot mEpo - \gamma_{Epo} \cdot Epo & (8) \end{aligned}$$

Figure 2 Detailed structure of the multi-level mathematical model proposed to describe effects of Epo signalling affecting differentiation and proliferation into mature red blood cells. Solid lines represent rate processes. The synchro/clock symbol refers to synthesis and degradation processes respectively. The 'block' symbol refers to a time-delay in the considered process.

Predictive Simulations

i. Loss of red blood cells

Based on our previous knowledge, we can verify that the deregulation of some important features in the JAK2-STAT5 pathway seems to induce important dynamical changes in the system and these changes could cause an unexpected loss of red blood cells (RB). Herein, we consider down-regulation of three important parameters (γ_{DpS} , $\gamma_{DpS_{in}}$ and S_{Hb}) accounting for dynamic features of the JAK2-STAT5 pathway in two ways (Fig. 3): 1. Individual down-regulation, we simulate repression of single parameter values. 2. Mutual down-regulation, we simulate down-regulation of two parameters at the same time, to observe the steady state level of RB.

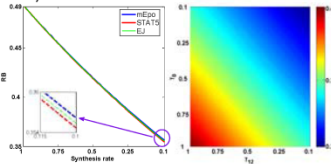


Figure 3 Steady state level of red blood cells (RB) for individual (left) and mutual (right) down-regulation of the specified parameters.

ii. Injection of erythropoietin

As we see, the down-regulation of specified proteins can lead to the loss of the red blood cells we model the injection of exogenous erythropoietin (Epo) to recover the RB to its basal level, ensuring the normal function of the whole system. The injection equation (Eq. 9) of Epo is derived from the pharmacokinetic equations described by Kato et al (Fig. 4) and we used the homologous experiment data to estimate the values of the coefficients.

$$Epo_{inj} = \frac{Epo_{max}}{A + B} \cdot (Ae^{-at} - Be^{-bt}) \quad (9)$$

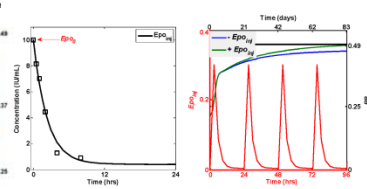


Figure 4 Parameter estimation for Epo injection dynamics (left) and the right figure illustrates the simulation for the effects of daily Epo injection (red solid line) on the levels of RB for weak down-regulation of STAT5 ($S_{Hb} = 0.72$) with (green solid line) or without (blue solid line) Epo injection. The black solid line represents the basal level of RB.

iii. Recovery of red blood cells

Via the exogenous injection of the Epo, it is possible to compensate the loss of RB when the individual down-regulation of specified protein happens, but when we simulate the repression of two proteins at the mean time, the level of RB can only trace back to its normal level under some conditions. As shown in Fig. 5, the minimal requirement of Epo_{inj} to cancel out the loss of RB for the down-regulation of γ_{DpS} and S_{Hb} (right) are much higher than the repression of another group γ_{DpS} and S_{Hb} (left). The maximum difference between the injection of Epo in both scenarios can reach 43 folds, suggesting that it is physiologically impossible to inject such a huge amount of Epo to restore the level of RB when extreme inhibition of both STAT5 and EJ hampers simultaneously.

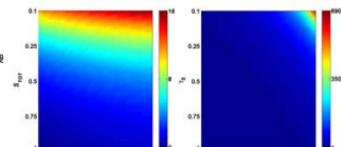


Figure 5 The simulation results of minimum Epo injection (Epo_{inj}) which is necessary to recover the healthy basal state for RB under the simultaneous down-regulation of two proteins involved in the system.

Parameter Estimation

In order to assign values to the parameters in our model, we proceed in the following manner: (i) we used the parameters values estimated from quantitative time series in our previous paper (Svetoslav et al. 2009) to characterize the equations accounting for the JAK2-STAT5 signalling (Eqs. 1-4); (ii) we extracted the data published by Koury and his colleagues (Koury et al. 1989) to estimate the values of the parameters accounting for Epo synthesis, and cell population dynamics (Eqs. 5-8), see Fig. 6; (iii) parameter γ_{DpS} was adjusted during step (ii) in order to make both parts of the model match.

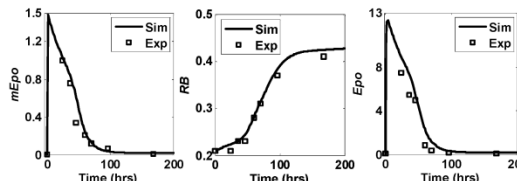


Figure 6 Data fitting of the selected solution for the observable messenger RNA of Epo (left), hematocrit levels (center) and serum levels of Epo (right). Solid lines represent the simulation results calculated by using the estimated parameter values, while square markers represent the experiment data from Koury et al. In the experiment, quantitative time series of hematocrit (RB), Epo and mEpo levels were measured after inducing acute anemia in mice.

Conclusions

- Our results suggest that this kind of multi-level model, integrating intracellular biochemical networks (cell signalling, metabolism and/or gene transcription), together with its effects in cell population dynamics and tissue organization, will be a very useful method in the coming phases for the development of Systems Biology.
- The main advantage of the multi-level data integration strategy through mathematical modelling will help the biologist to improve the design of experiments, reduce the experimental effort, and also be crucial for boosting drug discovery.
- Lacking of wet lab data could be the biggest barrier for modelers to set up a large-scaled multi-level model and integration of huge amount of diverse quantitative data is a challenge in the future.

References

- Lai X, Nikolov S, Wolkenhauer O, Vera J. (2009) A multi-level model accounting for the effects of JAK2-STAT5 signal modulation in erythropoiesis. *Comput Biol Chem*. 2009 Aug;33(4):212-24.
- Nikolov S, X. Lai, U. W. Liebel, O. Wolkenhauer, J. Vera (2009). Integration of Sensitivity and Bifurcation Analysis to Detect Critical Processes in a Model Combining Signalling and Cell Population Dynamics. *International Journal of Systems Science (in press)*.
- Stephen T. Koury, Mark J. Koury, Maurice C. Bonduant, Jaime Caro, and Stanley E. Greber. (1989) Quantitation of Erythropoietin-Producing Cells in Kidneys of Mice by In Situ Hybridization: Correlation With Hematocrit, Renal Erythropoietin mRNA, and Serum Erythropoietin Concentration. *Blood*. 74(2): 645-651.
- Kato M, Miura K, Kaniyama H, Okazaki A, Kumaki K, Kato Y, Sugiyama Y. (1998) Pharmacokinetics of erythropoietin in genetically anemic mice *Drug Metab Dispos*. 26(2):126-31.

www.sbi.uni-rostock.de

Supported by



Contact:

Xin Lai
Email: xin.lai@uni-rostock.de
Web: www.sbi.uni-rostock.de/cadys
Affiliation: System Biology & Bioinformatics Group
Institute of Informatics (University of Rostock, Germany)

Post address:

Ulmenstrasse 69,
Haus 3, 3.0 G
18057 Rostock
Mecklenburg-Vorpommern, Germany
Tel.: +49 0381 498 7604



Modeling miRNA regulation in signaling networks: miR-34a regulation of the p53/Sirt1 module

Xin Lai, Julio Vera and Olaf Wolkenhauer
Systems Biology and Bioinformatics Group, University of Rostock, Germany

Abstract

Micro RNAs are a family of small regulatory RNAs whose function is to regulate the activity and stability of specific messenger RNA targets through post-translational regulatory mechanisms. We studied a signaling module composed by p53, Sirt1 and the small regulatory miRNA, miR-34a, based on the integration of experimental evidence and quantitative data, with mathematical modeling. We further used the model to investigate different possible designs of the silencing mechanisms exerted by miR-34a on Sirt1, and to simulate the dynamics of the system under pathological conditions of deregulation of its components.

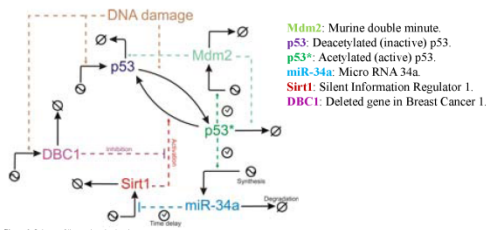


Figure 1: Scheme of the analyzed network.

Modeling

We used ordinary differential equations (ODEs) to describe the interactions of the components in the network. We then characterized the parameter values in the model by using the following strategies: (i) we fixed some parameter values by using the known protein half-life; (ii) for the rest parameters, we constrained them in an biologically meaningful interval and estimated them by combining the experimental data published by Yamakuchi et al. (2008) and Suzuki et al. (2009). We used the experimental data generated by Yamakuchi and Lowenstein (2009) to check the validity of the model.

$$\begin{aligned}\frac{d}{dt} Mdm2 &= k_{on_Mdm2} \cdot p53^* (t - \tau_1) - k_{deg_Mdm2} \cdot Mdm2 \\ \frac{d}{dt} p53 &= k_{on_p53} + k_{act_p53} \cdot Dd + \frac{k_{p_p53} \cdot p53^* \cdot Sirt1}{DBC1} - k_{p_p53} \cdot p53 \cdot Dd - k_{deg_p53} \cdot p53 \cdot Mdm2 \\ \frac{d}{dt} p53^* &= k_{p_p53} \cdot p53 \cdot Dd - \frac{k_{p_p53} \cdot p53^* \cdot Sirt1}{DBC1} - k_{deg_p53} \cdot p53^* \cdot Mdm2 \\ \frac{d}{dt} miR34 &= k_{on_miR34} + k_{act_miR34} \cdot p53^* (t - \tau_2) - k_{deg_miR34} \cdot miR34 \\ \frac{d}{dt} Sirt1 &= \frac{k_{on_Sirt1}}{miR34(t - \tau_3)} \cdot Sirt1 \\ \frac{d}{dt} DBC1 &= k_{on_DBC1} + k_{act_DBC1} \cdot Dd - k_{deg_DBC1} \cdot DBC1\end{aligned}$$

Predictive Simulations

i. Analyzing the mechanism of miR-34a post-translational repression of Sirt1

We expanded the initial mathematical model by introducing four different mechanisms of miR-34a-mediated Sirt1 repression (see Fig. 2 Top). We then simulated the model in five different conditions to predict whether an experiment with such design could help discriminate between the different regulatory mechanisms (see Fig. 2 Bottom).

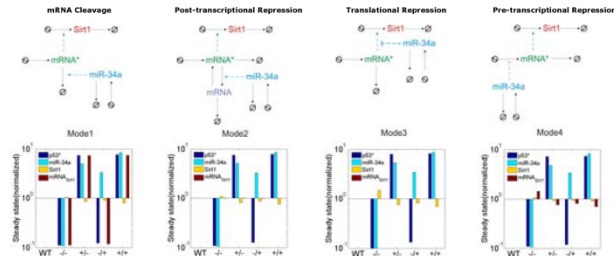


Figure 2: Top: The simplified scheme of four types of miRNA silencing mechanisms. Bottom: Simulation results of different miRNA silencing mechanisms under specific experimental condition. WT: wild type; +/-: up or down regulation of specific component. The model comparison suggests that total levels of mRNA would strongly differ in different experimental conditions for Mode 1 and 4, while they would keep similar in wild-type conditions for Mode 2 and 3. Moreover, the results also suggest that expression levels of Sirt1 are more affected in the simulated experimental conditions for the translational repression mode (Mode 3).

ii. miR-34a silences Sirt1 through translational repression

By comparing the biological data published by Ford et al. (2008) with model predictions, we found that only Mode 3 can repeat the behavior of the experimental data (see Fig. 3). Thus, we concluded that miR-34a represses Sirt1 expression through translational repression rather than the other three defined mechanisms. Interestingly, our conclusion is also in agreement with the results generated by Yamakuchi and his co-workers (2008).

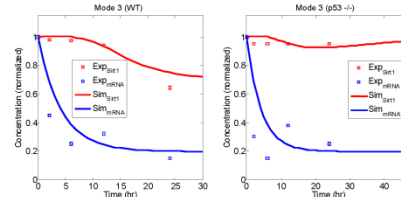


Figure 3: Prediction of mRNA silencing mechanism (Mode 3 in Fig. 2). Solid line: the model prediction. Square marker: biological data. Ford and colleagues measured mRNA and protein levels of Sirt1 after the stimulation with 5-FU in wild type (WT) or p53 mutated (p53 -/-) cell lines.

iii. Different regulatory effects of miR-34a and DBC1

We further investigated different negative regulatory effects on Sirt1 caused by its two inhibitors (miR-34a and DBC1). Interestingly, the simulations suggested that, although the concentration of DBC1 and miR-34a are perturbed in the same normalized interval, changes in the expression of DBC1 induce bigger modifications in the levels of active p53 than miR-34a (see Fig. 4 Top), implying a stronger role for DBC1 as enhancer of active p53 compared to miR-34a. Furthermore, we asked whether the two negative regulators of Sirt1 could compensate the loss of active p53 associated to experimental values in which Sirt1 is over-expressed, a condition related in the literature with tumour progression. As we found, only intensive enhancement of DBC1 is still able to cancel out the loss of active p53 due to the extreme up-regulation of Sirt1 (see Fig. 4 Bottom).

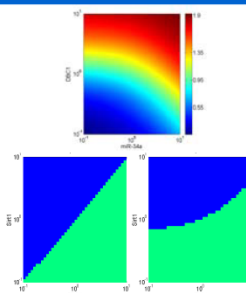


Figure 4: Top: Predictive simulation accounting for steady state level of active p53 under up and down-regulation of miR-34a and DBC1. Bottom: The ability of DBC1 and miR-34a to compensate the loss of active p53 for the abnormally high concentration of Sirt1 in cancerous cells. Active p53 is able (Green area) / unable (Blue area) to reach its basal level.

Summary

- We used a Systems Biology approach to set up a model accounting for the dynamical features of miRNA regulation in p53/Sirt1 signaling pathway.
- After qualitative validation of the model, we investigated two main features:
 - We modeled four different silencing mechanisms of miR-34 affecting on Sirt1 to predict the different observation that could be found in the specific experiment design.
 - By using a number of numerical computations, we compared the strength of the Sirt1's two negative regulators (DBC1 and miR-34a) and analyzed their impact on the status of active p53.
- Based on the analysis results, we concluded:
 - miR-34a silences Sirt1 through translational repression.
 - DBC1 is a more efficient negative regulator of Sirt1 than miR-34a.

References

- Ford, J., Ahmed, S., Allison, S., Jiang, M., and Milner, J., Cell Cycle 7, 3091-3097 (2008).
- Suzuki, H. I., Yamagata, K., Sugimoto, T., Kato, S., and Miyazono, K., Nature 460, 529-533 (2009).
- Yamakuchi, M., Ferlito, M., and Lowenstein, C. J., Proc. Natl. Acad. Sci. U.S.A 105, 13421-13426 (2008).
- Yamakuchi, M., and Lowenstein, C. J., Cell Cycle 8, 712-715 (2009).

Funded by



Federal Ministry of Education and Research



Xin Lai
Systems Biology & Bioinformatics Group
Institute of Computer Science, University of Rostock
18057 Rostock, Germany
URL: www.sbi.uni-rostock.de/calays
Email: xin.lai@uni-rostock.de

The Regulation of microRNA Target Hubs

Xin Lai¹, Ulf Schmitz², Olaf Wolkenhauer and Julio Vera¹

Department of Systems Biology and Bioinformatics, University of Rostock, Rostock, Germany

Abstract

In many signaling pathways there are critical target genes that can be simultaneously regulated by several miRNAs, the so called miRNA target hubs (Shalgi *et al.*, 2007). In this work, we propose a systems biology approach to investigate the regulation of target hub expression by miRNAs and transcription factors. We integrated knowledge from the biomedical literature, data from high-throughput experiments, and biological databases as well as hypotheses concerning the structure of the network into a mathematical model of miRNA target hub regulation. The model is used to test/construct biological hypotheses, design additional experiments, and predict complex biological scenarios associated to tissue-specific variability and oncogenic emergence via computational simulation.

To evaluate the methodology, we analyzed the regulation of the experimentally verified miRNA target hub Cyclin-dependent kinase inhibitor 1 (a.k.a. p21Cip1/Waf1), a cell cycle regulator related to DNA damage repairing and cancer emergence (Wu *et al.*, 2010). We constructed a comprehensive map of p21 regulation by miRNAs and transcription factors, and identified putative regulatory cooperation among p21-targeting miRNAs. Our map was used to detect and analyze putative feed-forward loops involving p21 transcriptional and post-transcriptional regulators that are activated in response to given critical cellular functions, like cell cycle and inflammatory response. Furthermore, the data-driven model was used to investigate hypothetical regulatory mechanisms involving couples of interacting miRNAs controlling p21 gene expression.

Background

p21 is a cyclin-dependent kinase inhibitor, a p53 mediator in growth suppression, and a marker of cellular senescence. p21 was identified as a miRNA target hub (Wu *et al.*, 2010), which can be repressed by two miRNA regulatory mechanisms: translation repression and deadenylation of p21 mRNA (Fig. 1).

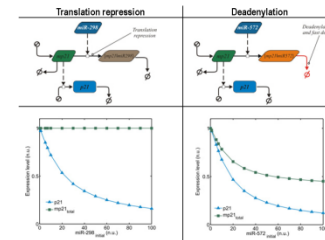


Figure 1. Illustrations of miRNA-mediated p21 regulation. Top: miR-200 binds to p21 mRNA and represses translation (left). miR-472 represses p21 by promoting p21 mRNA decay (right). Bottom: p21 protein and mRNA concentration in response to specific miRNA regulation. p21 mRNA concentration was predicted for the time point 48 hr after specific miRNA over expression.

Methodology

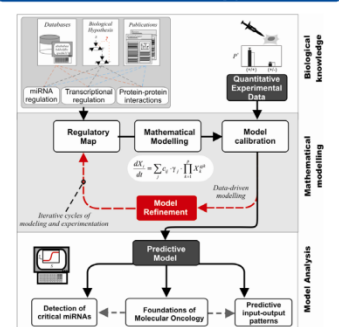


Figure 2. Schematic representation of the methodology. The methodology includes three modules: i) Collection of data from databases and the literature; ii) Model construction and calibration; iii) Simulation and analysis of the model.

Bioinformatics analysis

Two established target prediction algorithms (miRanda and RNA22) were used to identify binding sites for p21 targeting miRNAs in its 3' untranslated region (3' UTR; Fig. 3 top). A cooperation matrix was established based on the observations of Sætrom *et al.* (2007), in which it is suggested that the miRNAs with targeting sites in close proximity to other ones may result in stronger cooperative repression for their targets (Fig. 3 bottom).

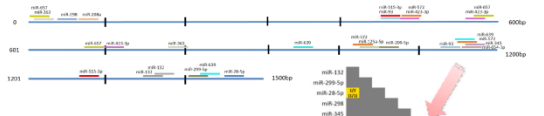


Figure 3. Bioinformatics analysis of p21-targeting miRNAs. Top: Predicted miRNA binding sites in the 3' UTR of human p21. The long blue line stands for the 3' UTR of human p21 and short color lines represent the targeting miRNAs located on their predicted binding sites. Bottom: Putative cooperation matrix of p21-targeting miRNAs. Yellow boxes account for potentially cooperating miRNA pairs whose binding sites are located in the cooperative proximity range. The numbers stand for the number of the cooperative miRNAs (before the forward slash) or the total binding sites (after the forward slash) for individual miRNAs displayed in the horizontal (top) or vertical (bottom) direction.

Model of p21 regulatory network

A model of the target hub (p21) regulation was constructed, in which p21 is repressed through single miRNA or cooperative miRNAs. Particularly, three hypothetical p21 regulatory mechanisms were modeled and the results revealed a sophisticated regulation mechanism by which the p21 expression is controlled (Fig. 4).

- (1) $\frac{dp21}{dt} = k_{on_mp21} - mp21 \cdot (k_{deg_mp21} + \sum_{i=1}^{15} k_{ass_miR_i} \cdot miR_i + \sum_{i,j=1}^{15} k_{ass_miR_i} \cdot miR_i \cdot miR_j)$
- (2) $\frac{d[mp21][miR_i]}{dt} = k_{ass_miR_i} \cdot mp21 \cdot miR_i - k_{deg_Cyt_i} \cdot [mp21][miR_i]$
- (3) $\frac{d[mp21][miR_i][miR_j]}{dt} = k_{ass_miR_i} \cdot mp21 \cdot miR_i \cdot miR_j - k_{deg_Cyt_{i,j}} \cdot [mp21][miR_i][miR_j]$
- (4) $\frac{dmiR_i}{dt} = k_{on_miR_i} - miR_i \cdot (k_{deg_miR_i} + mp21 \cdot (k_{ass_miR_i} + \sum_{j=1}^{15} k_{ass_miR_i} \cdot miR_j))$
- (5) $\frac{dp21}{dt} = k_{on_p21} \cdot mp21 - k_{deg_p21} \cdot p21$

Model equations. The state variables are p21 protein (p21), p21 mRNA (mp21), p21-targeting miRNAs (miR) and the complexes formed by mp21 and individual miRNA (mp21miR) or cooperative miRNAs (mp21miR_imiR_j). The parameters $k_{on_miR_i}$ and $k_{deg_miR_i}$ for each miRNA were estimated from experimental data published in Wu *et al.* (2010), others were fixed by using relevant biological information.

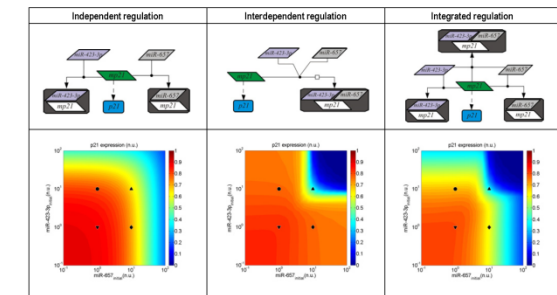


Figure 4. Simulation of three hypothetical p21 regulatory mechanisms, particularized for miR-457 and miR-423-3p. Left: Independent regulation, in which both miRNAs repress p21 independently. Middle: Interdependent regulation, in which p21 can be significantly silenced only when both of miRNAs are upregulated. Right: Integrated regulation, which is a combination of the independent and interdependent regulation mechanism. The markers in the figures represent four different initial expression conditions for miR-423-3p and miR-457: i) both miRNAs in normal expression (V), ii) over expression of both miRNAs (A), iii) and iv) over expression of only one miRNA (• and •).

Conclusions

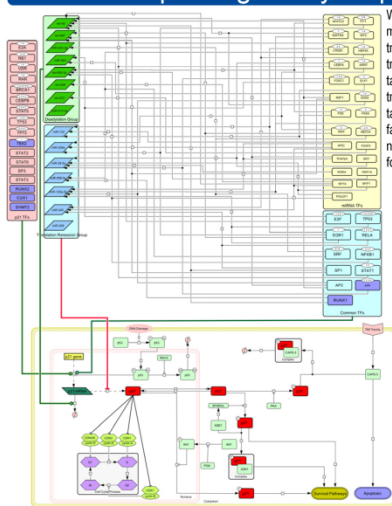
The integration of bioinformatics with mathematical modeling was used to study the experimental verified miRNA target hub (p21). By using such methodology:

- A sophisticated regulation mechanism considering the putative miRNA cooperation in downregulating p21 expression was revealed.
- A comprehensive p21 regulatory map was constructed.
- The feed forward loops existing in the p21 regulator network were detected and analyzed, and they were found to play a crucial role to maintain the robustness of the whole system.

References:
• Funahashi, A. *et al.*, Bioessays 1, 159 (2003).
• Shalgi, R. *et al.*, PLoS Comput. Biol. 3, 131 (2007).
• Sætrom, P. *et al.*, Nucleic Acids Res. 35, 2333 (2007).
• Le Novère, N. *et al.*, Nat. Biotechnol. 8, 735 (2009).
• Wu, S. *et al.*, Oncogene 29, 2302 (2010).

* These authors contributed equally to this work.

p21 regulatory map



We constructed a regulatory map accounting for transcriptional and post-transcriptional regulation of the target hub p21 and the transcriptional regulation of its targeting miRNAs (Fig. 5). This facilitates the detection of network motifs, e.g., feed forward loops.

Figure 5. Graphic representation of p21 regulatory network. Rectangles: The TFs for p21 (red) and its targeting miRNAs (yellow), and their common TFs (blue). Parallelograms: p21-targeting miRNAs, which are divided into two groups: deadenylation (blue) and translation repression (green). The map also sketches the most important signaling pathways in which p21 acts as a key regulator. The map was constructed using CellDesigner (Funahashi *et al.*, 2003) and follows the SBOL (Systems Biology Graphical Notation) specification (Le Novère *et al.*, 2009).

Funding
This work was supported by the German Federal Ministry of Education and Research (BMBF) as part of the project CALSYS (C.N. 0315264) under the FORSYS initiative.

FORSYS
Partner Initiative

Federal Ministry of Education and Research



Contact
xin.lai@uni-rostock.de
ulf.schmitz@uni-rostock.de
julio.vera@uni-rostock.de
Ulmenstrasse, 69, 18057 Rostock, Germany
www.sbb.uni-rostock.de

A Systems Biology Approach to Study Cellular Functions of MicroRNAs

Abstract

MicroRNAs (miRNAs) are potent effectors of posttranscriptional gene silencing and exert functions in affecting cellular and pathological processes such as apoptosis and cancer. Distinct interactions between miRNAs and their targets are designed to implement particular functions within cells. However, studying individual interactions between miRNAs and their targets is far from understanding the regulatory role of miRNAs at system-level.

The systems biology approach, combining bioinformatics analysis and quantitative mathematical modelling, provides a means to elucidate functions of miRNAs in gene regulatory networks and signalling pathways. By using this approach,

- we study the regulatory role of miR-34a in the p53/Sirt1 signalling pathway (Lai *et al.*, 2012a);
- we present a novel approach to construct the comprehensive gene regulatory network of p21, an experimentally verified miRNA target hub (Lai *et al.*, 2012b);
- we investigate the function of miR-146a in the early lung inflammatory response (Lai *et al.*, 2012c).

Systems Biology Approach

The systems biology approach is cyclical process including three modules (Figure 1):

- **Biological knowledge**
 - Collection of data from databases and relevant literature
 - Construct biological system
- **Mathematical modelling**
 - Model construction
 - Deterministic model (e.g., ordinary differential equations)
 - Model calibration
 - Parameter estimation
 - Parameter identifiability
 - Model validation
- **Model analysis and simulation**
 - Sensitivity analysis
 - Bifurcation analysis
 - Predictive simulation

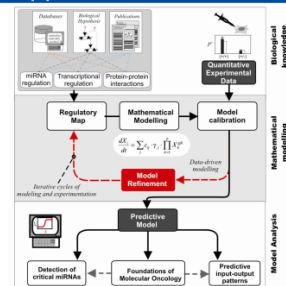


Figure 1. Workflow of the systems biology approach.

miR-34a regulation in signalling pathway

p53 is the most frequently mutated protein in human cancers. Reactivation of this protein in tumours, which induces cell cycle arrest and apoptosis, is therefore an appealing therapeutic strategy. Recently, miR-34a is a new component found to be involved in the regulation of the p53/Sirt1 signalling pathway, in which miR-34a can activate p53 through a feedback loop. In this loop, miR-34a, whose expression is transcriptionally promoted by p53, represses the production of Sirt1, which is an NAD-dependent deacetylase and can regulate apoptosis in response to oxidative and genotoxic stress through deacetylating p53. Besides, the other identified regulators (e.g., DBC1 and Mdm2) of p53 are also included in the pathway (Figure 2).

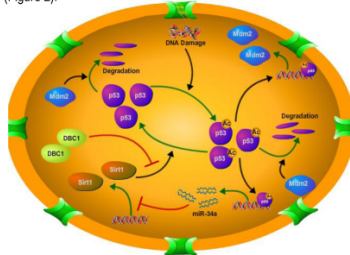


Figure 2. The scheme of the p53/Sirt1 signalling pathway. p53, deacetylated p53, ac-p53, acetylated p53, Mdm2, p53 binding protein Mdm2, Sirt1, NAD-dependent deacetylase sirtuin-1, DBC1, deleted in breast cancer 1.

For the investigation on the dynamic properties of p53 in the signalling pathway, we applied the systems biology approach. We set up and calibrated a mathematical model by using available experimental data and carried out the predictive simulations to illustrate the effects of miR-34a on the activation of p53 (Figure 3).

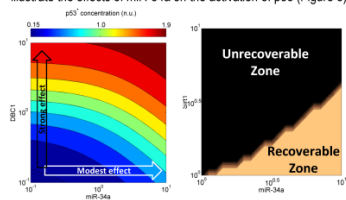


Figure 3. The regulatory effect on active p53 by miR-34a. Left: Up- and down-regulation of DBC1 and miR-34a to affect the concentration of active p53 (p53). Right: The ability of miR-34a to compensate the loss of p53, which is caused by the upregulation of Sirt1, mostly found in cancerous cells. n.u.: normalised unit.

miRNA target hub p21

miRNA target hubs are genes that can be simultaneously targeted by comparatively large number of miRNAs, non-coding RNAs that mediate posttranscriptional gene repression. Although the details of target hub regulation remain poorly understood, recent experiments suggests that pairs of miRNAs can cooperate if their binding sites reside in close proximity. To test this and other hypotheses, we established a novel approach to investigate mechanisms of collective miRNA repression and applied on the experimentally verified target hub p21.

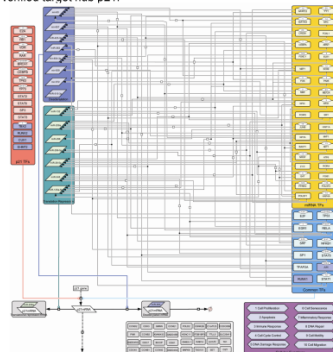


Figure 4. p21-centered regulatory map. The map includes the miRNAs targeting p21, the transcription factors (TFs) of p21 and the miRNAs (colourful rectangles) and the interacting proteins of p21 (grey rectangles). The cellular functions associated with the TFs are listed in the purple box.

We constructed a p21-centered regulatory map (Figure 4). Based on this map, we set up a kinetic model and performed computational analysis to decipher the p21 expression regulated by multiple and cooperative miRNAs (Figure 5).

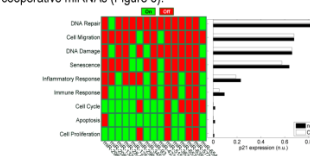


Figure 5. Cooperative miRNA regulation of p21 expression in different cellular functions. For different cellular functions, the distinctive combination of miRNA statuses (on/off) can result in different p21 steady-state levels when the miRNA cooperativity is considered (C) or not (no C).

miR-146a regulation in lung inflammation

Recently, regulations through miRNAs have been implicated in lung inflammation. Particularly, miR-146a seems to play a crucial role in the inflammatory response. Induction of miR-146a was observed after stimulation with different stimuli such as different bacterial Toll-like receptor (TLR) ligands and cytokines, and its expression is promoted in a NF- κ B-dependent way. Meanwhile, over expression of miR-146a can negatively regulate IL-8 and RANTES production. Thus, miR-146a plays a role in the TLR signalling pathway through targeting TRAF6 and IRAK1 in a negative feedback loop, suggesting miR-146a as an important regulator in lung inflammation (Figure 6).

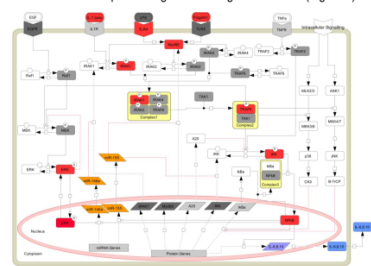


Figure 6. Key signalling pathways in lung inflammation involving miRNA regulation.

We designed and conducted experiments to measure the dynamics of important signalling pathway regulators (e.g., expression of miR-146a and IL-8; Figure 7), and these data were used to calibrate and validate the mathematical model. By using the model, we aim to identify the key processes that regulate intensity and duration of the immune response and to unravel the function of miR-146a in the early lung inflammatory response.

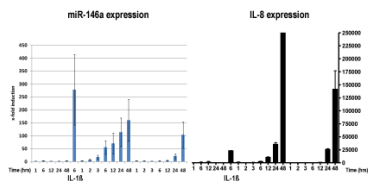


Figure 7. The measured experimental data used for mathematical modelling. Q-PCR data for miR-146a expression (left) and IL-8 expression measured by ELISA (right). A549 cells were stimulated with either wild type Legionella (wt) or its non-flagellated mutant (Δ fda). Unstimulated cells served as negative control (ctrl), cells stimulated with the cytokine IL-15 [1 ng/ml] served as positive control (IL-15).

Conclusions

The systems biology approach provides us an efficient and systematic way to understand the functions of miRNA that are difficult to be dissected by pure experimental methods and to generate the hypotheses that can push forward our understanding of the regulatory role of miRNA in signalling pathways and gene regulatory networks.

References:

- Lai *et al.* (2012a). Modelling miRNA regulation in cancer signalling systems: miR-34a regulation of the p53/Sirt1 signalling module. In: *Computational Modeling of Signaling Networks*, Liu, X., Schmitt, W., eds. Springer, ISBN: 978-1-177-78230-2.
- Lai *et al.* (2012b). Computational analysis of target hub gene expression regulated by multiple and cooperative miRNAs (submitted).
- Lai *et al.* (2012c). Unravel the regulatory role of miR-146a in the early inflammatory response to Legionella pneumophila (under preparation).

Funding
This work was supported by the German Federal Ministry of Education and Research (BMBF) as part of the project CALSYS (C.N. 0315264) under the FORSYS initiative as well as the DFG project WO 991/4-1.

FOR
Partner Initiative

Federal Ministry of Education and Research

DFG

Contact
Xin Lai, Ulf Schmitt, Julia Vera, Otf Wolkowhauser
Department of Systems Biology and Bioinformatics
University of Rostock
xin.lai@uni-rostock.de
www.sbi.uni-rostock.de

Curriculum vitae

Xin Lai



Personal Information

Work address	Department of Systems Biology and Bioinformatics Institute of Computer Science University of Rostock 18051 Rostock, Germany
Telephone	0381-498-7684
Email	xin.lai@uni-rostock.de
URL	sites.google.com/site/xinlairostock
Date of birth	21 st April 1983
Place of birth	Chengdu, China
Nationality	Chinese

Education

2008-2012	Ph.D. in Systems Biology and Bioinformatics University of Rostock, Germany Dissertation: A systems biology approach to unravel the cellular function of microRNAs
2005-2008	M.Sc. in Computational Engineering University of Rostock, Germany Thesis: Mathematical modelling and optimization of biochemical systems: a method of analysis in biotechnology and biomedicine
2001-2005	B.Sc. in Computer Science Technology University of Chengdu, China

Honour and Award

2012	Best Poster Award Symposium on Remodeling, Repair and Regeneration in Lung Diseases Marburg, Germany
2005	Excellent Graduate Award Technology University of Chengdu, China
2002, 2004, 2005	First Class Scholarship Technology University of Chengdu, China

Research Project and Position

2008-2012	Postgraduate Research Assistant Investigating the Cancer and Aging Link through Systems Biology Department of Systems Biology and Bioinformatics University of Rostock, Germany
July-December 2007	Undergraduate Research Assistant Computational Systems Biology of Cell Signalling Department of Systems Biology and Bioinformatics University of Rostock, Germany

Teaching and Administration Experience

2009-2012	Hands on Lectures in Systems Biology I and II Mathematical modelling of cell signalling pathways using SBtoolbox2 Mathematical modelling of biochemical networks using SYCAMORE Principles of advanced parameter estimation for biochemical models
2008-2012	Research Group Seminar Organizer www.sbi.uni-rostock.de/students/courses/researchseminar
2008-2012	Web Creator and Administrator for BMBF-Funded Research Project CALSYS www.sbi.uni-rostock.de/calsys
2011	A Practical Lecture for Collaborators from Medical Departments Mathematical modelling of biochemical networks
2009	Organization Assistant in Transatlantic Summer School on Cancer Systems Biology, Rostock, Germany
2008	Organization Assistant in Systems Biology for Medical Applications Summer School, Tenerife, Spain

Promovieren im Fach Biotechnologie

Interview von Anke Wilde auf www.academics.de veröffentlicht

Beide promovieren sie in der Krebsforschung - sie darüber, wie bestimmte Wirkstoffe sich per Impfung am besten in ein Tumorgewebe transportieren lassen, er darüber, wie man eben diese Wirkstoffe und ihre biochemischen Reaktionen über ein mathematisches Modell beschreiben kann. Sie wollte schon immer bei einem Pharmariesen unterkommen, er träumt davon, an seiner Heimatuniversität einen Fachbereich für Systembiologie zu gründen. Zwei Wege, in der Biotechnologie eine Promotion abzuschließen.



Xin Lai, Promovend der Biotechnologie an der Uni Rostock, möchte an seiner Heimatuniversität einen Fachbereich für Systembiologie gründen.

Xin Lai kann endlich ein wenig durchatmen. Gerade hat der 29-jährige Chinese an der Universität Rostock seine Doktorarbeit abgeschlossen. Es war schon mitten in der Nacht, als er die letzten Korrekturen vorgenommen, das Dokument gespeichert und in den Druck geschickt hatte. Jetzt kommt erst einmal ein Wochenendtrip mit der Ehefrau nach Kopenhagen, dann steht wieder die Forschung auf dem Plan. Anna Maria Städtler hat das alles noch vor sich. Die 26-Jährige hat vor einem Jahr mit ihrer Promotion bei der Bayer Pharma AG begonnen, die sie im Rahmen eines durch das BMBF geförderten Verbundprojektes absolviert. An die ersten Tage dort kann sie sich noch sehr gut erinnern - sehr straff durchorganisiert seien die gewesen, es sei ihr, der Neuen, sehr leicht gemacht worden, sich in die neue Arbeitsumgebung einzufinden. Dann sei eine längere Lektürephase gekommen, in der sie sich ausschließlich dem aktuellen Forschungsstand in ihrem Thema gewidmet hat.

Forschungsziel: Medikamente gegen den Krebs

Ihr Thema umfasst die Evaluierung von Nanotransportsystemen für sogenannte small interfering RNAs, kurzkettige Ribonukleinsäure-Moleküle, die direkt in die Tumorzellen eingeschleust werden. Dort schalten sie - genregulierenden Prozessen sei Dank - gezielt die Gene ab, die dafür sorgen, dass die Zellen sich ungebremsst teilen können und damit bösartige Wucherungen verursachen. Problematisch ist allerdings, diese Moleküle zielgerichtet dorthin zu transportieren, wo sie wirken sollen. An sich sind RNA-Moleküle in der freien Blutbahn nämlich nicht vorgesehen, sie werden abgebaut. Auch das Immunsystem erkennt sie als feindliche Eindringlinge und reagiert darauf. Deshalb braucht es eine Art schützendes Transportsystem, so Anna Maria Städtler. "Das sind in unserem Fall neue sehr verzweigte Moleküle, die die RNA binden und in die betroffenen Zellen einschleusen, wobei das Tumorstadium zum Stillstand gebracht werden kann."

Zwei Transportsysteme, die vom Verbundpartner, der Arbeitsgruppe Haag der Freien Universität Berlin synthetisiert worden sind, seien mittlerweile erfolgversprechend in vivo, das heißt im Mausorganismus getestet worden. Ein drittes, das in vitro, sprich im Reagenzglas, bereits gut funktioniert, soll nun ebenfalls in vivo untersucht werden. "Das ist alles sehr anwendungsbezogen", sagt Städtler begeistert. "Es geht eben darum, am Ende ein Medikament zu entwickeln, das einem Patienten neue, lebensverlängernde Therapieoptionen eröffnet." Diese Anwendungsbezogenheit beim Promovieren, der Transfer von Wissenschaft in eine medizinische Therapie, sei ihr sehr wichtig, und den finde man eher in einem Unternehmen als an der Universität.

Forschungsziel: Modelle für das Verhalten von Molekülen

Auch Xin Lai befasst sich mit kleinen RNA-Schnipseln, die Tumorzellen von ihrem bösartigen Treiben abbringen sollen. Sein Ansatz ist allerdings ein komplett anderer. In seiner Heimatstadt Chengdu in Zentralchina hatte er Informatik studiert, und in seiner Doktorarbeit ging es darum, ein mathematisches Modell zu schaffen, welches das Wirken der in die Zelle eingeschleusten RNA präzise beschreibt. Zu den Parametern, die in ein solches Modell einfließen, gehört beispielsweise die Reaktionsgeschwindigkeit, eben wie schnell ein Protein verarbeitet oder in ein anderes Molekül umgewandelt wird.

Ist ein solches Modell gut, dann kann man ganz ohne Tests im Reagenzglas oder auch an Mäusen vorhersagen, wie eine Zelle sich unter bestimmten Umständen verhalten wird. "So ein Modell muss dann natürlich auch auf seine Tragfähigkeit überprüft werden", sagt Xin Lai. In seinem Fall übernimmt das eine Arbeitsgruppe aus Leipzig, die in dem Forschungsprojekt mit der Universität Rostock zusammenarbeitet. "Man muss sich das so vorstellen: Aus der Literatur und aus den Experimenten der Kollegen holt man sich alle verfügbaren Daten. Die fügt man in das Modell ein, und dann wird wieder im Experiment untersucht, ob sich die Voraussagen des Modells auch wirklich erfüllen." Wenn nicht, wird das Modell korrigiert.

Promovieren in der Industrie oder in der freien Forschung - ein Gegensatz?

Eine Industriepromotion oder eine Doktorarbeit an der Universität oder einem Forschungsinstitut - beide Varianten haben ihre Verfechter und ihre Gegner. Doktoranden in der akademischen Forschung halten der Industrieforschung fehlende Freiheiten und eine zu große Ausrichtung auf lukrative Projekte vor. Umgekehrt besteht die Kritik, die öffentlich geförderten Forschungsinstitute seien schlechter ausgestattet und achteten zu wenig auf praktische Anwendbarkeit der Forschungsergebnisse.

Anna Maria Städtler findet die Kritik an einer Promotion in einem forschenden Unternehmen unbegründet. Sie erfahre bei Bayer eine sehr gute fachliche Betreuung und werde ermutigt, ihre Forschungsergebnisse auch auf Konferenzen und in Publikationen der wissenschaftlichen Öffentlichkeit zu präsentieren. "Natürlich muss ich vorher absprechen, ob damit patentrelevante Themen angeschnitten werden", räumt sie ein. Aber das sei an den Universitäten nicht anders - wer sich an seinen neu entwickelten Technologien ein Patent sichern wolle, spreche vorher auch nicht öffentlich darüber.

Auch Xin Lai ist mit den Rahmenbedingungen seiner Promotion zufrieden. Er konnte an vielen Konferenzen teilnehmen und musste seine Arbeit nicht durch endlose Verwaltungsakte unterbrechen, sagt er. Und auch wenn seine Arbeit zunächst die Grundlagenforschung voranbringe, so sei der Anwendungsbezug ja dennoch gegeben. "Schließlich können solche Modelle helfen, Therapien gegen bislang unheilbare Krankheiten zu entwickeln", gibt er zu bedenken.

Die fachliche Expertise gibt den Ausschlag

Und was sagen die Personaler? Claudia Israel ist Recruiting Managerin bei der Firma Qiagen im nordrhein-westfälischen Hilden. Deutschlandweit sind in dem Biotechnologie-Unternehmen etwa 1.400 Mitarbeiter angestellt, weltweit sind es 4.000. Von den promovierten Bewerbern in ihrer Firma haben die meisten den Dokortitel an der Universität erworben, sagt sie. Inzwischen aber beobachtet sie, dass die Industriepromotion allmählich an Bedeutung gewinnt. "Das liegt einfach daran, dass die Unternehmen gut qualifizierten Nachwuchs möglichst frühzeitig entdecken und an sich binden wollen", meint sie. Aus ihrer Sicht ist es jedoch nicht so wichtig, ob der Titel an einer renommierten Universität oder bei einem führenden Unternehmen erworben wurde - das Worüber, die erworbenen Kompetenzen und fachlichen Methoden wögen deutlich schwerer. Studienabsolventen rät sie deshalb, sich genau zu überlegen, was ihr Karriereziel ist, und entsprechend den Weg dahin zu wählen. Anna Maria Städtler hatte schon lange mit einer Karriere bei dem international operierenden Pharmaunternehmen geliebäugelt, und darum hatte sie sich auch vor über einem Jahr bei Bayer beworben. Xin Lai dagegen will im akademischen Sektor forschen und am liebsten in seiner Heimatstadt Chengdu an der Universität ein eigenes Forschungslabor gründen oder eine Abteilung für Systembiologie. Gemessen an den Zielen, die sie erreichen wollen, haben wohl beide die richtige Sprosse auf ihrer persönlichen Karriereleiter erklommen.

Theses

- The utilisation of a systems biology approach, which combines biological data with mathematical modelling, provides a promising way to understand the function of microRNAs in cellular systems.
- Kinetic modelling, using nonlinear ordinary differential equations, is an appropriate method to simulate and predict temporal dynamics of interacting components in signalling pathways and gene regulatory networks.
- A combination of local and global optimization methods provides an efficient means to estimate model parameter values. Sensitivity and bifurcation analysis are useful tools for unravelling dynamic properties of kinetic models.
- Kinetic modelling of the p53/SIRT1 signalling pathway, which consists of the interactions among p53, SIRT1 and miR-34a, identifies the mechanism by which miR-34a represses SIRT1 and shows the ability of miR-34a to recover the loss of active p53 in certain cancerous condition, in which the expression of SIRT1 is aberrantly upregulated.
- A novel approach, combining transcriptional factor and microRNA target prediction algorithms with data from the literature and databases, provides guidance to the construction of microRNA target hub networks. This is demonstrated with a comprehensive regulatory map of p21.
- Identification of microRNA-mediated feedback and feedforward loops in the regulatory map of p21 shows their crucial role in maintaining the proper regulation of p21. For example, a feedforward loop mediated by miR-125a-5p is shown to be important for maintaining the proper regulation of p21 during cell cycle.
- A data-driven kinetic model, derived on the basis of the p21 regulatory map deciphers the regulation of p21 by multiple and cooperative microRNAs in different biological scenarios. For example, the synergistic regulation of p21 is shown to be a consequence of a pair of experimentally verified cooperative microRNAs; the model can be also used to investigate response of p21 to different types of stimuli and the distinct p21 expression levels for different cellular functions.

Selbständigkeitserklärung

Ich versichere hiermit, die vorliegende Arbeit selbständig und ausschließlich unter Verwendung der angegebenen Mittel und ohne unerlaubte Hilfen angefertigt zu haben. Ich versichere, dass ich die Regularien, die Voraussetzungen, sowie die Vorgehensweisen für Promotionsverfahren an der Universität Rostock gelesen habe und ihnen zustimme.

Rostock, 29. August 2012

Xin Lai